REVIEW ARTICLE

The solar magnetic field

Sami K. Solanki, Bernd Inhester, and Manfred Schüssler

Max-Planck-Institut für Sonnensystemforschung, 37191 Katlenburg-Lindau, Germany

E-mail: `solanki@mps.mpg.de`

Abstract. The magnetic field of the Sun is the underlying cause of the many diverse phenomena combined under the heading of solar activity. Here we describe the magnetic field as it threads its way from the bottom of the convection zone, where it is built up by the solar dynamo, to the solar surface, where it manifests itself in the form of sunspots and faculae, and beyond into the outer solar atmosphere and, finally, into the heliosphere. On the way it, transports energy from the surface and the subsurface layers into the solar corona, where it heats the gas and accelerates the solar wind.

1. Introduction

After 5 billion years, the Sun is still popping and boiling, unable to settle down into the decadent middle age that simple theoretical considerations would suggest. (...) It appears that the radical element for the continuing thread of cosmic unrest is the magnetic field.
(E.N. Parker, Cosmical Magnetic Fields, 1979)

What Eugene Parker [1] wrote for the Universe is certainly true for the Sun. In the absence of a magnetic field, the Sun would be a considerably simpler object: it would show only minor deviations from spherical symmetry due to differential rotation and meridional circulation, while convection and the oscillations and waves that it excites would provide some background noise. Although these processes themselves provide a rich field of study, they pale in comparison with the overwhelming variety of phenomena and processes existing and acting on the real Sun. Without a magnetic field, phenomena as diverse as sunspots and coronal loops, faculae and solar flares, the solar wind and prominences, the solar cycle and irradiance variability, to name but a few, would be unknown to us.

It is therefore not surprising that the magnetic field holds a central position within solar research, although this is sometimes masked by the fact that the indirect manifestations of the Sun's field (e.g. the relatively cool gas within sunspots or the very hot gas in the corona) are much easier to detect than the magnetic field itself. Direct in-situ measurements of the Sun's magnetic field are restricted to locations accessible to spacecraft, i.e. up to now to distances greater than $60\,R_\odot$ (sampled by the Helios space probes [2, 3]). Only a small fraction of the Sun's total magnetic flux reaches out to this distance. We therefore rely on remote sensing in order to detect more than just the tip of the proverbial iceberg. The magnetic field near the solar surface is usually measured using the Zeeman effect, which is best observed in spectral lines formed

in the solar photosphere. Although observations based on cyclotron resonance, the Hanle effect and Faraday rotation, as well as the recording of the Zeeman effect in non-photospheric spectral lines are becoming increasingly important, the vast majority of all recordings of the magnetic field still refer to measurements of the Zeeman effect in the photosphere.

Hence the photospheric magnetic configuration of, e.g., sunspots is known with considerable accuracy, while our knowledge of the strength and structure of the magnetic field in the corona owes as much to the extrapolation (using potential or force-free fields) from photospheric measurements and the use of proxies (e.g., EUV images of coronal loops) as to direct measurement. This is extremely unfortunate since the magnetic field plays a comparatively minor role in the photosphere, but completely dominates proceedings in the corona. The absence of sensitive and high-resolution coronal magnetic field measurements may be the largest single factor blocking progress in coronal physics and frustrating our attempts to answer questions related to coronal heating, the triggering of flares and coronal mass ejections, as well as the acceleration of the fast and slow solar wind.

Our conception of the Sun's magnetic field is a prototype for the magnetism of other cool stars. Many of these very common stars show signs of magnetic activity, such as X-ray and EUV emission typical of stellar coronae, or the brightness modulations due to the passage of starspots across the stellar disc [4]. The sum of all cool stars in the solar neighborhood can supply information on the generation and manifestation of stellar magnetic fields which cannot be obtained from the Sun alone, so that their investigation indirectly provides an enrichment of our knowledge of the Sun. Examples are the dependence of activity level, of the surface magnetic flux and activity cycle parameters or of starspot latitudes on stellar rotation rate, mass and evolutionary state. The investigation of stellar magnetism is, however, strongly hampered by the inability to resolve stellar surfaces at the spatial scales at which many of the physical processes take place, not withstanding the success of techniques such as (Zeeman) Doppler imaging [5, 6, 7]. For example, it is estimated that Doppler imaging resolves only a small fraction of the starspots on active stars [8]. Only on the Sun do we (nearly) achieve the necessary spatial resolution to get at the heart of the physics. Thus it is not surprising that both physical mechanisms proposed to explain the presence of high-latitude spots on rapid rotators [9, 10] are extrapolations to the relevant stellar parameters of mechanisms known to act on the Sun. Magnetically driven processes occur also in systems such as accretion disks around evolved stars or supermassive black holes at the centres of galaxies and other astrophysical systems. Once more, the Sun provides access to similar processes at the fine spatial scales at which many of them occur.

In addition to being a normal star the Sun is also the central star of the solar system and the main source of energy for the Earth. The magnetically variable Sun can influence the Earth in multiple ways. Changes in the radiative output of the Sun affect the Earth's energy balance and influence stratospheric chemistry. The cyclic variations of the Sun's open magnetic flux modulates the cosmic ray flux reaching the Earth. These and other solar variables have been proposed as drivers of global climate change. The evidence for such an influence is increasing [11, 12]. In addition, coronal mass ejections, large eruptions that fling coronal gas into interplanetary space, inject particles and energy into the magnetosphere, ionosphere and upper atmosphere. There they produce aurorae, substorms and other phenomena combined under the heading of space weather. Since all the relevant solar phenomena (e.g. irradiance variations and

coronal mass ejections) are magnetically driven, a better understanding of Sun-Earth relations also requires a good knowledge of the Sun's magnetic field and its evolution on timescales from minutes to millenia.

Finally, the Sun's magnetic field and in particular its interaction with solar convection and rotation also presents a variety of problems of basic physical interest (e.g., self-excited dynamos, magnetoconvection, interaction of radiation with magnetized gas, magnetic reconnection). Indeed, in a diagram of the location of laboratory and natural plasmas in the n-T plane (where n is the particle density and T the temperature) the plasma in the solar core, corona and heliosphere occupies parameter regimes that other plasmas in the laboratory or elsewhere in the solar system do not. Thus, the Sun is a unique laboratory of magnetized plasmas.

This review is aimed both at the young solar researcher entering the field, as well as physicists working in other, possibly related fields. We have reduced mathematical descriptions to a minimum and have not aimed at completeness in the references. The review is structured as follows. We start by giving a very brief overview of the Sun's magnetic field and introducing a few relevant parameters (Sect. 2). This is followed by a description of the large scale structure of the field and the solar cycle (Sect. 3). After that, the physics of the solar magnetic field is described step by step. We start in the solar interior (Sect. 4), discuss the dynamo (Sect. 5), and then move upward to the solar photosphere (Sects. 6 and 7), for which the largest amount of empirical data is available. Proceeding further outward, we discuss the magnetic structure of the solar corona (Sect. 8) and end in the heliosphere (Sect. 9).

2. Overview and basic considerations

A dynamo mechanism operating in the lower part of the solar convection zone is generally considered to be the source of the Sun's magnetic field. Current models (see Sec. 5) place the dynamo at the interface between the convection zone and the radiative core, a layer marked by convective overshooting and a strong radial shear in the Sun's differential rotation. Strands of strong azimuthal (toroidal) magnetic field generated by the dynamo break out from the overshoot layer owing to magnetic buoyancy and related instabilities, rise through the convection zone and emerge at the visible solar surface in the form of bipolar magnetic regions, finally forming loop structures whose tops usually lie in the corona. The locations where the legs of a loop intersect the solar surface are visible as either sunspots or faculae. Higher in the atmosphere, in the chromosphere, the latter appear as bright plages. The upper layers of a loop radiate at EUV and X-ray wavelengths.

The structure of the field and its properties undergo a remarkable transition with height. In the photosphere the field is highly filamented. Most of the magnetic energy resides in magnetic flux tubes, concentrations of magnetic field that can be roughly described as bundles of nearly parallel field lines with a relatively sharp boundary, although these cover less than 5% of the solar surface. The flux tubes visible at the surface range from the very small and bright (magnetic elements) to the very large and dark (sunspots). The strength of the flux tube fields at the solar surface is remarkably homogeneous, however, being around 1–2 kG† when averaged over their cross sections.

---

† Throughout this review, we write all equations according to the SI unit system. However, when giving values of the magnetic field strength and the magnetic flux, we mostly follow the practice in the astrophysical literature and use cgs units. The relationship between both systems of units is: $1\,\text{Tesla} = 10^4\,\text{Gauss}$ (magnetic flux density) and $1\,\text{Weber} = 10^8\,\text{Maxwell}$ (magnetic flux).

Owing to the pressure exerted by the magnetic field, radial force balance across the tube boundary implies that the flux tubes are strongly evacuated. This evacuation leads to considerable buoyancy, which ensures that, on average, the magnetic field remains nearly vertical.

Because of the evacuation, the plasma β $(= 2\mu_0 p/B^2)$ at the solar surface is in the range 0.2–0.4, if the gas pressure p is taken within a flux tube. Thus, locally the magnetic energy density can exceed the thermal energy density, although, because of the small area coverage by strong fields, globally most of the energy is in the form of the thermal energy of the gas. Below the solar surface the plasma β increases rapidly with depth, reaching values estimated to be 10^5 or higher near the bottom of the convection zone.

Another relevant ratio is that of magnetic to kinetic energy density, $B^2/\mu_0\rho v^2$, which indicates whether the magnetic field locally dominates the bulk motions or vice versa. Taking values for velocity, v, and density, ρ, typical of the surface convection (granulation) and B typical of the flux tubes, one obtains a value of the order of 10 (while it can become of order unity for the supersonic peaks of the granular flow). Globally, the energy in the granulation is of the same order of magnitude as the energy in the magnetic field. In the convection zone, the value of $B^2/\mu_0\rho v^2$ is more uncertain, but there are indications for values significantly above unity in intense flux tubes located in the lower convection zone.

The situation changes rapidly as one moves higher into the atmosphere. Initially, both the gas pressure and the field strength decrease exponentially with height, so that β remains approximately constant, but above a certain height, which typically lies in the chromosphere, the expanding magnetic flux tubes fill the whole volume. Beyond this height, the field strength drops more sedately, although still with a large negative power of r (the radial distance from the solar center). It drops much more rapidly than a locally monopolar ($\propto r^{-2}$) or dipolar ($\propto r^{-3}$) configuration. This comes from the fact that, in addition to the increasing volume available to be filled, the field lines loop back to the solar surface. Hence, with increasing r one moves beyond the tops of an increasing number of loops. Alternatively, the magnetic field in the corona, if described as a linear combination of multipoles, requires that very high orders are included, which drop with a correspondingly high power of r. Nonetheless, the gas pressure and density drop even more rapidly with height than the field (exponential vs. power law decrease). Consequently, we have $\beta \ll 1$ and $B^2/\mu_0\rho v^2 \gg 1$ in the corona, so that the energetics and dynamics are dominated by the magnetic field.

As a consequence of these conditions, the magnetic Lorentz force cannot be balanced by any other force, so that the coronal magnetic field has to arrange itself into a force-free configuration, which is rather homogeneous in strength (compared to the photosphere or convection zone), but not so in direction. Owing to the presence of loops reaching up to different altitudes, all values of the field inclination can be found at a given height in the corona, so that the situation is exactly the opposite to the photosphere, where the field is inhomogeneous in strength, but mainly vertically oriented.

At $r \gtrsim 2$–3 $R_\odot$, most of the remaining field lines are 'open', i.e., they reach out into the heliosphere. Only a small fraction (a few percent) of the total flux that emerges from the solar surface is in the form of such open field lines. Finally, even further out, in the regime of the solar wind the relative importance of the various energy densities changes again, with $\rho v^2/2 > B^2/2\mu_0 > P$ beyond the point where the kinetic energy density of the solar wind equals the magnetic energy density (the

Alfvén radius). This point is located 10–20 $R_\odot$ from the solar surface, for the fast and slow wind, respectively. The kinetic energy of the solar wind dominates and forces the magnetic field lines to follow the radially directed wind. In combination with solar rotation this results in a spiral pattern of the magnetic field.

3. Large-scale structure and solar cycle

While the solar magnetic field is strongly structured down to scales at the limit of observational resolution, it shows, at the same time, a remarkable degree of large-scale spatio-temporal order and organization. Properties of the bipolar magnetic regions on the solar surface (like their mean emergence latitude and the spatial orientation of their polarities) and the direction of the global dipole field vary systematically in the course of the solar activity cycle. Magnetic flux is organized in network structures defined by convection patterns and becomes globally redistributed by large-scale flows.
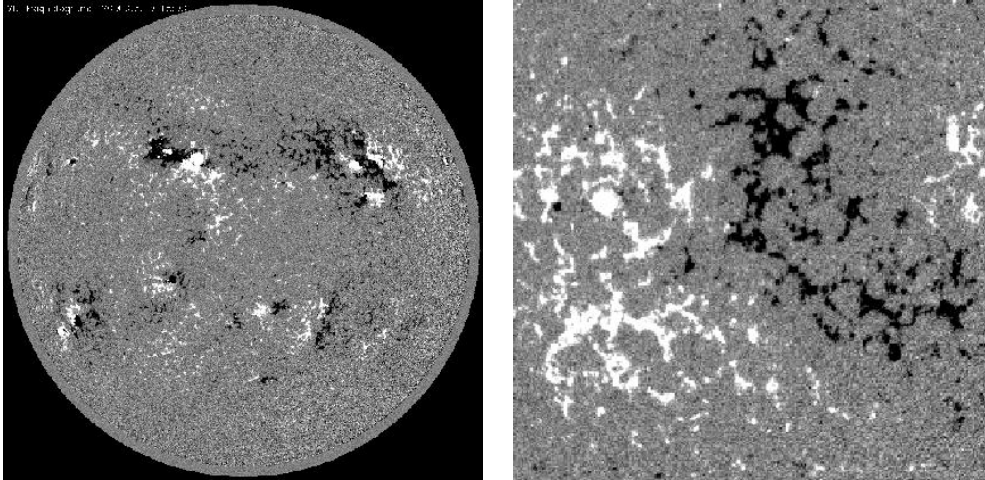
3.1. Flux distribution on the solar surface

Maps of the magnetic field on the visible solar surface (the thin layer where the solar plasma becomes transparent for light in the visible wavelength range) displays structures on a wide range of scales. During periods of high solar activity, large bipolar magnetic regions indicate the locations of recent magnetic flux emergence from the deep solar interior (see Figure 1, left panel). Large areas of apparently unipolar field result from the decay and spread of the bipolar regions. During most of the time, such unipolar regions can be found around the solar poles; they define the global dipole component of the solar magnetic field, which is roughly aligned with the rotation axis during most of the time.

3.1.1. Bipolar regions. Magnetic flux appears at the solar surface in the form of bipolar magnetic regions with a wide range of values for the (unsigned) magnetic flux and lifetimes [13, 14]. While the largest *active regions* reach fluxes of nearly 10^{23} Mx (10^{15} Wb) and lifetimes of months, the smallest *ephemeral regions* contain less than 10^{19} Mx and live less than a day before their magnetic flux cancels or merges with the pre-existing background flux. Large bipolar regions form conspicuous sunspot groups while the smaller regions can only be detected through magnetic field measurements.

Figure 2 shows that the emergence rate of bipolar regions as a function of flux (or size) roughly follows a power law, which possibly extends down to the ephemeral regions, indicating a common origin of all emerging flux. On the other hand, the variation of the emergence rate in the course of the solar cycle is different: large active regions vary by about a factor 8, while ephemeral regions hardly vary at all and may actually show a slight variation in antiphase [14].

Bipolar active regions exhibit a number of systematic properties, providing information on the magnetic structure of the source region near the bottom of the convection zone from where the surface flux emerges (see Sect. 3.2.2). Active regions (a) are generally orientated roughly in the East-West direction, (b) are systematically tilted in latitude, (c) appear only in low and middle latitudes (below 45 degrees), (d) show different proper motions of the two opposite-polarity patches with respect to the surrounding plasma. During and shortly after their emergence at the surface, these properties are displayed by the bipolar regions in a statistical sense; smaller regions show a larger scatter [14, 4].

Figure 1. Distribution of magnetic flux in the visible solar surface layers. The circular polarization of a spectral line due to the Zeeman effect serves as a quantitative measure of magnetic flux. Black and white indicate positive and negative magnetic polarity, respectively, while grey signifies low magnetic flux levels. *Left*: Magnetic image of the visible hemisphere on July 31, 2000, near the maximum of the current activity cycle. The map is dominated by large bipolar magnetic regions and extended unipolar domains. The Sun rotates from left to right. *Right*: Close-up of a decaying bipolar region of about $400 \times 400 \,\mathrm{Mm}^2$ size, showing the network structure outlining the convective flow pattern of supergranulation (Images taken with the *Michelson Doppler Imager (MDI)* on board the *Solar and Heliospheric Observer (SOHO)*, a joint ESA/NASA mission).

3.1.2. Magnetic network. The relative importance of induction versus diffusion effects in the temporal evolution of the magnetic field in a plasma with bulk flow is described by the *magnetic Reynolds number*, $R_\mathrm{m} = U\,L/\eta$, where U is a typical flow velocity, L the length scale of the flow, and η is the magnetic diffusivity (inversely proportional to the electrical conductivity). For all relevant flow patterns in the Sun we have $R_\mathrm{m} \gg 1$, so that the magnetic field evolution is governed by induction, with the magnetic field lines being fixed to the fluid elements (*Alfvén's theorem*, 'flux freezing' [15]). As a consequence, the magnetic flux distribution at the solar surface reflects the dominant patterns of convection: magnetic flux is transported by the horizontal flows to the convective down drafts and forms a network pattern on both the scales of granulation (the dominant scale of convective energy transport with $L \simeq 1 - 2\,\mathrm{Mm}$, see Sect. 7) and supergranulation ($L \simeq 30\,\mathrm{Mm}$, see Figure 1, right panel).

3.1.3. Magnetic flux transport. The dominance of induction effects has the consequence that the evolution of the magnetic flux through the solar surface after its emergence is largely governed by the large-scale velocity fields. These are (a) differential rotation (the equator rotating about 30% faster than the polar regions), (b) a meridional flow of about 10–25 m s^{-1} from the equator towards the poles, and (c) supergranulation. At large length scales, the effect of the latter can be described by a random-walk process with an effective ('turbulent') magnetic diffusivity of the order of $5\,10^8\,\mathrm{m}^2\,\mathrm{s}^{-1}$ [16]. The main consequences of this transport of magnetic flux on the solar surface are: (a) the spreading of bipolar regions in time, (b) the development of quasi-rigidly rotating magnetic patterns, and (c) the transport of magnetic flux to the
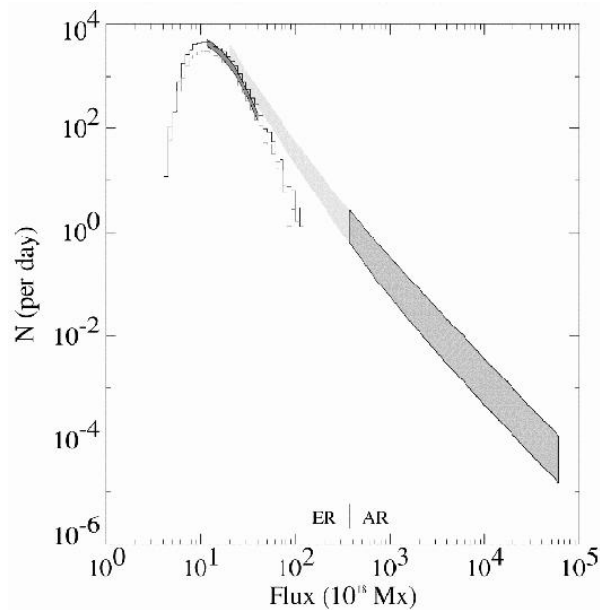
Figure 2. Emergence rate of bipolar regions per (unsigned) flux interval of 10^{18} Mx. The dark grey band shows the distribution for larger regions (AR: active regions [13]); the variation by about a factor of 8 through a typical activity cycle is indicated by the width of the band. The variation for the smallest ephemeral regions (ER) is much smaller and possibly in antiphase with the sunspot cycle (dark shading); full histograms are shown for 1997 October (black, solar minimum) and 2000 August (gray, solar maximum). The turnover below 10^{18} Mx reflects the detection threshold of the instrument. The lightly shaded area between the smallest ephemeral regions and the active regions is conjectural (from [14]).

poles. In connection with the tilt of the bipolar region with respect to the East-West direction (see Sect. 3.2.2) the latter process leads to reversals of the polar fields: the westward polarity patch of a bipolar region is at somewhat lower latitudes and thus preferentially cancels with its opposite-polarity counterparts on the other hemisphere, so that a net flux of eastward polarity is transported to the poles by the meridional flow.

The observed evolution of the large-scale solar magnetic field on a time scale of months to years, including the polarity reversals of the polar fields, is remarkably well reproduced by two-dimensional flux-transport models [17, 18, 19, 20], which describe the passive transport of a purely vertical (radial) magnetic field by differential rotation, meridional flow, and turbulent diffusion. The input required for this kind of models is the temporal and spatial distribution of magnetic flux emergence in bipolar magnetic regions. The results indicate that the evolution of the observable magnetic flux after emergence is largely a surface phenomenon, so that inferences about the generation of magnetic flux and the dynamo in the solar interior can only be drawn from the properties of bipolar regions in their early phases.

3.2. The 11(22)-year cycle

The magnetic activity of the Sun, as most apparent by the coming and going of dark sunspots (strongly magnetized regions on the visible surface, see Sect. 6) and the
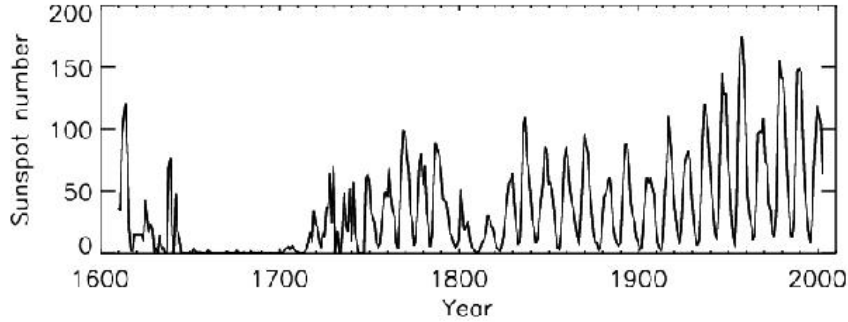
Figure 3. The record of yearly averaged group sunspot numbers [21]. Besides the dominant 11-year cycle, there is a long-term modulation of sunspot activity with extended periods of almost vanishing sunspots (1640-1700, Maunder minimum) or rather few sunspots (1800-1820, Dalton minimum).

eruptive phenomena in the upper atmosphere and corona of the Sun, shows a cyclic (but not strictly periodic) variation with a mean period of about 11 years. There is a remarkable degree of regularity in the large-scale properties of this *solar cycle*, which underlies the seemingly random appearance and evolution of the magnetic features in the turbulent surface layers of the Sun. The systematic reversals of the polar magnetic fields and the polarity orientation of sunspot groups show that a complete magnetic cycle covers two 11-year activity cycles.

3.2.1. Sunspot numbers. The longest systematic direct record of solar activity is the series of sunspot numbers, which starts soon after the invention of the telescope in the beginning of the 17th century. By compilation of the records of many observers it was possible to derive a series of sunspot numbers which reaches back to 1611 [21].

Figure 3 shows the existing record of (yearly averaged) sunspot numbers. While the 11-year cycle is obvious, there is also a modulation of the sunspot activity on longer time scales. Most remarkable is the second half of the 17th century (the Maunder minimum [25]), when sunspots were almost completely absent. We now know that this is just one case of the occasional 'grand minima' of solar activity (see Sect. 3.3); a less marked example is the Dalton minimum at the beginning of the 19th century.

Although the definition of the sunspot number appears to be somewhat arbitrary, it is in fact very well correlated with more objective measures like the total solar radio flux at 10.7 cm wavelength or the total (unsigned) surface magnetic flux and thus represents a quantitatively valid measure of solar magnetic activity [26] (see Figure 4).

3.2.2. Sunspot latitudes, polarity rules, and tilt angle of bipolar regions. The average latitudes of newly appearing sunspots show a systematic variation in the course of the 11-year activity cycle. Sunspots emerge in two broad latitude belts, which are roughly symmetric with respect to the solar equator. At the beginning of a cycle, these belts are centered around $\pm 30°$ latitude. In the course of the cycle, the sunspot belts migrate towards the equator and reach about $\pm 5°$ average latitude towards the end of the cycle. In a latitude-time diagram of sunspot occurrence, this drift leads to a characteristic butterfly-shaped pattern, which is also clearly visible in the related diagram of the surface magnetic field (see Figure 5).
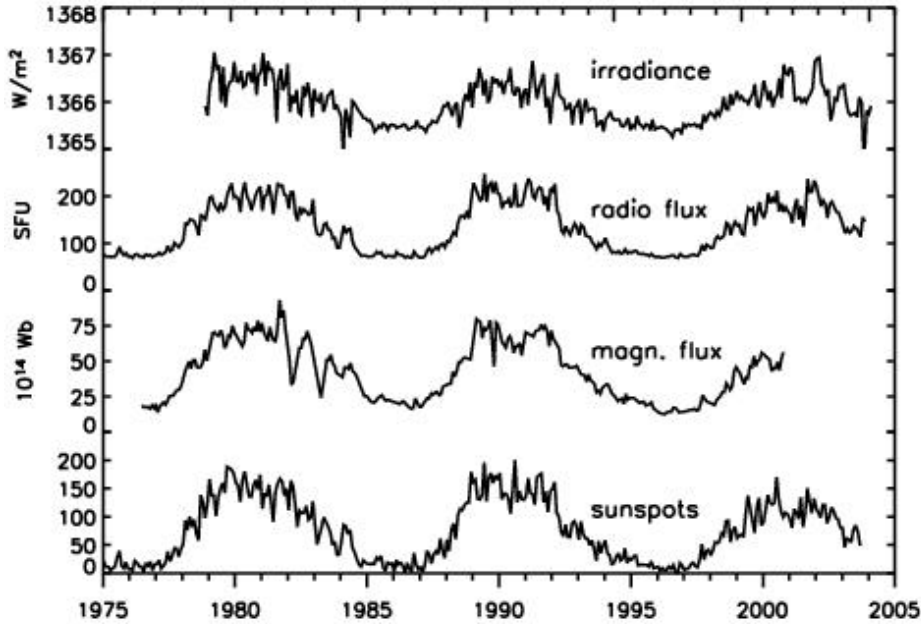
Figure 4. Various quantities varying in phase with the 11-year cycle of sunspots (lowest curve: monthly sunspot number provided by the Royal Observatory of Belgium, Brussels): total solar irradiance at the top of the Earth's atmosphere in W/m^2 (source: [22, 23]), 10.7 cm (2800 MHz) solar radio flux in 'solar flux units' (SFU) of $10^{-22}\,\mathrm{J\,s^{-1}\,m^{-2}\,Hz^{-1}}$ (source: Radio Astrophysical Observatory, Penticton, Canada) and the total (unsigned) magnetic flux in the solar photosphere (source: Wilcox Solar Observatory, Stanford, USA [24]).

Sunspots typically appear in groups embedded in magnetically bipolar regions, whose local magnetic polarity they share in most cases. The bipolar regions are roughly oriented in East-West-direction (the direction of solar rotation, see Figure 1) and their polarities are arranged according to the following set of *polarity rules* (*Hale's law,* first formulated on the basis of magnetic field measurements in sunspot groups [28]):

1) The magnetic orientation of bipolar regions remains the same in each hemisphere during an 11-year activity cycle.

2) The bipolar regions in the Northern and Southern hemispheres have opposite magnetic orientation.

3) The magnetic orientation of the bipolar regions reverses from one cycle to the next.

As a consequence of these rules, the pattern of magnetic orientations repeats itself with a period of two activity cycles, i.e., the magnetic cycle of the Sun has a duration of about 22 years.

Another systematic property of bipolar regions is their deviation from a precise East-West orientation: on both hemispheres, the more westward located polarity (leading with respect to the direction of rotation) is nearer to the equator than the

LONGITUDINALLY AVERAGED MAGNETIC FIELD
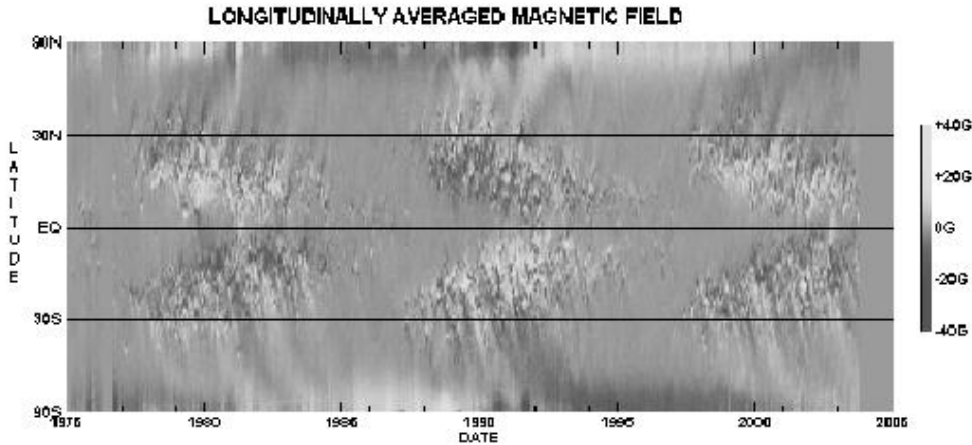
Figure 5. Time-latitude diagram of the longitudinally averaged magnetic field in the solar photosphere for the last three activity cycles. The emergence of magnetic flux in active regions leads to characteristic structures in the lower latitudes, which have been first described in similar 'butterfly diagrams' based on sunspot observations [27]. The combined effects of convection, and meridional circulation lead to the magnetic flux transport to high latitudes and thus cause reversals of the polar magnetic fields in phase with the activity cycle (courtesy D. Hathaway, NASA).

following polarity. On average, the corresponding tilt angle with respect to the East-West direction, γ, is proportional to the mean heliographic latitude, λ, of the bipolar region: $\gamma \simeq 0.5\lambda$ (Joy's law [29]).

Larger bipolar regions obey the polarity rules and Joy's law more strictly than smaller regions (without sunspots), which are probably more strongly affected by disturbances and deformation of the underlying magnetic structure by convective motions.

The systematic properties of large bipolar regions are important constraints for models of solar magnetic activity and the solar cycle. Together with the polarity reversals of the global magnetic field, they indicate a remarkable degree of large-scale order and self-organization that is not obvious considering the non-stationary nature of the convective motions, from which the solar magnetic field must ultimately derive its energy (see Sect. 5).

3.2.3. Effect on solar rotation Magnetic activity affects the differential rotation of the solar plasma only very slightly. Helioseismological measurements have not revealed a systematic change of the shear layer (tachocline) at the bottom of the convection zone in the course of the 11-year cycle, but there are indications of a time variation of the rotation near the bottom and below the solar convection zone with a period of about 1.3 years [30]. It is presently unknown whether this oscillation is related to the magnetic field. A clearer relationship exists in the case of the (somewhat misleadingly named) 'torsional oscillations', a pattern of slightly slower and faster rotating bands differing from the average rotation by well below 1%. The bands propagate in latitude toward the equator and are related, at low latitudes, to the migration of the sunspot zones as well as to variations in the pattern of the meridional flow on the solar surface

[31]. The torsional oscillation was first observed by Doppler measurements of surface flows [32] and later found to penetrate at least a third of the convection zone depth [33, 34]. Suggestions concerning the physical origin of the alternating bands include driving by the magnetic Lorentz force [35] and geostrophic flows driven by surface cooling in active regions [36].

3.2.4. Irradiance variation and other impacts of the solar cycle The variation of magnetic activity in the course of the 11-year solar cycle affects not only 'magnetic' quantities like magnetic flux or sunspot number; the radiative output of the Sun is also modulated in phase with the solar cycle. This variation is particularly pronounced for the radiation originating from the hot plasma in the upper layers of the solar atmosphere (chromosphere to corona). Here, the dominating magnetic forces and the dissipation of magnetic energy determine the atmospheric structure, which therefore strongly changes in the course of the activity cycle (see Sect. 8). As a consequence, the radiation at UV, EUV and radio wavelengths varies by factors in the range $2 \ldots 10$ between solar activity minimum and maximum while the soft X-ray flux changes by a factor of order 100 [37]. Moreover, the total (frequency-integrated) solar irradiance at Earth's orbit as measured with bolometric instruments in space also changes slightly (of the order of 0.1%) in phase with the solar cycle (see Figure 4, [23]). The fact that the Sun brightens during activity maximum in spite of the larger fraction of the surface covered by dark sunspots is due to the effect of small-scale magnetic fields, which locally enhance the radiative flux in so-called faculae (see Sect. 7).

The variability of the solar irradiance has potential effects on terrestrial climate, both on time scales of the solar cycle and, probably even more importantly, on centennial and longer time scales [38]. While changes in the total irradiance concern the basic energy input into the climate system, the (relatively much stronger) variability of the UV radiation affects the temperature structure of the stratosphere through photochemical reactions involving ozone [39]. A third possible route by which solar variability may affect the terrestrial climate is via the modulation of the galactic cosmic ray flux by the varying heliospheric magnetic field [40] (see Sect. 9). It has been suggested that cosmic rays trigger cloud formation, so that their variation could possibly affect the total cloud cover and thus climate [41].

3.3. Long-term modulation of magnetic activity

As already apparent from the record of sunspot numbers shown in Figure 3, there is a long-term amplitude modulation of the 11-year sunspot cycle, including periods of low or even almost vanishing sunspot activity. The detection of further regularities or periodicities is hampered by the short length of the directly measured sunspot record. Quantitative information about the solar activity before 1611 can be obtained through proxies like the concentrations of the 'cosmogenic' isotopes ^{10}Be and ^{14}C [45]. These isotopes are produced from atmospheric oxygen and nitrogen by spallation reactions caused by galactic cosmic rays (mainly protons and α-particles). The modulation of the cosmic ray flux (in antiphase with the solar cycle) by the varying heliospheric magnetic field [46] imprints the signature of the solar cycle and the strength of solar activity upon the production rate of the cosmogenic isotopes: the higher the solar activity, the lower the production rate, and vice versa. The isotopes are subsequently removed from the atmosphere and incorporated in 'archives' of past solar magnetic activity in the form of yearly layers of polar ice shields (^{10}Be, by precipitation) or tree
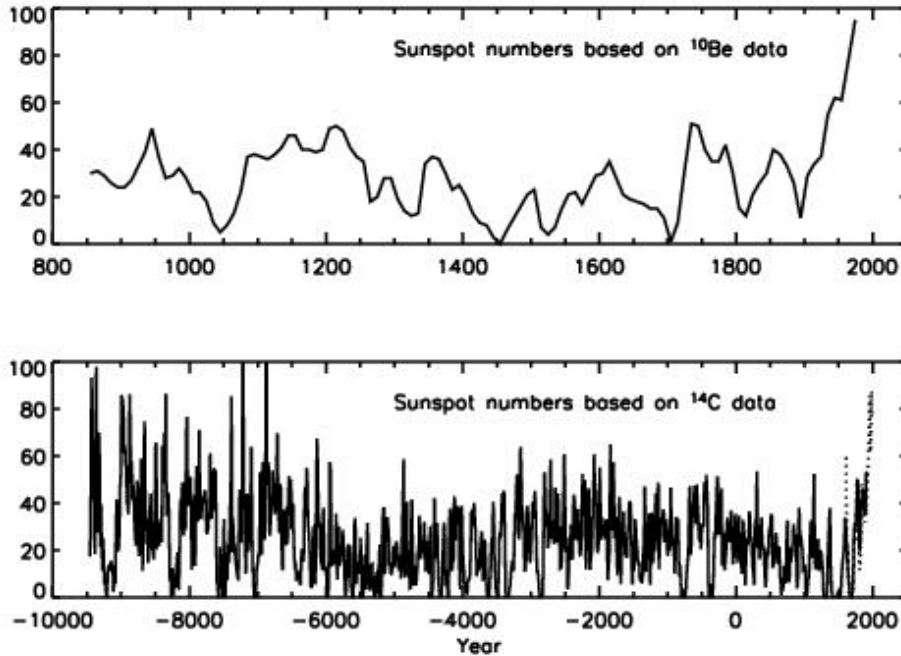
Figure 6. Reconstructions of the (10-year averaged) sunspot number from the measured concentrations of cosmogenic isotopes. *Upper panel:* Sunspot number since AD 850 based on [10]Be data [42, 43]. *Lower panel:* Reconstruction from 9455 BC until AD 1900 based on ^{14}C data from tree rings [44] (full line). After $\simeq$ 1900, the ^{14}C record is strongly contaminated by the burning of fossil fuels (Suess effect) and cannot be used for the reconstruction. The dotted line gives the 10-year averaged actual group sunspot number from 1611 AD onward.

rings (^{14}C, by plant metabolism).

By inverting the various components of the chain of processes connecting the measured isotope concentration with characteristic measures of solar activity (like the sunspot number), it is possible to reconstruct the latter for periods greatly exceeding the length of the directly measured record. As an example, Figure 6 shows the (11-year averaged) reconstructed sunpot number based upon [10]Be data from Greenland and Antarctica (from AD 850 onward [42]) and a reconstruction from ^{14}C in tree rings (for the whole holocene from the year 9400 BC onward [44]). Both reconstructions demonstrate that periods of very low activity like the Maunder minimum in the 17th century are not uncommon. Furthermore, they also show that episodes of consistently high average activity (like the current period since about 1940) are much more rare; in fact, similarly long periods of comparable activity levels can only be found more than 8000 years before present.

The cosmogenic isotope records permit also the search for other periodicities than the 11/22-year basic sunspot cycle. Spectral analysis of the isotope data in fact reveals significant signals at periods around 90 years (the Gleissberg cycle, which is also found in the sunspot record [47]), 210 years, and 2200 years [45, 48, 49].

3.4. A 'fossil' magnetic field in the radiative interior?

Owing to the skin effect, the oscillating magnetic field of the solar cycle can penetrate the radiative interior by only a few km. In the absence of turbulent convection, the skin depth is determined by the molecular magnetic diffusivity, $\eta = (\mu_0 \sigma)^{-1}$, which is in the range $10^{-2} \ldots 1 \, \mathrm{m^2 \, s^{-1}}$ (σ is the electrical conductivity).

On the other hand, such values of the diffusivity in the interior together with the large size of the system lead to a very long diffusive decay time for a large-scale magnetic field, $\tau_d \simeq R_\odot^2/\eta$, exceeding the age of the Sun. It is therefore conceivable that a slowly decaying 'fossil' magnetic field resides in the solar interior. This field could be a remnant from the magnetization of the interstellar cloud out of which the Sun formed or it could be a trapped field from a dynamo acting during the very early evolutionary phase of the Sun when it was fully convective [50, 51]. It is also conceivable that the combination of differential rotation and magnetic instability of a toroidal magnetic field leads to dynamo generation of magnetic field in the radiative interior of the Sun [52].

However, there is no direct observational evidence for such a magnetic field in the solar interior. In fact, the existence of a sharp transition between the differentially rotating convection zone and the almost uniformly rotating radiative interior in form of a narrow radial shear layer (the solar 'tachocline' [53]) indicates that any fossil magnetic field is closely confined to the radiative part and thus has no surface manifestations. On the other hand, at least a weak internal magnetic field seems to be required to maintain both the uniform rotation of the solar interior [54, 55] and the sharpness of the tachocline [56, 57, 58].

4. Magnetic fields in the convection zone

In a convecting medium with large magnetic Reynolds number, magnetic flux is expelled from regions of closed streamlines and assembled in flux concentrations between the convection cells [59, 60]. This process of flux expulsion, which can be directly observed in the flux distribution on the solar surface (see Sect. 7), leads to a strongly intermittent distribution of magnetic flux. By analogy as well as through qualitative minimum-energy arguments [61] and numerical simulations [62], such intermittency of the magnetic field is also suggested to prevail throughout the whole solar convection zone. The question is whether intermittent structures generated by flux expulsion can become sufficiently strong and large to decouple themselves from the convective velocity field to be governed by their internal dynamics. Sunspots are an example of such an 'autonomous' structure, but observations show that they are not formed by flux expulsion by surface flows but emerge as coherent (albeit initially fragmented) entities from below. In fact, the sunspot polarity rules and other systematic features indicate that the magnetic flux responsible for the formation of sunspots and (large) bipolar regions is not dominated by non-stationary convective motion but originates from a source region of largely ordered and azimuthally oriented magnetic flux in the deep convection zone [63, 64]. These observations are in accordance with the picture of a 'rising tree' [65, 66]: strands of magnetic flux detach from the source region, rise through the convection zone and emerge at the surface in a dynamically active way to form bipolar magnetic regions and sunspots. Only after the initial stage of flux emergence and after fragmenting into small-scale flux concentrations, does the surface field come progressively under the influence of

convective flow patterns and large-scale surface flows, so that its large-scale evolution can be well described by flux transport models (see Sect. 3.1.3). Consequently, it is necessary to consider the dynamics of magnetic structures in the convection zone in order to make the connection between the observed properties of the surface fields and the dynamo process generating the magnetic flux in the first place (see Sect. 5).

4.1. Magnetic flux tubes and flux storage

The dynamics of magnetic structures can be conveniently described using the concept of *isolated magnetic flux tubes.* These are defined as bundles of magnetic field lines (comprising constant magnetic flux), which are separated from their non-magnetic environment by a tangential discontinuity (surface current) in ideal MHD or a narrow resistive boundary layer. As a consequence, the coupling between an isolated flux tube and its environment is purely hydrodynamic and mediated by pressure forces.

If the diameter of a flux tube is small compared to all other relevant length scales (scale heights, wavelengths, radius of curvature, etc.) the *thin flux tube approximation* can be employed, a quasi-1D description that greatly simplifies the mathematical treatment [67, 68]. The forces which are most important for the dynamics of a magnetic flux tube are the buoyancy force, the magnetic curvature force, the Coriolis force (in a rotating system), and the aerodynamic drag force (for motion relative to the surrounding plasma). Very thin flux tubes are effectively coupled to the motion of the surrounding plasma by the drag force, while larger (but still 'thin' in the above sense) tubes can move relative to the surrounding plasma owing to the action of the other forces, similar to a flexible solid body immersed in a fluid.

An upward directed buoyancy force results from the density deficit in a flux tube arising from the necessity to compensate the magnetic pressure by a reduced gas pressure [69, 70]. Such *magnetic buoyancy* has important consequences for dynamo models. It is the obvious mechanism to drive the rise and eruption at the surface of magnetic flux generated by the dynamo, but it is so efficient that fields of equipartition strength are lost from the convection zone in a time much shorter than the 11-year time scale for field generation and amplification by the dynamo [70]. This problems is actually made even more severe by the unstable superadiabatic stratification of the convection zone, which leads to convective buoyancy and even faster flux loss [71], and by the intrinsic instability of magnetic flux tubes in an unstably stratified medium [72, 73, 74].

The buoyancy problem and the resulting 'storage problem' could possibly be somewhat alleviated by 'convective pumping' [75, 76, 77]. This effect provides a net transport of magnetic flux toward the bottom of a strongly stratified convecting layer or into an underlying stable layer [78]. The cause of this process is the strong asymmetry between up- and downflows in stratified convection: while most of the rising fluid has to turn horizontal owing to the decreasing density after ascending for about a scale height, the downflows accelerate, converge and merge, and can traverse many scale heights. The magnetic buoyancy is therefore reduced by the 'pummeling' from above by strong downflow plumes. It is not clear, however, whether the numerical simulation results which prompted this suggestion are applicable to the realistic solar situation. The effects of limited grid resolution and numerical diffusion may well lead to an overestimate of the flux transport by pumping [79].

In any case, the storage problem for magnetic flux resulting from magnetic buoyancy in the convection zone can be resolved by assuming that the azimuthal

magnetic flux which, upon emergence at the surface, leads to large active regions and sunspot groups is generated and stored in a stably (subadiabatically) stratified layer of overshooting convection below the convection zone proper [80, 81, 82, 83], where it can reach a stable equilibrium configuration [84, 74]. This layer overlaps with the region of strong radial differential rotation (tachocline) and thus also provides the rotational shear required for building up a strong azimuthal magnetic field.

There are two classes of possible magnetic configurations in the overshoot layer: a continuous layer of magnetic flux and an ensemble of isolated magnetic flux tubes. In the case of a layer of azimuthal magnetic field in mechanical equilibrium, the magnetic Lorentz force is balanced by a combination of gas pressure gradient and Coriolis force due to a field-aligned flow [85]. The relative importance of both forces for the balance of the magnetic curvature force depends on the degree of subadiabaticity of the stratification as measured by the quantity $\delta = \nabla - \nabla_{\mathrm{ad}}$, where ∇ and $\nabla_{\mathrm{ad}} = (\mathrm{d}\ln T/\mathrm{d}\ln p)_{\mathrm{ad}}$ represent the actual and the adiabatic logarithmic temperature gradient (i.e., the logarithmic temperature gradient in a homentropic stratification), respectively. In a strongly subadiabatic region (like the radiative core of the Sun with $\delta < -0.1$), the latitudinal pressure gradient is dominant for the magnetic equilibrium, while the contribution of the Coriolis force is small. For $\delta \simeq -10^{-3}$, both contributions are similar, while for a value of $\delta \simeq -10^{-6}$, as is probably realistic for a layer of convective overshoot, the magnetic curvature force is balanced practically by the Coriolis force alone. For a field strength of the order of 10^5 G (10 Tesla), an azimuthal velocity of the order of $100\,\mathrm{m\,s}^{-1}$ relative to the background rotation is required, so that the profile of differential rotation would be significantly modified.

Another important point is the stability of a magnetic layer. In the simplest case, the decrease of the field strength at the top of such a layer drives an instability of Rayleigh-Taylor type, whose nonlinear evolution leads to the formation of tubular magnetic structures [86, 87]. In the absence of diffusion effects, a magnetic layer in the overshoot region becomes unstable to flux tube formation when the field strength exceeds a value of the order of the equipartition field strength with respect to the kinetic energy density of the convective velocities [88]. The limiting field strength for stability may be even smaller if doubly-diffusive instability becomes relevant in the case of a dominating thermal diffusion due to radiation [89]. Another road to the fragmentation of a magnetic layer into flux tubes is the Kelvin-Helmholtz-type instability due to the shear flow [90].

As long as they remain within a stably stratified region, the flux tubes formed by the instability of a magnetic layer can find a new equilibrium governed by the balance of curvature force and Coriolis force [84], which is similar to the equilibrium of a magnetic layer in a slightly subadiabatic region [85]. To obtain mechanical equilibrium in the idealized case of an azimuthal flux tube, i.e. a flux ring contained in a plane parallel to the equator, the buoyancy force must vanish since its component parallel to the axis of rotation cannot be balanced by any other force. In the direction perpendicular to the axis of rotation, the magnetic curvature force is balanced by the Coriolis force due to a faster rotation of the plasma within the flux ring compared to its nonmagnetic environment.

4.2. Flux-tube instability

If the dynamo-generated azimuthal magnetic flux is stored in the convective overshoot layer in the form of a non-buoyant equilibrium configuration, a trigger mechanism is

required to initiate the rise of flux tubes towards the surface. One possibility is radiative heating [91, 92], which leads to a slow rise of flux tubes through the overshoot layer until they enter the convection zone proper, whereupon they rapidly rise to the surface owing to convective and magnetic buoyancy [71].

As the field strength of a flux tube is intensified by differential rotation, at some stage it exceeds the threshold for the onset of the *undulatory instability* [72, 73]. This instability in most cases sets in for non-axisymmetric perturbations of an equilibrium flux ring as sketched in the left panel of Figure 7. A downflow of plasma along the field lines within the flux tube leads to an upward buoyancy force acting on the outward displaced parts and a downward force on the troughs, so that the perturbation grows. As a consequence, flux loops form, rise through the convection zone, and finally emerge at the surface to form sunspot groups and active regions.

A detailed linear stability analysis [74] shows that flux tubes in the solar convective overshoot layer are strongly stabilized by the combined effects of stratification, rotation, and magnetic curvature forces. It requires a field strength of the order of 10 Tesla (10^5 G) for the formation of a rising loop that eventually emerges at the solar surface. This threshold value is about an order of magnitude larger than the equipartition field strength with respect to the kinetic energy density of the convective motions in the deep convection zone.

4.3. Numerical simulations of rising flux tubes

Simulations of the nonlinear development of the undulatory instability on the basis of the thin flux tube approximation have revealed the important role played by the Coriolis force (angular momentum conservation) for the evolution of a rising flux tube in the solar convection zone [94]:

1) The expanding flux loop experiences a retarding Coriolis force directed perpendicular to the rotation axis. For sufficiently weak field, the Coriolis force can balance the corresponding component of the buoyancy force. The unbalanced axial component of the buoyancy force then leads to a motion of the flux loop parallel to the axis of rotation, deflecting its motion to high latitudes. It demands a sufficiently strong buoyancy force to let the loop emerge in low latitudes, as observed on the Sun; this requires initial field strengths of the order of 10 Tesla (10^5 G) [95, 96, 97, 98]. The lower part of Figure 7 shows the quite different behavior of emerging flux loops with initial fields of 12 Tesla (left panel) and 1 Tesla (equipartition field strength, right panel).

2) The strong stratification of the convection zone leads to a draining of mass from the rising part by a flow along the loop. The Coriolis force on the horizontal component of this flow (corresponding to an expansion) leads to a twist of the rising loop (clockwise in the northern and anti-clockwise in the southern hemisphere). Upon emergence of the flux loop at the surface, this twist manifests itself as a tilt angle of the leading and the following parts of the newly-formed bipolar region with respect to the azimuthal direction (see Sect. 3.2.2). A quantitative agreement with the observed tilt angles requires a strength of the dynamo-generated magnetic field at the bottom of the convection zone in the range of 3–10 Tesla [99, 93].

3) Angular momentum conservation retards the azimuthal motion of the upper parts of a rising loop and leads to a geometric asymmetry: the preceding part in the
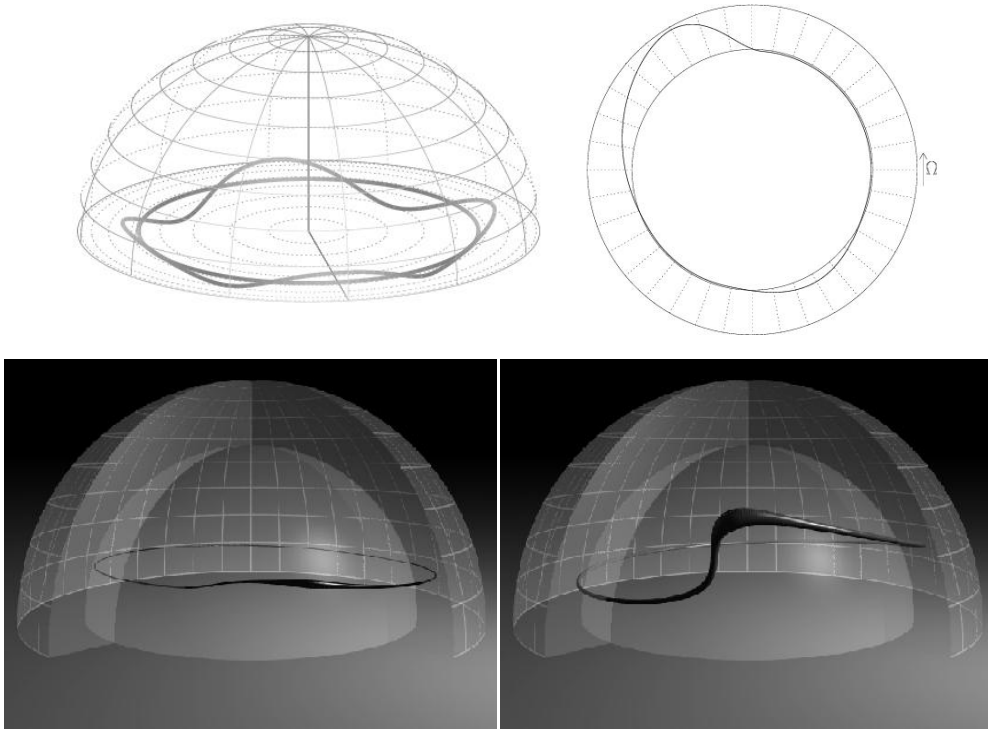
Figure 7. Instability and rise of magnetic flux tubes. *Upper left:* Sketch of the undulatory instability. An initially axisymmetric magnetic flux tube (a flux ring) in force equilibrium at the bottom of the convection zone is perturbed by a displacement with azimuthal wavenumber $m = 4$. A downflow of plasma from the crests into the troughs lets the summits rise while the valleys sink. *Upper right:* Polar view of an emerging loop resulting from the nonlinear development of the undulatory instability (azimuthal wave number $m = 2$) of a flux tube with an initial field strength of about 12 Tesla. Shown is the projection of the tube onto the equatorial plane. Note the distinct geometric asymmetry between the two legs of the emerging loop resulting from the Coriolis force. *Lower left:* Three-dimensional view of the rising flux tube shown in the upper right panel. The two transparent half-spheres correspond to the solar surface and the bottom of the convection zone, respectively. The geometry of the rising loop is in accordance with the observed properties of bipolar regions: low emergence latitude, positive tilt angle with respect to the azimuthal direction, and geometric asymmetry between the two legs of the loop. *Lower right:* Emerging flux loop with initial equipartition field of 1 Tesla carrying the same magnetic flux as the tube on the left side. The loop emerges at much too high latitude and the tilt angle even has the wrong sign (from [93]).

direction of rotation is more inclined with respect to the vertical than the following part [100, 101]. The asymmetry can clearly be seen in the upper right panel of Figure 7. The rise of such an asymmetric structure leads to the characteristic proper motions and geometrical asymmetries observed in young sunspot groups [102].

2D and 3D simulations of buoyantly magnetic flux tubes confirm the basic results based on the thin-tube approximation [103, 94]. Moreover, they show that a rising magnetic flux tube is liable to fragmentation [104] unless it is sufficiently strongly twisted, i.e., has an azimuthal field component in addition to the axial field [105, 106, 107]. At a later stage of the rise, the twist can lead to kink instability, the signature of which

is indicated in X-ray images [108]. The effects of rotation and convection further complicate the picture [109, 110].

4.4. Origin of super-equipartition fields

The requirement of a field strength of the order of 10 Tesla for the azimuthal magnetic field in the source region of large bipolar active regions and sunspot groups is based on a number of reasons: (1) the criterion for undular instability, (2) the low emergence latitudes of active regions, (3) the tilt angles of sunspot groups, and (4) the preservation of the coherence of the flux tube during its rise in view of the surrounding turbulent convection [111].

It is unclear, however, how such a strong field is generated in the Sun. The magnetic energy density of a field of 10 Tesla is two orders of magnitude larger than the kinetic energy density of the convective motions in the lower solar convection zone. This largely excludes flux expulsion by convection as a mechanism. It is conceivable that convective flows could *locally* be much stronger (for instance, in concentrated downflows) and compress the field; however, such local concentrations would correspond to large azimuthal wave numbers ($m > 10$, say), for which the undulatory instability requires a field strength well in excess of 10^6 G (100 Tesla). Since the velocity differences over the tachocline are of the same order as the convective velocities, the same argument applies to stretching by differential rotation as a mechanism for the generation of the strong field: the back-reaction via the Lorentz force of the growing magnetic field upon the shear flow limits the field strength to about equipartition values. Moreover, this would lead to a strong variation of the tachocline flows during the solar cycle, which is not observed [112].

A possible field intensification mechanism that does not rely on mechanical stress is related to the sudden weakening of the field strength at the apex of a slowly rising flux loop that remains in approximate hydrostatic equilibrium along the magnetic field lines [113, 79]. Since the plasma in the flux loop is almost isentropic while the surrounding convection zone shows a decreasing entropy with height, the pressure within the flux tube decreases less rapidly than the external pressure. At some critical height in the convection zone, both pressures become equal, so that the magnetic pressure formally has to vanish: the flux tube 'explodes' at its apex and a region of weak field develops between the two remaining 'stumps' of the loop. After such an explosion, the high-entropy material within the tube streams out of the stumps owing to its buoyancy. Numerical simulations indicate that this outflow continues for a sufficiently long time, so that lateral pressure balance leads to a significant field amplification in the non-exploded sections of the loop, including the deep, still stored part of the flux tube [114, 115]. This represents an amplification process for the magnetic field that does not rely on the mechanical energy of the convective or rotational motions but directly utilizes the huge amount of potential energy residing in the superadiabatic stratification of the convection zone.

5. The solar dynamo

The regular reversals of the global magnetic field in the course of the solar cycle indicate that induction effects by bulk flows of the electrically conducting solar plasma dominate over diffusion effects in determining the evolution of the solar magnetic field. In the radiative interior, radially overturning motions are strongly suppressed by the

very stable stratification and the rotation is almost rigid, so that it can harbor only a slowly decaying fossil field (see, however, [52]). The magnetic fields responsible for the solar cycle therefore most probably originates in the overlying convection zone, where the convective motions and differential rotation lead to strong induction effects. The field reversals in the 11-year time frame, which is extremely short compared to the diffusion time scales, indicate that these flows have to provide mechanisms for both the fast generation and for the efficient removal and dissipation of magnetic flux. While the latter process can be ascribed to the drastic enhancement of the effective magnetic diffusivity for a large-scale magnetic field by turbulent flows in the convection zone ('turbulent diffusivity'), the mechanisms for flux generation starting from a small initial seed field is the crucial issue of solar dynamo theory. Various possibilities have been considered and a number of models have been constructed, but a fully consistent and predictive theory is still lacking. In what follows, a brief sketch of the basic concepts and the present state of research on the solar dynamo is given. Recent comprehensive reviews can be found in [116, 117, 118].

5.1. Basic concepts

In the framework of magneto-hydrodynamics (MHD), the dynamo problem can be stated as the search for solutions of the MHD equations (the combination of the non-relativistic Maxwell equations, Ohm's law, and the hydrodynamic equations [15]) with non-vanishing magnetic energy as time goes to infinity. In order to exclude trivial or unrealistic cases, the flow providing the induction effects is restricted to a compact volume and has to be regular (finite kinetic energy and gradients). Moreover, the magnetic field must not be maintained by sources (currents) at infinity [119, 120]. We can define a self-excited dynamo by the instability of the solution with vanishing magnetic field, a trivial solution of the MHD equations. The evolution of a magnetic field, **B**, under the influence of a velocity field, **u**, and a magnetic diffusivity, η, is described by the *induction equation*, viz.

$$\frac{\partial \mathbf{B}}{\partial t} = \nabla \times (\mathbf{u} \times \mathbf{B}) - \nabla \times (\eta \nabla \times \mathbf{B}) . \tag{5.1}$$

For dynamo action, the induction term (first term on the right-hand side) has to overcome (in a global sense) the diffusion term (the second term). Consequently, a necessary requirement for dynamo action is that the order-of-magnitude ratio of both terms, the magnetic Reynolds number, is larger than unity.

Another necessary requirement for a working dynamo results from *Cowling's theorem*, which states that a rotationally symmetric magnetic field (like a dipole field) cannot be maintained by dynamo action under rather general circumstances [121, 122]. Accordingly, the solar magnetic field is clearly non-axisymmetric. Another important such 'anti-dynamo' theorem is due to Elsasser [123] and states that differential rotation alone (or, more generally, a purely toroidal motion in an expansion of the velocity field into spherical harmonics) cannot drive a dynamo in a sphere, provided that the magnetic diffusivity is constant on spherical surfaces [124, 125]. As a consequence of these restrictions, a working dynamo requires a complex three-dimensional and non-axisymmetric structure of both the generated magnetic field and the driving velocity field.

In the case of the Sun, differential rotation and convective flows are considered to be the most important ingredients of self-excited dynamo action. For high magnetic Reynolds numbers, the magnetic field lines are fixed to the fluid elements, so that the
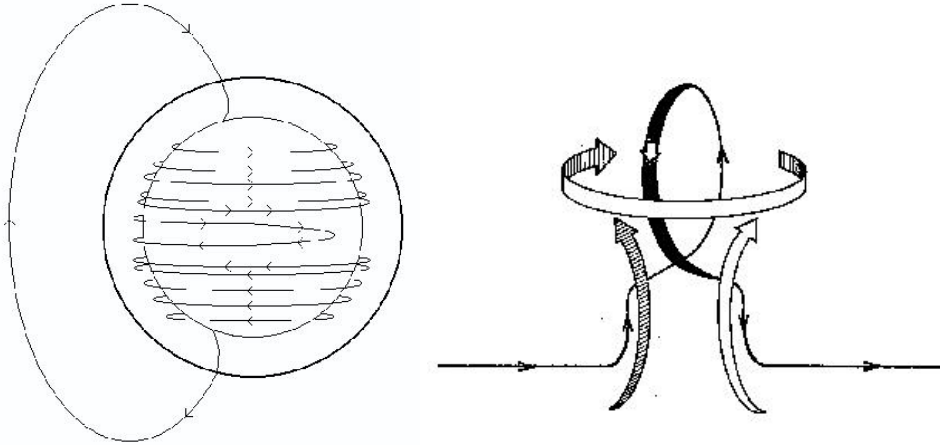
Figure 8. *Left:* Generation of an azimuthal magnetic field through winding of meridional magnetic field lines by differential rotation. Sketched here is the case of a latitude-dependent angular velocity with a faster-rotating equatorial region (courtesy D. Hathaway, NASA). *Right:* Sketch of the Parker loop. An expanding convective upflow comes into vortical motion owing to the action of the Coriolis force in a rotating system (clockwise in the Northern hemisphere, where the rotation vector has an upward directed component, counter-clockwise in the Southern hemisphere). A magnetic field line frozen into the plasma is twisted into a loop with magnetic field components perpendicular to the plane of projection (after [126]).

shearing effect of the latitudinal and radial gradients of the angular velocity of rotation leads to the generation and amplification of an azimuthal magnetic field (aligned with the direction of rotation) from a meridional field with radial and latitudinal components (see left panel of Figure 8). Elsasser's theorem shows that differential rotation alone is not sufficient to maintain the solar magnetic field; a flow regenerating the meridional part of the field is required in addition. The conceptual basis for most convection-based models of this process is the *Parker loop* [126], which describes how convective up- and downflows in a rotating system generate meridional flux loops through twisting of the field lines due to the action of the Coriolis force on the flow (see right panel of Figure 8). Upflows expand and downflows contract owing to the pressure stratification of the convection zone. This leads to the same sense of twisting by the Coriolis force in one hemisphere and, consistently, to the opposite sense in the other hemisphere. For an azimuthal field of opposite polarity in both hemispheres as generated from a dipolar field by differential rotation (cf. left panel of Figure 8), the superposition of many such meridional loops forms a large-scale meridional field of reversed polarity with respect to the original field from which the azimuthal field had been wound up in the first place. Therefore, the Parker loop provides a simple explanation for the polarity reversals of the large-scale meridional field of the Sun. In connection with the winding by differential rotation it leads to periodic reversals of both meridional and azimuthal magnetic field and thus accounts for the observed basic features of the solar cycle: large-scale field reversals and the polarity rules of sunspots groups (assuming that the latter originate from the azimuthal field component, see Sect. 4).

The Parker mechanism escapes Cowling's prohibition of a dynamo-generated axisymmetric field through the intrinsic non-axisymmetry of the loop formation while the spatially averaged generated field may well have a dominating axisymmetric component.

5.2. Mean-field theory

The Parker mechanism has been mathematically formalized and greatly generalized in the theory of 'mean-field electrodynamics' first developed by Krause, Rädler and Steenbeck [120], which describes the evolution of a suitably averaged magnetic field in a turbulent flow of an electrically conducting fluid. Magnetic field and velocity are written as sums of their mean (denoted by angular brackets in what follows) and fluctuating parts (with zero mean, denoted by primes). Under certain conditions (e.g., a clear separation of scales), a spatial, temporal or azimuthal average can be considered, but mathematically more convenient are ensemble averages, which always satisfy the Reynolds rules (like interchangeability of averaging and differentiation [117]).

Averaging the induction equation (5.1), one obtains an equation for the time evolution of the mean magnetic field, viz.

$$\frac{\partial \langle \mathbf{B} \rangle}{\partial t} = \nabla \times (\langle \mathbf{u} \rangle \times \langle \mathbf{B} \rangle + \langle \mathbf{u}' \times \mathbf{B}' \rangle) - \nabla \times (\eta \nabla \times \langle \mathbf{B} \rangle) . \tag{5.2}$$

The term $\langle \mathbf{u}' \times \mathbf{B}' \rangle$ describes the effect on the mean field of the correlations between the fluctuating quantities. A corresponding equation for $\mathbf{B}'$ is obtained by subtracting Eq. (5.2) from Equation (5.1). Under certain conditions (e.g., if the magnitude of the fluctuations is small compared to the mean field), an approximate solution of this equation in terms of the mean field can be found. In the case of (locally) isotropic and homogeneous turbulence, a series expansion in terms of the spatial derivatives of $\langle \mathbf{B} \rangle$ then leads to

$$\langle \mathbf{u}' \times \mathbf{B}' \rangle = \alpha \langle \mathbf{B} \rangle + \beta \nabla \times \langle \mathbf{B} \rangle + \dots, \tag{5.3}$$

where

$$\alpha = -\frac{\tau_c}{3} \langle \mathbf{u} \cdot (\nabla \times \mathbf{u}) \rangle \quad \text{and} \quad \beta = \frac{\tau_c}{3} \langle \mathbf{u} \cdot \mathbf{u} \rangle . \tag{5.4}$$

Here, τ_c denotes the correlation time of the fluctuating part of the velocity field. Inserting Equation (5.3) into Equation (5.2) yields

$$\frac{\partial \langle \mathbf{B} \rangle}{\partial t} = \nabla \times (\langle \mathbf{u} \rangle \times \langle \mathbf{B} \rangle + \alpha \langle \mathbf{B} \rangle) - \nabla \times [(\eta + \beta) \nabla \times \langle \mathbf{B} \rangle] . \tag{5.5}$$

If non-vanishing, the contribution $\alpha \langle \mathbf{B} \rangle$ to the mean electric field (the so-called *α-effect*) drives a mean current parallel to or anti-parallel to the mean magnetic field. The α-effect term therefore generates a meridional field from an azimuthal field, and vice versa. The pseudo-scalar α is only non-vanishing for flows lacking mirror symmetry, i.e., flows possessing a finite average helicity, $\langle \mathbf{u} \cdot (\nabla \times \mathbf{u}) \rangle$, resulting from a net correlation between velocity and vorticity. These conditions are fulfilled in the case of convection in a rotating stratified medium ('cyclonic convection'), since the Coriolis force leads to the required correlation between velocity and vorticity. Therefore, the mean-field approach yields a formalization of the dynamo mechanism illustrated by the Parker loop.

Equation (5.5) shows that the positive quantity β formally is equivalent to an additional magnetic diffusivity, the *turbulent diffusivity*. It describes the enhanced

effective diffusion of the mean magnetic field due to the (random-walk type) transport of magnetic field lines by the fluctuating velocity field and the creation of small-scale structure and enhanced dissipation through the development of a turbulent cascade. The turbulent diffusivity in the deep solar convection zone is many orders of magnitude larger than the molecular diffusivity $\eta \simeq 1...10 \, \mathrm{m^2 \, s^{-1}}$: with typical values of $10 \, \mathrm{m \, s^{-1}}$ for the fluctuating convective velocity and about a month for the correlation time, we find $\beta \simeq 10^8 \, \mathrm{m^2 \, s^{-1}}$, so that the molecular magnetic diffusivity can be neglected for the evolution of the mean magnetic field. In fact, such values of the turbulent diffusivity lead to typical decay times of the order of decades, which is the right order of magnitude for the solar cycle.

Inserting differential rotation for the mean flow, $\langle \mathbf{u} \rangle$, in Equation (5.5) and using simple estimates for α and β leads to excited dynamo solutions, i.e., a mean field growing from a small seed field. If the induction effect of the α-term is much smaller than that of differential rotation (also called the Ω-*effect*), the solutions are oscillatory with periodic reversals of both the meridional and the azimuthal field components. Moreover, the solutions of such $\alpha\Omega$-dynamos represent latitudinally propagating waves for predominantly depth-dependent differential rotation. Whether such dynamo waves propagate equatorward or poleward depends on the sign of $\alpha \partial\Omega/\partial r$, where Ω is the angular velocity and r the radial coordinate [127, 128]. The period of the oscillatory solutions is basically determined by the diffusion time based upon the turbulent diffusivity, which yields the value for the solar cycle to within an order of magnitude.

The presentation above covers only the most basic aspects of mean field theory. In general, the coefficients of the expansion given in Equation (5.3) are (pseudo)tensors, so that, depending on the preferred directions in the system (due to stratification and rotation), anisotropic turbulent diffusion and transport as well as anisotropic dynamo coefficients result [120, 129]. While the symmetric part of the general α-tensor represents the dynamo effect, the antisymmetric part describes a turbulent transport of the mean field. The simplest of such effects is *turbulent diamagnetism* [130, 131], the expulsion of magnetic field from regions of intense turbulence. In fact, numerical simulations of convection in rotating systems indicate that the α-tensor is highly anisotropic, with the term describing the generation of meridional field from azimuthal field generally dominating [132, 133, 134].

So far we have only considered the linear (kinematic) aspects of the dynamo process: magnetic field lines are passively carried and twisted by the convective flows. As the field strengths grows in the course of the dynamo process, the back-reaction of the magnetic field on the generating velocity fields through the Lorenz force becomes important. This limits the field strength that can be reached in the course of the dynamo process (at least roughly to order of magnitude) to the 'equipartition field' B_{eq}, i.e., the field strength for which the magnetic energy density equals the kinetic energy density of the generating motions:

$$\frac{B_{\mathrm{eq}}^2}{2\mu_0} \simeq \frac{1}{2}\rho v^2 \,, \tag{5.6}$$

where ρ is the density and v the velocity amplitude. For the lower half of the solar convection zone we find $B_{\mathrm{eq}} \simeq 10^4$ G if we use current estimates of the convective velocity.

There are basically two non-linear effects to be considered in mean-field theory. One is the back-reaction of the magnetic field on the statistical properties of the velocity field (like the flow helicity in cyclonic convection) that give rise to dynamo

action in the first place. This leads to a dependence of the α-effect on the magnetic field (also called α-*quenching*). Simple models give just an algebraic relationship (like $\alpha \propto B^{-2}$), but the incorporation of effects with long time scales in situations characterized by large magnetic Reynolds numbers (like the evolution of the spectrum of the current helicity, the product of the magnetic field with the electrical current density [135]), leads to a dynamic (differential) equation for α [136]. Under certain circumstances, α-quenching can become 'catastrophic' in the sense that α becomes inversely proportional to the magnetic Reynolds number and the magnetic field saturates at very low levels in systems characterized by large magnetic Reybolds number [137]. The second non-linear effect results from the mean Lorentz force due to the mean field, driving a mean flow. The induction effect of these flows, in turn, reacts back and contributes to limiting the growth of the mean field [138, 104]. This effect includes also the modification of the differential rotation in $\alpha\Omega$-dynamos [139, 140].

Mean-field $\alpha\Omega$-dynamo models are capable of reproducing many of the key features of the solar cycle, namely, the periodic field reversals, the polarity rules of the sunspot groups, and the equatorward drift of the activity zones – given that the parameters (α-effect, magnetic diffusivity, and differential rotation) are suitably chosen. Elementary considerations on the basis of the Parker loop already show that the (pseudo-scalar) α generated by convection should be positive in the northern hemisphere and negative in the southern hemisphere of the Sun. Equatorward propagation of dynamo waves would then require that the dominant component of differential rotation should be a radially inward increase of the angular velocity. This is in clear contrast to the results of helioseismology, which show almost no radial differential rotation in the convection zone and an inward *decrease* of the angular velocity in the low-latitude tachocline [53]. On the other hand, the velocity correlations leading to the α-effect reverse near the bottom of the convection zone, so that the sign of α reverses also and the correct sense of dynamo wave propagation ensues in low latitudes.

5.3. Dynamo simulations and fast dynamos

Local simulations of compressible magneto-convection describing small parts of the solar convection zone have been carried out mostly in cartesian geometry [141, 142]. These simulations show excited dynamo action, albeit they produce only little 'mean' field on the scale of the computational box. While the total magnetic energy saturates at a small fraction of the kinetic energy in the flow, the magnetic field is locally intensified in flux-tube-like structures ('flux cigars') with about equipartition field strength.

Self-consistent simulations of the generation of differential rotation and dynamo action by convection in a spherical shell were already attempted in the 1980s [143, 144, 145]. Excited dynamo action was found, but the generated fields indicated poleward dynamo wave propagation in disagreement with the empirical facts. More recent attempts ([146, 147], see also [148]) showed the generation of an intermittent 'turbulent' magnetic field but failed to reproduce the large-scale ordered fields responsible for the 22-year solar cycle.

Numerical simulations have also provided a few examples of 'fast dynamos' [149], i.e., dynamos whose growth rate remains finite in the limit of infinite magnetic Reynolds number, R_m. This is an important issue since the very large value of R_m for the flows in the solar convection zone must not restrict the growth time of the

dynamo to time scales exceeding the solar age. Typically, fast dynamo action appears for flows with chaotic stream lines, corresponding to positive Lyapunov exponents, so that the magnetic field lines are repeatedly stretched, twisted, and folded. In fact, numerical simulations of Boussinesq convection in a closed box show fast dynamo action and strong intermittency of the generated magnetic field [150]. At present it is unclear, however, how these concepts can be applied to the study of dynamo action by solar convection and rotational shear or which fraction of the small-scale field at the solar surface could possibly be generated by such local fast dynamo action. Another topic of considerable current interest is the dependence of small-scale dynamo action on the value of the magnetic Prandtl number, ν/η, the ratio of kinematic viscosity and magnetic diffusivity of the fluid, which is a small number in many astrophysical contexts [151, 152, 153].

5.4. Magnetic helicity conservation

A conceptually important quantity in the study of dynamo action in flows with large magnetic Reynolds number is the *magnetic helicity,* viz. the quantity

$$H = \int_V \mathbf{A} \cdot \mathbf{B} \, \mathrm{d}V , \qquad (5.7)$$

where $\mathbf{A}$ is the vector potential of the magnetic field and the volume V contains the magnetic field, so that the normal component of $\mathbf{B}$ vanishes at its boundary. H is gauge-invariant under these conditions and its evolution equation is given by

$$\frac{\mathrm{d}H}{\mathrm{d}t} = -2\eta \int_V \mathbf{j} \cdot \mathbf{B} \, \mathrm{d}V , \qquad (5.8)$$

which shows that the magnetic helicity is a conserved quantity under ideal conditions ($\eta = 0$), which is also true in the limit $\eta \to 0$ [154]. Note that the velocity field does not explicitly appear in the evolution equation for H, so that there is no turbulent diffusion of H: the net magnetic helicity in a flow with large magnetic Reynolds number changes only on the very long time scale of molecular diffusion. This represents a relevant constraint on dynamo models for the Sun, since the 11/22-year period of the solar cycle is very much shorter than the resistive time scale based upon (microscopic) diffusion [155, 156]. For dynamos based upon helicity and/or shear, the build-up of a large-scale magnetic field is necessarily connected with the build-up of large-scale magnetic helicity. This growth can happen in a time significantly smaller than the resistive time scale only if (approximately) the same amount of magnetic helicity of the opposite sign resides in a location separated either spatially (e.g., on the other hemisphere, as for helicity generation by differential rotation) or in wavenumber (i.e., in small scales, as in the case of the α-effect due to helical flows). In any case, the Sun has to shed magnetic helicity in the course of the solar cycle [157], either in the form of resistive dissipation at very small scales, by cross-hemispheric transport, or by losses into outer space (possibly in the form of coronal mass ejections [158]).

5.5. Current models

Conventional models of $\alpha\Omega$-dynamos working in the bulk of the convection zone have difficulties to reproduce the latitudinal migration of the sunspot zone since the radial rotational shear is much smaller than the latitudinal shear in the convection zone and dynamo waves propagate along isolines of angular velocity [127] (see, however, [128]
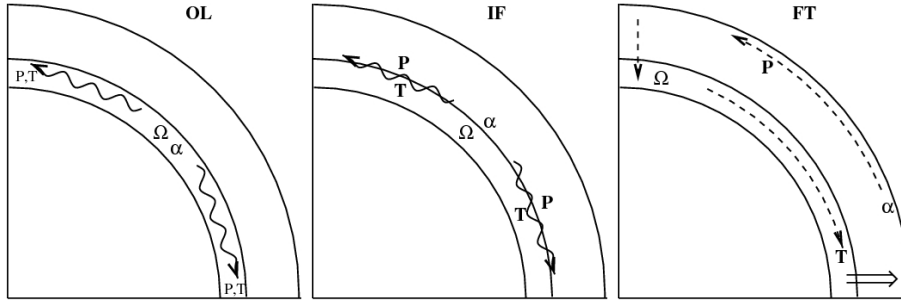
Figure 9. Schematic illustration of the key features of various classes of dynamo models. The images represent a quadrant from a meridional cut through the Sun, indicating the radiative core (inner part), the layer of convective overshoot and radial shear (inner shell, not to scale), and the convection zone proper (outer shell). *Left panel:* overshoot layer dynamo (OL). Differential rotation (Ω) and α-effect are both confined to the overshoot layer; dynamo waves (wavy line) of poloidal (P) and toroidal (T) magnetic field propagate in latitude, according to the sign combination of the radial shear and the α-effect. *Middle panel:* interface dynamo (IF). The α-effect acts in the convection zone proper while the radial shear is confined to the overshoot layer (tachocline). Both regions are connected by (turbulent) diffusion. The dynamo waves take on the character of a surface wave along the interface between overshoot layer and convection zone. *Right panel:* flux transport dynamo (FT). The poloidal field generated by an α-effect in the convection zone (for instance, from the tilt induced near the surface by the Coriolis force on rising flux tubes) is transported by a meridional circulation (dashed lines) poleward and down to the tachocline, where the rotational shear generates a toroidal field. This field is transported equatorward by the return flow of the meridional surface flow and, owing to magnetic instability, erupts at low latitudes (double-lined arrow) (adapted from [116].)

and a recent re-appraisal of distributed dynamo action in the convection zone, [159]). Moreover, such models are neither capable of producing and storing strongly super-equipartition azimuthal fields nor can the turbulent α-effect of cyclonic convection act efficiently upon such strong fields. Various possibilities to overcome these problems have been suggested. In most of these models, it is assumed that a layer of overshooting convection overlapping with the tachocline is the location where a strong azimuthal magnetic field is generated and stored. The models can be classified into the following three types (for detailed reviews see [117, 116, 160, 161]):

1) *overshoot layer dynamos:* α-effect is restricted to the overshoot region;

2) *interface dynamos:* Ω-effect is dominant in the overshoot region and a conventional α-effect operates in the convection zone above, both regions being coupled by magnetic diffusion;

3) *flux transport dynamos:* the radial transport of magnetic flux into the overshoot layer and the latitudinal migration of the magnetic field are dominated by advection by a large-scale meridional flow.

The basic concepts of these three classes of models are illustrated in Fig 9. In the first case of a dynamo working completely in the overshoot region, the regeneration of the meridional (poloidal) field has to be reconsidered because the strong fields suppress the turbulent flows and the kinematic α-effect would hardly work. Possible alternative mechanisms rely on instabilities of strong magnetic fields driven by buoyancy [162, 163, 164, 165], radial shear flow in the tachocline [166], or latitudinal differential rotation [167]. In contrast to the conventional kinematic dynamo models, the velocity field is not prescribed but consistently determined from the (linearized)

MHD equations. Super-equipartition fields pose no problem but are actually required in some models for the mechanism to operate, since the instability must be excited. On the other hand, in most of these models, the dynamo is not truly self-excited since the instability requires the field strength to exceed a certain threshold value. Consequently, a turbulent dynamo as a 'starter' is required to work in the background. A frequent problem of overshoot dynamo models is the considerable overlap of the individual cycles in a time-latitude diagram of the azimuthal field [168], which is in disagreement with the corresponding observational diagrams of active-region occurrence at the solar surface.

The interface dynamos circumvent the problem of the suppression of the α-effect by a spatial separation of the generation region for the azimuthal and the meridional magnetic fields [169]. Radial differential rotation builds up a strong azimuthal field in the overshoot region, while the regeneration of the meridional field is achieved by the 'classical' α-effect operating in the bulk of the convection zone. The connection between the two regions is accomplished via (turbulent) diffusion, with the magnetic diffusivity in the overshoot layer being reduced by a factor $\sim 10^2...10^3$. As a result, the magnetic field is strong below the interface and sufficiently weak above for the α-effect to work. The resulting dynamo wave takes on the character of a surface wave propagating along the interface between the convection zone and the overshoot layer [170, 171, 172]

The most often studied examples of flux transport dynamos are the 'Babcock-Leighton dynamos' [173, 174], named so owing to some similarities with early models for the solar cycle [175, 176]. In these models, the regeneration of the meridional field from the azimuthal field component is assumed to originate from the twist imparted by the Coriolis force on azimuthal flux tubes rising through the upper layers of the convective envelope. This twist becomes apparent as the latitudinal tilt of active regions at the solar surface. If the radial shear in the tachocline dominates the Ω-effect, the two induction effects are widely separated in space. It is assumed that the generated poloidal field is transported by a large-scale meridional circulation in the convection zone, a combination of the observed poleward surface flow and a conjectured equatorward subsurface return flow [177, 178, 179, 180, 181, 182, 183]. The deep return flow controls the migration of the dynamo wave such that it can propagate equatorward (in accordance with the observed latitude drift of the sunspot zone) even if the sign combination of α-effect and angular velocity gradient would lead to poleward propagation in the absence of a meridional flow. Furthermore, the resulting cycle period is largely determined by the flow speed of the circulation. An example of such a model is shown in Figure 10. Flux transport by meridional flow has also been considered in some models of overshoot-layer dynamos [184] and interface dynamos [185, 186].

5.5.1. Long-term modulation and grand minima In order to understand the origin of the long-term modulation of the solar cycle in terms of dynamo theory, various mechanisms have been proposed:

1) a modulation of the differential rotation through the nonlinear back-reaction of the magnetic field,

2) a stochastic fluctuation of the α-effect,

3) a variation in the meridional circulation, and

4) on-off intermittency owing to a threshold field strength for dynamo action.
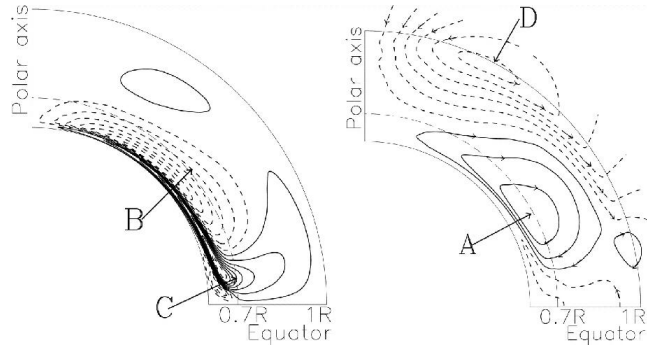
Figure 10. Snapshot from a simulation of a Babcock-Leighton type flux-transport dynamo with a realistic profile of angular velocity at a time close to 'sunspot minimum', after reversal of the high-latitude polar magnetic field. The meridional circulation (not shown in the figure) is poleward in the upper part of the convection zone and equatorward in the lower part. Contour lines of the azimuthal magnetic field strength (left) and field lines of the meridional magnetic field component (right) are plotted in a meridional quadrant, with the long-dashed line indicating the interface between the radial shear layer (overshoot layer) and the convection zone proper. Solid contours correspond to positive (clockwise-oriented) azimuthal field (meridional field line), with opposite polarity (orientation) denoted by dashed contours. The meridional flux system located around A is acted upon mostly by the (positive) latitudinal differential rotation, since the radial shear vanishes at mid-latitudes. This leads to the growth of the azimuthal flux system at B. The azimuthal flux system near C is the (decaying) remnant of the cycle just completed, and that at B represents the new cycle just beginning. The latter is already contributing to the generation of a surface meridional field at D, of opposite polarity to the meridional flux system in A. The finite time required for meridional circulation to advect the magnetic field from D to A introduces a time lag in the dynamo process (from [187]).

The back-reaction of the large-scale magnetic field on the differential rotation in the tachocline can lead to complicated nonlinear behaviour, including long-term amplitude modulations, intermittency and chaos as well as symmetry-breaking bifurcations, so that the generated field may flip between dipole and quadrupole states in a grand minimum [188, 189, 190, 191].

A different approach to account for the modulation of the solar cycle is the stochastic behaviour of the dynamo itself [192, 193]. Defining averages over longitude in a mean-field dynamo model and considering a finite number of large convective cells, all mean quantities, including the α-effect, retain a stochastic component [194, 195]. Such a variation can lead to the occasional excitation of higher dynamo modes as well as to long intervals of low activity [196].

Fluctuations of both the meridional flow and the α-effect have been studied in connection with flux-transport dynamos [187]. The results suggest that the meridional circulation speed, the primary determinant of the cycle period, acts as a clock and thus maintains the phase stability of the cycle [197]. The model also exhibits a clear correlation between the azimuthal field strength of a given cycle and the strength of the high-latitude surface magnetic field of the preceding cycle, which is in qualitative agreement with observational inferences [198]. Producing extended periods of reduced activity, however, turns out to be rather difficult in the framework of these models.

The dynamic α-effect due to magnetic buoyancy only sets in beyond a threshold field strength [163, 166]. Therefore it requires a starting mechanism in the form of fluctuating magnetic fields transported by downdrafts from the turbulent convection zone into the overshoot region. At the same time, such fluctuations, when destructive,

can lead to a sequence of low-amplitude cycles or even drive the dynamo subcritical until another, constructive magnetic fluctuation restarts the dynamo again. This leads to on-off intermittent solutions, which can be related to the occurrence of grand minima [199] .

5.6. Magnetic activity and dynamos of other stars

While the proximity of the Sun allows us to study its magnetic activity and the underlying dynamo process in detail, observations of other stars open up the possibility to investigate the dependence of magnetic activity on stellar parameters like age, rotation rate, and depth of the convection zone, thus providing opportunities to test dynamo theories [200].

Magnetic fields have been detected on many stars of various types [201]. However, solar-like magnetic activity characterized by strong surface inhomogeneity, hot chromospheres and coronae, rapid time variability and flaring, etc., seems to be restricted to stars with outer convection zones. These are comparatively cool stars in various evolutionary stages ranging from very young stars still accreting matter over hydrogen-burning stars to evolved giant stars [4]. In some cases, the magnetic field can be directly measured through the Zeeman effect, but most often 'proxies' of magnetic activity like photometric variations, emission in chromospheric lines, and coronal X-ray emission are used to infer the stellar activity. Large starspots can also be detected by the spectroscopic techniques of (Zeeman) Doppler imaging [202, 203].

The magnetic activity of cool stars is related to their rotation rate: faster spinning stars are more active. This is in general accordance with turbulent dynamo theory, which predicts an increase of the α-effect with rotation rate. For a number of stars there are detections of cyclic activity variations with periods between 7 and 14 years, while others exhibit either irregular variations on a high activity level or have a flat low activity level, possibly indicating a grand minimum [204]. Typically, stars with a cyclic or flat activity level rotate slowly, while those with a irregular variations are rapid rotators [205].

6. Sunspots

Sunspots are the most readily visible signs of the interaction between concentrated solar magnetic fields and the solar plasma, with the largest sunspots being visible to the (suitably protected) naked eye. Although sunspots have been extensively studied for almost 400 years and their magnetic nature has been known for practically a century, our understanding of a number of their basic properties is still evolving.

The first telescopic observations of sunspots by Galilei, Scheiner and others around 1611 marked the beginning of the systematic study of the Sun in the western world and heralded the dawn of research into the Sun's physical character. Over the ages the prevailing view on the nature of sunspots has undergone major revisions. The breakthrough came in 1908 when G.E. Hale [206] first measured a magnetic field in sunspots. This was the first time that a magnetic field had been measured outside the Earth. Since then the magnetic field has become firmly established as the root cause of the sunspot phenomenon.

Recent overviews of the structure and physics of sunspots are given in the proceedings edited by Thomas and Weiss [207], Schmieder et al. [208], Strassmeier et al. [5], as well as in the review article by Solanki [209].
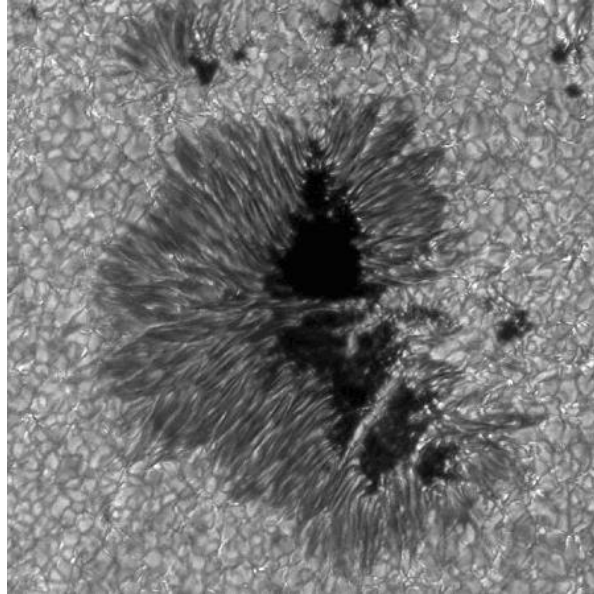
Figure 11. A white-light image of a sunspot. The dark core is the umbra, the radially striated part the penumbra. The surrounding bright cells with dark boundaries are granular convection (Image obtained with the German Vacuum Tower Telescope on Tenerife, courtesy Kiepenheuer Institut für Sonnenphysik).

6.1. Brightness and thermal structures

An image of a sunspot is shown in Figure 11. Each sunspot is characterized by a dark core, the umbra, and a less dark halo, the penumbra. The presence of a penumbra distinguishes sunspots from the usually smaller pores. In addition, some sunspots contain light bridges, i.e. bright bands crossing the umbra (two bright light bridges and a fainter one are visible in Figure 11).

Integrated over wavelength, the intensity of the radiation coming from the umbra is approximately 20% of that of the quiet Sun, that of the penumbra is approximately 75%. Since the penumbral area is roughly four to five times as large as the umbral area, the averaged, wavelength integrated intensity of a sunspot is roughly 60–70% of that of the quiet Sun.

The brightness and thus the temperature of a sunspot are functions of spatial position within the spot. They change on large scales, e.g. gradually in the umbra, but small-scale structure is also prominent. The umbra harbors small bright structures, primarily umbral dots. An image of a sunspot umbra taken in the TiO band-head at 705.5 nm is shown in Figure 12. It reveals the presence of many umbral dots, which have diameters ranging from the spatial resolution of the observations to roughly 600 km, with the number decreasing quadratically with increasing size [210, 211]. This suggests that many umbral dots are spatially unresolved. The exact brightness of umbral dots is not established beyond doubt, but the majority is probably significantly darker than the undisturbed photosphere outside sunspots [212, 213, 214].

The sunspot penumbra is dominated by small-scale structure, most prominently the elongated bright and dark penumbral filaments, but also the point-like penumbral grains, which have similarities to the umbral dots. At the highest currently reachable
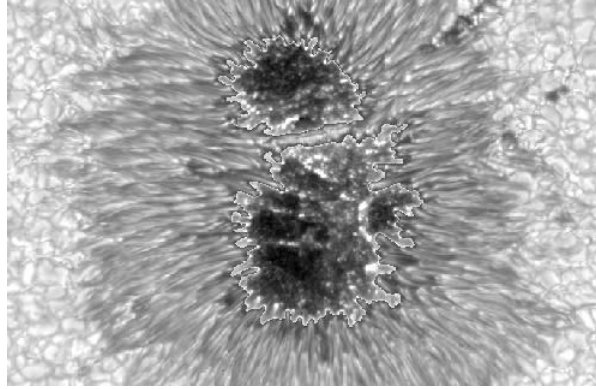
Figure 12. Image of a sunspot made in the band head of the TiO molecule at 705.5 nm wavelength with the Swedish Solar Telescope on La Palma by V. Zakharov and A. Gandorfer. The umbral brightness is artificially enhanced in order to show the numerous umbral dots more clearly.

resolutions the bright penumbral filaments or fibrils show a sharp dark lane running inside them [215] and there is evidence that even these observations have not resolved all the fine structure [216]. In the cores of spectral lines formed in the middle and upper photosphere this brightness modulation appears to be washed out or, at least, to be restricted to larger spatial scales [217].

6.2. Sizes and lifetimes

Sunspots exhibit a considerable range of sizes, which is well approximated by a lognormal size distribution [218, 219]. Very large sunspots can occasionally reach diameters of 60 000 km, but are relatively rare. Sunspots smaller than 3000 km in diameter are also rare. Smaller photospheric magnetic structures usually manifest themselves as pores or magnetic elements (see Sect. 7).

Small sunspots live for hours, the largest ones for months. The lifetime, T, increases linearly with maximum area, A_0: $A_0 = WT$, where $W \simeq 3.1\,10^7\,\text{km}^2\,\text{day}^{-1}$ [220, 221]. Sunspots decay steadily soon after they reach their maximum size. The decay is thought to be driven by turbulent diffusion of the magnetic field [222, 223].

6.3. Magnetic structure

Sunspots have a field strength of $B = 2500$–3500 G in their darkest portions and 700–1000 G at their outer edges. At the 'centre' of a spot (i.e., at the location of the largest field strength) the field is vertical (i.e., the zenith angle of the magnetic vector, ζ, is close to zero) while it is inclined by $\zeta \simeq 70° \ldots 80°$ to the vertical at the visible sunspot boundary. Measurements of the radial profiles of magnetic field and inclination angle in almost circular sunspots are shown in Figure 13 [224]. Other observations made in the visible and infrared spectral ranges [225, 226, 227, 228, 229] give similar, although not completely identical, results. Such regular, isolated sunspots do not appear to show significant global azimuthal twist of the field [230, 226, 231, 224, 232]. Fits to such data assuming a 'buried' dipole are reasonable, but not perfect. This suggests that the global structure of the field inside regular sunspots is close to but not exactly potential. The observations also indicate that sunspot magnetic fields are bounded by

current sheets, i.e., at the sunspot boundary B falls off rapidly within a radial distance that is small compared to the size of the sunspot [233].

From the measured profiles $B(r)$ and $\zeta(r)$ it is possible to determine the relative amounts of magnetic flux emerging through the umbra and the penumbra [234, 233]. The observations imply that over half of the magnetic flux emerges in the penumbra. Consequently, sunspot penumbrae are deep, i.e. the lower boundary of the field in the penumbra is inclined and lies significantly below the solar surface, at least in the inner penumbra. The outer part of the penumbra could be shallow, however [235].

Above the visible solar surface, the field lines of a sunspot fan out rapidly, so that the magnetic field forms an almost horizontal *canopy,* which overlies the nearly field-free plasma below. The interface between these two regions (the canopy base) is found to lie in the photosphere [236, 237, 227, 238]. The field strength above the canopy base decreases steadily outward.

Modern techniques allow the 3-D structure of the magnetic vector in the lower solar atmosphere to be determined. Within the visible outline of the sunspot, the field strength decreases with height. At photospheric levels, $\partial B/\partial z \approx 0.5\text{--}3$ G km^{-1} [239, 240, 241]. When averaged over a height range of 2000 km or more, values around $\partial B/\partial z \approx 0.3\text{--}0.6$ G km^{-1} are found in the umbra [242, 243, 244, 235]. These values are in rough agreement with simple theoretical predictions of 0.5–1 G km^{-1} [245]. More recently, discrepancies have been found between gradients deduced in the penumbra from visible and infrared spectral lines, respectively [246, 228]. Such seeming inconsistencies can be reconciled if the fine structure of the penumbra is taken into account, in particular, the presence of horizontal flux tubes interspersed with the inclined field, as described below [247, 248].

At small scales, the penumbral magnetic field is filamented into two components, an inclined component and a horizontal component [249, 250, 251]. The filaments associated with each component are found to run uninterrupted across the entire width of the penumbra [252]. The horizontal magnetic component is restricted in height and is well described by horizontal flux tubes that are embedded in an inclined field ([253], see Figure 14). However, there is still considerable controversy regarding the exact magnetic structure. One controversial point is the actual width of the horizontal flux tubes, with proposed values ranging between very slender, completely optically thin flux tubes and structures that are a few hundred km thick [254, 255, 256]. Recently, is has also been proposed that the magnetic structure is quite different, with field-free gas intruding into (or nearly into) the photosphere and the horizontal field overlying this field-free material [257].

6.4. Dynamic structure

The dominant signature of dynamics in the photospheric layers of sunspots is the Evershed effect, named after its discoverer J. Evershed. It is composed of a shift and asymmetry of spectral lines, with opposite signs on the limbward and centreward sides of the penumbra† [259, 260, 261, 262, 246, 263]. This observational signature is generally interpreted in terms of a nearly horizontal, radial outflow of material.

† As a sunspot moves over the visible solar disc owing to the rotation of the Sun, the line of sight towards the observer changes its inclination with respect to the locally vertical (radial) direction: when the sunspot is near the center of the disc, the spot is observed vertically, while sunspots near the limb are seen under a large inclination. It is important to take these geometrical effects into account when it comes to measuring quantities (like Doppler shift) which reflect the line-of-sight component of a vector.
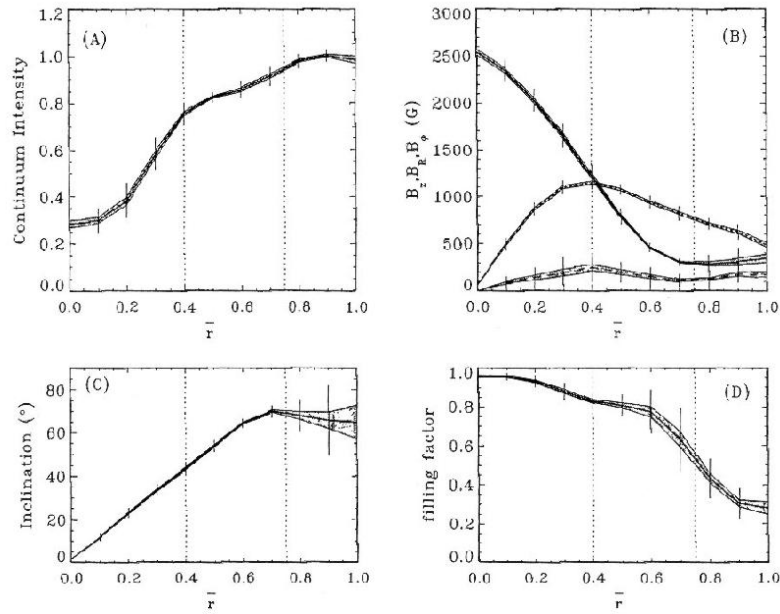
Figure 13. Intensity and magnetic parameters vs. normalized radial distance, $\overline{r}$, from sunspot centre, as determined from 16 observations of sunspots. Vertical dotted lines indicate the umbra (left) and the penumbra (right) boundaries. Plotted are the continuum intensity in Panel A, vertical (B_z, solid curve), radial (B_r, dotted curve) and azimuthal (B_ϕ, dashed curve) components of the magnetic field in Panel B, magnetic inclination in Panel C, and magnetic filling factor in Panel D. $\overline{r}$ is normalized to a radius well outside the visible sunspot. (from [224]).
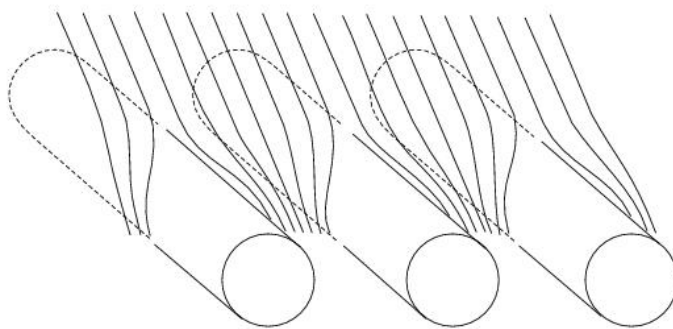
Figure 14. Detail of the fine-scale magnetic structure of the penumbra, as derived from observations. Small-scale horizontal flux tubes are surrounded by inclined field lines (adapted from [253]).
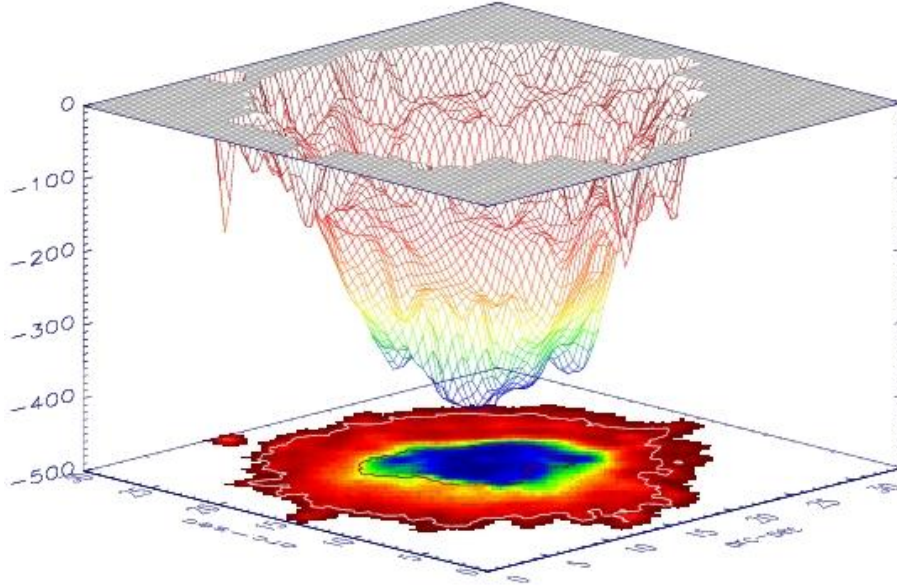
Figure 15. Wilson depression (Z, downward shift of the layer of optical depth unity) of a regular sunspot obtained from spectro-polarimetric observations in the infrared. The inner and outer contours overplotted on the horizontal plane represent the umbral and penumbral boundaries obtained from the continuum image, respectively (from [258]).

Depending on the spectral line used speeds of up to 6–9 km s^{-1} have been inferred [264]. There has been considerable controversy about whether the Evershed effect continues beyond the outer penumbral boundary, or not [265, 266, 267]. It is now accepted that the Evershed effect does continue outside the boundary, but mainly above the base of the magnetic canopy [268]. The mass flux in the penumbra is found to be larger than in the canopy region beyond the visible penumbra [268, 238], so that some of the mass carried by the Evershed flow must return into the solar interior within the confines of the sunspots. The problem raised by this finding was solved by the discovery of downflows near the penumbral edge [269], which suggests that the excess mass flows again into the solar interior there. The flow is also found to be structured in the sense that the outflow follows the nearly horizontal component of the magnetic field [251, 270].

The Evershed effect is restricted in height. The line shifts decrease rapidly with height of line formation (e.g. [259, 267]) and at sufficiently large heights (above the temperature minimum) even change sign, so that the flow in the chromosphere is directed inwards (inverse Evershed effect, e.g., [259, 266, 271]). This inflow is seen at temperatures up to a few 10^5 K, i.e. in both chromospheric and transition region gas. The transition region flow is both more vertical and faster than the flow at chromospheric temperatures, and is also seen as an almost vertical flow above the umbra. In spite of the larger flow speeds, the mass flux transported by the inverse Evershed effect is only a few percent of the mass flux flowing out from the umbra in the much denser photosphere.

With the help of local helioseismic techniques it is now starting to become possible to detect flows below the solar surface. Sunspots are found to have a distinctive

signature, with a downflow below them [272] and an inflow feeding this downflow just below the surface (this flow pattern is termed a collar flow and was proposed by Parker [273] to help hold sunspots together). This suggests that the Evershed flow and the adjacent moat flow (a horizontal outflow surrounding the sunspot) do not extend more than a couple of Mm into the solar interior.

Besides such steady flows, sunspots are also rich sources of oscillations and waves. The most prominent are oscillations with a period of about three minutes, which are measured in chromospheric layers above umbrae [274]. Above penumbrae, waves traveling horizontally outwards (so called running penumbral waves) are dominant [275]. Finally, the oscillations in the photospheric layers are found to have a period of five minutes with similar properties as the acoustic oscillations of the quiet Sun. They are identified as magnetoacoustic oscillations [276].

6.5. The Wilson depression

For sunspots near the solar limb, the umbra and often the part of the penumbra nearer to the centre of the visible solar disk are no longer visible. This effect is called the Wilson effect after its discoverer, A. Wilson. The Wilson effect is best explained if the visible light within the umbra arises 400–800 km deeper than in the quiet Sun [277, 278, 279]. The presence of such a *Wilson depression* implies that the gas pressure within the sunspot must be significantly smaller at the same geometric level than outside, in accordance with the idea that the magnetic field is confined mainly by horizontal balance of total (gas plus magnetic) pressure.

The Wilson depression may also be estimated by introducing measured values of magnetic field strength and temperature into the horizontal component of the magnetohydrostatic force-balance equation [280, 281, 282]. Comparison of the Wilson depression estimated in this manner with observation indicates that the magnetic curvature forces within the sunspot are significant, but do not dominate over pressure gradient forces. Spatial maps show that the Wilson depression is largest in the darkest parts of the umbra, where B is largest [258]. Also, there is a relatively abrupt change of the Wilson depression at the umbral boundary. The Wilson depression surface of a regular sunspot obtained in this manner is plotted in Figure 15.

6.6. Theoretical models of the magnetic structure

The magnetic structure of sunspots is generally modelled assuming axial symmetry for reasons of theoretical tractability, although most sunspots possess an irregular shape. The field is confined by the external gas pressure and the magnetohydrostatic equilibrium is described by

$$\mu_0^{-1} \operatorname{curl} \mathbf{B} \times \mathbf{B} = \nabla p - \rho \mathbf{g} \ ,$$

where $\mathbf{B}$ is the magnetic vector, p is the gas pressure, ρ the gas density and $\mathbf{g}$ denotes gravitational acceleration. Usually significant additional assumptions have to be made since otherwise the computation of the magnetic configuration would require the treatment of all relevant spatial and temporal scales (which span very wide ranges, e.g., spatially between 10 km and 10^5 km). A complete theoretical sunspot model would also require the simultaneous and consistent solution for the magnetic and thermodynamic structures, i.e., a solution of a complete energy equation (with
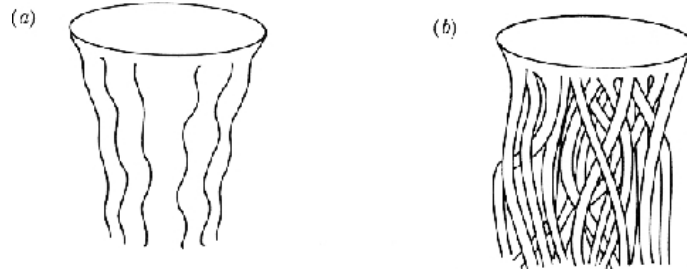
Figure 16. Sketch of the monolithic (a) and cluster (b) models of the subsurface structure of sunspot magnetic fields (from [207]).

radiative transfer and a consistent treatment of magneto-convection) in addition to the force balance.

The most comprehensive existing models of the magnetic structure of sunspots [283, 284] have a threefold structure that consists of the umbra, the penumbra, and the surrounding nonmagnetic stratification, each separated by current sheets. Such models, which also could include electrical body currents (leading to deviations from a potential magnetic field) provide acceptable fits to the observations of the global magnetic structure of sunspots and are the most promising for future study. One basic assumption underlying all attempts to quantitatively model the global magnetic structure of sunspots is the assumption that the sunspot is monolithic below the solar surface. Recent helioseismic work, however, suggests that this assumption may not be valid (see below).

Parker [285, 286, 287] proposed that just below the surface the magnetic field of a sunspot breaks up into many small flux tubes due to the fluting (interchange) instability [288]. Later is was found, however, that magnetic buoyancy protects sunspots with magnetic flux $\phi > 10^{20}$ Mx from this instability, at least in the first 5–10 Mm depth [289]. Nevertheless, a cluster model of sunspots (see Figure 16) can readily explain umbral dots as field-free intrusions into the sunspot from below [287, 290], thus providing the high thermal energy flux of the umbra, which cannot be transported by radiation alone. The strongest (but still indirect) support for a cluster model comes from measurements made with the technique of local helioseismology, which can (with some restrictions) image the subsurface thermal and velocity structure [272]. At least in one case, signs of a nearly horizontal flow that passes a few Mm underneath a sunspot has been found [291]. Since the magnetic field is nearly frozen in the plasma, the field lines at the surface are nearly vertical, and the spot is stable, such a flow cannot occur if the spot is monolithic below the surface.

One idea concerning the nature of the small-scale magnetic structure of the penumbra considers it to be dynamic and its complexity to result from the convective exchange of flux tubes [292, 234]. In the framework of this scenario, a flux tube at the outer boundary of the penumbra (the magnetopause) is heated by the field-free convecting external plasma. The subsurface section of the heated tube becomes buoyant and rises, eventually coming to the surface near the outer penumbral edge. Later, portions of the tube closer to the umbra reach the solar surface. At the surface, the tube cools by radiation, loses its buoyancy, becomes more horizontal, and eventually sinks down again, so that the cycle can be repeated. Part of this scenario has been studied by numerical simulation [293, 294]: a flux tube lying at the

magnetopause does indeed rise to the surface until it lies there horizontally through much of the penumbra. Hot material continues to rise along the flux tube and flows horizontally outward along the flux tube. This flow reproduces some properties of the Evershed effect, suggesting that the magnetic and velocity structure are intimately connected. Evidence supporting the presence of magnetic structure consistent with these simulations has been provided [295, 296]. However, the simulations carried out so far do not reproduce the second half of the convective transport cycle: the horizontal flux tubes do not sink back down again, but remain at the surface. In this respect, the simulations are in accordance with observed time series of magnetograms that display little change in the magnetic structure with time [297]. An alternative proposal assumes that the fluted structure of the penumbral field is produced by upwellings of hot, field-free material, which parts the penumbral field lines approximately like two curtains and reaches very close to the surface. Above these intrusions, the field is nearly horizontal, beside them more vertical [257].

6.7. Models of the brightness and thermal structure

L. Biermann [298] first proposed that the reduced brightness of sunspots is due to the inhibition of convective motions by the magnetic field, whereby the criterion for the onset of convection is modified by the presence of the magnetic field [299]. Since convection dominates energy transport below the observable layers, quenching of convection turns a sunspot into an obstacle to the outward heat flux through the convection zone. This leads to a diversion of energy away from the sunspot, which reduces the energy flux through the spot and produces a darkening. The diverted energy flux is mainly stored in the convection zone and released very slowly over its thermal time scale of 10^5 years, much longer than the lifetime of a sunspot [300, 301, 302]. The recent rediscovery of a (very faint) bright ring around large sunspots ([303]; see Waldmeier [304] for the original discovery) has only served to show just how efficiently the blocked energy is redistributed within the convection zone. Since only a few percent of the blocked energy flux immediately re-emerges in the bright ring, the presence of sunspots at the solar surface leads to a global darkening of the Sun.

A complete quenching of convection so efficiently reduces the heat flux that the question to ask is not why umbrae and penumbrae are so dark, but rather why they are so bright, in particular the penumbrae. The observed brightness can only be explained if efficient mechanisms of heat transport act within sunspots in spite of the strong magnetic field.

Of the approaches that have been taken to solve the problem basically two are still considered viable. The first is to form the sunspot out of a cluster of small flux tubes (see Section 6.6). Owing to the tapered shape of each small flux tube, larger amounts of field-free gas are present between them at increasing depth. Consequently, below the sunspot, convection can penetrate relatively unhindered until close to the surface. In addition, for a sunspot composed of N small flux tubes the surface area of the side walls of the flux tubes, over which the convective gas can radiate into the magnetized gas, is $\sqrt{N}$ times larger than for a simple monolithic sunspot. A larger side-wall surface compared to the horizontal cross-sectional area leads to a more efficient heating of the tubes. Note that, instead of flux tubes, marrow flux sheets als lead to an enhanced energy flux at the surface.

The second proposal considers convective transport within a monolithic sunspot

umbra. Magnetoconvection is a vast subject in itself and we refer the reader to reviews devoted specifically to this topic (e.g., [305, 306, 307]. Here we only mention two results. The character of the convection below a sunspot umbra depends largely on the parameter $\zeta = \eta/\kappa$, where η is the magnetic diffusivity and κ is the (radiative) thermal diffusivity. For $\zeta < 1$ the convection is oscillatory, while for $\zeta > 1$ overturning convection is the preferred mode [222]. Since $\zeta \approx 10^{-3} \ll 1$ at the solar surface, but increases rapidly with depth, the current picture is that oscillatory convection dominates in the first 2 Mm below the surface, while overturning convection takes over in the deeper layers. In any case, such modes of magneto-convection lead only to moderate variations of the magnetic field strength between the upflow and the downflow regions [308].

Recent 3-D simulations exhibit cases of filamentation. For magnetic fluxes appropriate to sunspot umbrae, islands of upwelling hot gas with a relatively weak magnetic field were found, surrounded by cooler, strong-field material [309, 310]. These hot upwellings are reminiscent of umbral dots. Unfortunately, such magnetoconvection simulations cannot as yet be used to decide between the monolithic and the cluster model. This is partly because the parameters and geometries for which these computations are carried out are still significantly removed from real sunspots.

The problem of heating the umbra pales in comparison with that of heating the penumbra with its nearly 4 times higher radiative flux. One possibility would be a 'flat penumbra', such that the sunspot magnetopause were to lie within a few photon mean-free-paths of the solar surface under the whole penumbra [311]. However, the measured magnetic field structure excludes such a model, since it does not account for the amount of magnetic flux emerging in the penumbra [233]. Most other options, such as interchange convection (see previous subsection), the excess heat brought to the surface by the gas feeding the Evershed flow, or heating by magnetic reconnection between the inclined and the horizontal field, face problems. For example, the first runs afoul of observations suggesting that the penumbral magnetic structure does not change sufficiently rapidly to provide the necessary heat flux [312, 297]. A steady outflow of matter as the source of the heat could work, but only if the flow dips below the solar surface multiple times during its passage across the penumbra. Another possibility is a special mode of magneto-convection in an inclined magnetic field (e.g., [313], or the intrusion of field-free material between the penumbral field lines, making the penumbra locally shallow [257].

6.8. Models for the Evershed effect

The simplest interpretation of the Evershed effect is that it is produced by a steady, almost radial outflow. This scenario was put on a solid physical footing by Meyer and Schmidt [314, 315], who presented a siphon flow model of the Evershed effect. The field strength in the outer penumbra (700–900 G) is smaller than in typical small-scale magnetic elements (1000–1500 G), so that the gas pressure is expected to be larger in the outer penumbra. If the field lines from the outer penumbra are connected to elements of concentrated magnetic flux outside the sunspot (see Sect.7), then the gas pressure difference at equal geometrical height drives a flow from the penumbra to the magnetic elements. At the same time, this model also explains the inverse Evershed effect. The field strength in the umbra (2000–3000 G) is larger than in small external magnetic elements, so that a field line connecting the umbra with a magnetic element should support an inflow into the umbra. The relative simplicity and intuitive appeal

of this model has led to a number of investigations (e.g., [316, 317]).

Observations indicate that the outflow associated with the Evershed effect is largely restricted to the penumbra, with downflows present in the outer penumbra [269], so that only a small fraction of the mass continues into the superpenumbral canopy [268]. Since the (average) field strength decreases by roughly a factor of two from the inner to the outer penumbra, this would lead to a siphon flow directed towards the umbra, opposite to the observed flow. Only a difference in the heights (i.e., Wilson depression) to which the field strength observations correspond leaves a possibility to obtain the correct flow direction [317]. However, another solution is also possible. The horizontal component of the field supporting the Evershed flow changes very little in strength between umbral boundary and outer spot boundary [318, 248] while the more vertical background component of the field displays a strong outward decrease. The balance of total pressure between these two components leads to a strong radial gas pressure gradient in the flow-carrying horizontal flux tube, which can drive an outward flow.

7. Small-scale magnetic structure

7.1. Introduction

The magnetic field in the photospheric layers is concentrated in active regions and in a network distributed over the whole Sun. In active regions (outside sunspots) the magnetic field is concentrated into more or less discrete features that together form faculae or plage regions.† In the quiet Sun (i.e., outside active regions) the magnetic flux elements form a network outlining the borders of supergranular cells with a length scale of 20–40 Mm. Another type of magnetic feature in the quiet Sun are the internetwork elements, which are located in the interiors of supergranular cells. On a more localized scale, the magnetic elements forming faculae and the network, and very likely also those in the internetwork, are located in the downflow lanes between granules [319, 320].

There is a whole spectrum of magnetic features having very different sizes and properties on the solar surface. Sunspots (Sect. 6) are the largest and rarest. Even at times of greatest solar activity they cover only a fraction of a percent of the solar surface. On average smaller than sunspots are pores, although the largest pores can be bigger than the smallest sunspots. Pores typically have diameters of a couple of thousand km and are dark. They are distinguished from sunspots by the fact that they have no penumbra, appearing like isolated umbrae [321]. Even smaller, and far more common, are magnetic elements, bright structures with diameters smaller than a few hundred km. High resolution observations show magnetic features with sizes right at the achievable spatial resolution of 150 km [322]. In the quiet Sun, indirect estimates suggest the existence of features of the internetwork field with a diameter of at the most 50 km [323]. Finally, observations indicate an omnipresent turbulent field in photospheric layers.

The current picture of the magnetic elements is that they have many features in common with sunspots (although at first sight the differences may appear to

† Historically, a plage is defined as an extended bright region seen in cores of stronger chromospheric spectral lines. Plages are roughly co-spatial with photospheric faculae, bright areas seen near the solar limb in the continuum or in photospheric spectral lines. Both, plages and faculae, are caused by a large density of small-scale elements of concentrated magnetic flux, so that often the terms plage or faculae are used to denote areas densely populated by such magnetic elements.

dominate). In particular, both structures, as well as pores, are thought to be manifestations of intense concentrations of magnetic flux and are usually described by the theory of magnetic flux tubes. Overviews of the properties of magnetic elements can be found in [324, 325].

The magnetic structure in both active regions and in the quiet Sun network is very similar: the magnetic field is concentrated into more or less discrete elements of magnetic flux separated by regions with comparatively little magnetic flux (to first approximation they are considered to be field free, although they probably harbor a considerable turbulent magnetic field; see Sect. 7.7). Hence the measured intensity from a part of the Sun can, employing a simple 2-component model, be written as:

$$I_{\mathrm{obs}} = f I_{\mathrm{m}} + (1 - f) I_{\mathrm{b}}, \tag{7.1}$$

where I_{obs} is the observed intensity, I_{m} the intensity of light from the magnetic feature, I_{b} from the "field-free" background and f is the magnetic filling factor, i.e. the fraction of the observed part of the solar surface covered by intense magnetic fields. Equation 7.1 is based on the assumption that the spectra of magnetic elements and background are the same everywhere, or, alternatively, it describes average properties. One reason why Equation 7.1 has been widely used is that many magnetic features are not resolved by spectropolarimetric observations, which usually do not reach the spatial resolution achievable in broad-band images. Although I_{m} and I_{b} do to a certain extent depend on f, to first order on different parts of the Sun I_{obs} can be determined simply by changing f, while leaving I_{m} and I_{b} unchanged. When considering the net polarization (as described by the Stokes parameters Q and U for net linear polarization and Stokes V for net circular polarization) produced by the Zeeman effect to first order

$$S_{\mathrm{obs}} = f S_{\mathrm{m}}, \quad \text{where} \quad S = Q, U, \text{or } V. \tag{7.2}$$

In reality, the relationship is more complex, but Equation 7.2 does indicate one major advantage of using the polarized Stokes parameters when studying small-scale magnetic elements, specially when they are spatially unresolved: to first order the field-free atmosphere does not contribute to the polarized Stokes profiles.

7.2. Field strength measurements

The first evidence for magnetic fields outside sunspots was found by G.E. Hale [326] in what he termed 'invisible sunspots'. Such features were first mapped with the photoelectric magnetograph by Babcock and Babcock [327]. Although the field strength averaged over the spatial resolution element of the magnetograph (typically a few Mm on the Sun) was on the order of tens to a few hundred G, evidence kept accumulating that the intrinsic field strength of these features is much larger [328, 329, 330]. The difference between the apparent and intrinsic field strength can be explained if the features are spatially not resolved, i.e., $f \ll 1$ in Equations (7.1) and (7.2). Finally, a technique involving the ratio of a carefully chosen line pair was used by Stenflo [331] to show that magnetic elements intrinsically have kG field strength (cf. [332, 333, 334]). The strong fields have been confirmed by a number of other techniques and diagnostics in the meantime, most prominently the spectral lines of neutral iron (Fe I) at 1.56 μm, which are sufficiently Zeeman-sensitive to directly reveal the splitting by the kG field [335, 336, 337]. More recently, line profile inversions, which allow the magnetic field to be determined consistently with the other atmospheric parameters have confirmed and refined the results obtained with

other techniques [338, 339, 340]. At the same time, the spatial resolution of the observations has also been increasing, in some cases allowing magnetic elements to be nearly resolved [322], although simulations of magnetoconvection show many features that lie below the best currently achievable spatial resolution (see Sect. 7.5).

The magnetic field strength drops rapidly with height. In the deep photosphere, the field strength is around 1500–1700 G [335, 336, 337]), dropping to roughly 1000–1200 G in the middle photosphere [333]), and to 200–500 G near the temperature minimum [341, 342]). How strongly the field strength drops with height in still higher layers depends on the filling factor. Owing to magnetic flux conservation, the magnetic features expand with decreasing field strength (increasing height) until neighboring flux tubes merge, at least in the case when they have the same magnetic polarity, which is typical of active regions. This case is illustrated in Figure 17. Above the merging height, the field strength is expected to drop much more slowly. Observations have also provided evidence for the expansion of the flux tubes and their merging [342, 343]. In a mixed polarity environment like the quiet Sun, the situation is more complex since field lines can bend over and return to the solar surface relatively close by.

The field strength of magnetic elements increases slowly with increasing filling factor, f, and also with increasing cross-sectional area of the elements [337, 344]. Thus between the quiet network and strong active region plage the field strength increases by roughly 10% at a given geometrical height, although f can change by nearly an order of magnitude. At very small filling factors or magnetic fluxes, as found mainly in supergranule cell interiors, however, the situation is less clear. Observations using the infrared iron lines at 1.56μm show that B drops rapidly with decreasing flux [323, 345, 346]. High resolution observations in the visible spectral range, on the other hand, suggest the presence of strong fields throughout the supergranule cell interiors [347, 348]. The dependence of the intrinsic field strength on the spatially averaged field, as deduced from 1.56μm lines, is shown in Figure 18.

High resolution images suggest that the average size of magnetic features increases as the filling factor increases. This is also supported by the comparison of spectropolarimetric data with MHD simulations [349]. These results indicate that the increase in field strength with filling factor may mainly reflect a dependence on flux-tube size.

7.3. Formation and evolution

New magnetic flux emerges into the solar atmosphere in the form of bipolar magnetic regions. During emergence, the field initially is relatively weak (being a few hundred Gauss) and predominantly horizontal [350]. At this point we are seeing the top of the emerging Ω loop. As the loop continues to rise, its two photospheric footpoints move apart, the field gets stronger and nearly vertical.

Right from the beginning, the field interacts with convection. At the location of flux emergence, the granulation is heavily disrupted, with long thin parallel dark and light striations being visible instead of normal granules [351]. This interaction continues throughout the lifetime of the magnetic flux, although the field and convection segregate early (such that the magnetic flux then lies in the intergranular convective downflow lanes). As the granules evolve and move, the flux located between them is forced to move along, wandering with the intergranular lanes. Finally, it is probably the turbulence associated with convection which buffets and twists the field on a small scale, bringing opposite polarities together and thus allowing for the
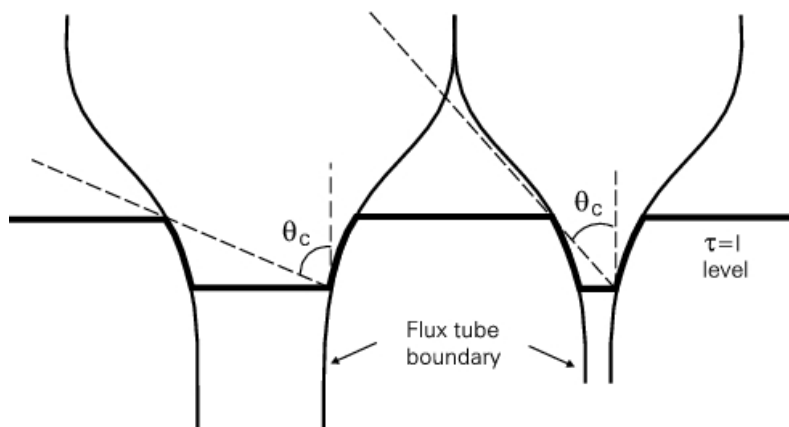
Figure 17. 'Wine glass model' of magnetic elements. The bounding field lines (current sheets) of two neighbouring magnetic elements are indicated by the curved, nearly vertical lines, the solar surface (i.e. the continuum unit optical depth, $\tau = 1$, level) by the thick line. Also indicated are the angles θ_c at which the bright walls of the flux tubes are best visible. Note that θ_c is larger for the thicker flux tube.
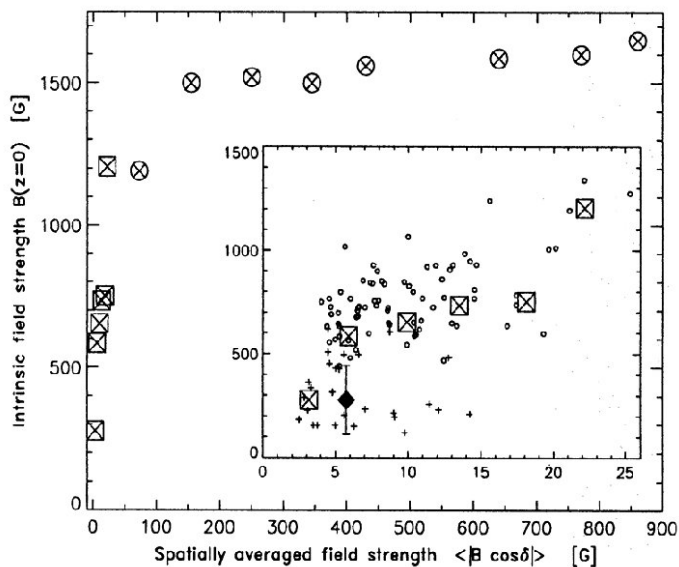
Figure 18. Intrinsic magnetic field strength at the solar surface, $B(z = 0)$, vs. the unsigned, spatially averaged longitudinal field strength $\langle |B \cos \delta| \rangle$, where δ is the angle between the direction of the magnetic vector and the line of sight of the observer. Plotted are binned values resulting from quiet Sun (squares) and plage (circles) observations. The inset shows only the left-most part of the main figure, with the squares being identical to those in the main figure. The small circles and crosses represent individual measurements. The diamond denotes the value of B derived from the profile averaged over all the magnetic features denoted by crosses, which individually lie below the noise level (from [345]).

dissipation of magnetic energy.

The currently favored physical picture of the formation of magnetic elements involves a two-stage process. In a first step, the convection (i.e. the granular flow) expels the initially weak and relatively homogeneously distributed magnetic flux into the intergranular downflow lanes [59, 60, 309, 352]. This process is called flux expulsion and can concentrate the field until it is roughly in equipartition with the flow, i.e., the magnetic energy density equals the kinetic energy density, $B \simeq \sqrt{\mu_0 \rho}\, v$, where ρ is the gas density and v is the average horizontal convective flow speed. For the solar photosphere values of 100–400 G are thus obtained, depending on the height to which they refer (ρ drops exponentially with a scale height of ≈ 100 km) and on the value of the convective velocity assumed. Of considerable importance for the further concentration of the magnetic flux is an instability, the so-called convective collapse, which is driven by the cooling, through radiative losses at the solar surface, of the gas trapped between the field lines [353, 354]. As the gas cools, its density increases, so that it sinks and settles in deeper layers, leading to low pressure in the upper layers of the flux concentration. The pressure of the surrounding gas pushes the field lines together, thus strengthening the field to kG values at the solar surface. A field of this strength quenches convection and stops the instability from growing further. Radiative heating (mainly through the side walls of the flux concentration; see Sect. 7.5) keeps the gas from cooling further and thus allows the magnetic element to approach a stable magneto-static state [355]. Since the lateral influx of heat is more efficient for more slender flux tubes (which have a larger ratio of wall area to volume and which are less optically thick), the less flux in a small-scale magnetic feature, the lower the final field strength [356]. Observations confirm this theoretical prediction [345].

In reality, the various stages of the above multistep process (emergence, brightening, flux expulsion and convective collapse) seem to run in parallel [357]. The emerging field already has equipartition field strength and is very rapidly swept into the intergranular downflow lanes, where is becomes intensified by the convective collapse process. As the field becomes stronger, the buoyancy force increases $\propto B^2$, so that an initially inclined field quickly becomes nearly vertical [358]. Indeed, a strong correlation is found between inclination and the strength of the field in an emerging flux region [350] and is also observed in simulations of magnetoconvection appropriate for regions of mixed magnetic polarity [359].

The non-stationary granulation appears to be the major driver of the evolution of individual magnetic features, although on a larger scale the evolution of the supergranulation and possibly the mesogranulation (i.e., a velocity pattern on an intermediate scale of 5–10 Mm) play the more important role [360]. Individual magnetic features are dragged along as intergranular lanes change and move [361, 362]. Polarimetric observations have so far provided only limited information on the evolution of individual magnetic elements, with proxies revealing much of what we know. Proxy observations (see Sect. 7.4) show, e.g., the splitting and merging of bright points [361]. However, a deeper insight is given by MHD simulations (see Sect. 7.5).

The most common mode of decay of the magnetic field is through cancellation with features of opposite magnetic polarity, as has been revealed from time series of magnetograms [363, 364]. Again, the spatial resolution of the observations is not sufficient to learn more about the exact processes acting during the cancellation. However, after the emergence of a bipolar loop, its individual footpoints generally keep moving apart and finally cancel with opposite polarity elements belonging to

another bipole (or merge with field of the same polarity). Hence, the cancellation must be accompanied by magnetic reconnection of some form, i.e. with some amount of energy release. This process has been proposed as the source of the observed X-ray bright points [365].

7.4. Facular brightening and proxies of the magnetic field

The measurement of the magnetic field often suffers from a low signal-to-noise ratio, in particular when considering regions with low magnetic flux (or filling factor). Since net circularly polarized light needs to be recorded at high spectral resolution, the low signal level necessitates longer integrations, which results in a loss of spatial resolution caused by smearing due to fluctuations of the refractivity index in the turbulent terrestrial atmosphere. This has led to the use of more easily accessible proxies, generally the intensity in some (narrower or broader) spectral band in which the magnetic features exhibit a particularly large contrast. These proxies are useful since they are more rapidly recorded, permit a simpler instrument setup and do not suffer from polarization cross-talk. Magnetic elements are generally visible as bright structures. Their visibility thus depends on the amount of excess heating which they undergo.

The intrinsic brightness of magnetic features depends on their size. In general, the intrinsic brightness of a magnetic feature located near the centre of the visible solar disc (so that the observational line of sight is vertical) increases steadily with decreasing cross-sectional area or magnetic flux per feature. Such a relationship also holds if instead of size the magnetic flux per pixel, or filling factor f, is considered [366, 367]. However, unless the spatial resolution is very high or a region located near the solar limb is observed, magnetic elements cannot be recognized in continuum radiation. This behavior can be understood in terms of a flux-tube model (see below). The dependence on magnetic flux itself depends on the height from which the radiation originates (e.g., [368]). Thus, pores are dark in the visible continuum, but bright in radiation coming from the chromosphere (e.g., emitted in the core of the strong spectral line of ionized calcium, Ca II K). Quite generally, the contrast of the magnetic features located near solar disc centre increases with increasing height of emission or absorption of the radiation (within the photosphere and chromosphere). Hence the best wavelengths at which to study magnetic elements are those for which the radiation is emitted in the mid-photosphere or higher and where the intensity is particularly temperature sensitive. This is illustrated by Figure 19, which shows the large difference between the contrast of magnetic features measured in the visible continuum (bottom), and the cores of spectral lines. Clearly, the contrast saturates and decreases again in the continuum for increasing magnetic flux (formation of pores), but continues to increase in the line cores.

Recent G-band observations with a resolution of 100 km or better have unveiled new aspects of the morphology and dynamics of small-scale magnetic features. Their morphology strongly depends on the amount of magnetic flux that they harbour. In regions of low magnetic flux (quiet Sun) the features are more point-like, while in strong plage (active regions) they reveal are more ribbon-like appearance, often exhibiting a rather convolved shape. The features continuously evolve along with the granulation, changing their form, buckling at their edges, breaking up or coalescing [369, 370].

Quite distinct is the behavior of the brightness contrast (with respect to the quiet

Sun) of magnetic elements as a function of their distance from the centre of the solar disk (centre-to-limb variation of contrast due to an increasing angle between the line of sight and the local vertical direction on the Sun). In white light or at continuum wavelengths, faculae are often almost invisible near the centre of the solar disk, but become bright near the limb even at relatively low spatial resolution. This dependence on limb distance also is a strong function of the amount of magnetic flux or filling factor [371, 367]. The steep increase in contrast towards the limb is typical of regions with a high flux density, with features that are dark at the centre of the disk appearing bright near the limb. At small f, the contrast peaks closer to the centre of the disk, although it is comparatively flat as a function of limb distance. The contrast of chromospheric plage and the chromospheric network is much higher and is roughly independent of position on the solar disk. This suggests that different mechanisms are responsible for the excess brightness of magnetic elements in the lower photosphere than in higher layers.

Although broad-band brightness is the most easily recorded quantity, it is not the best proxy of the magnetic field. The continuum contrast of magnetic elements is small, being a couple of percent under typical to good observational conditions. This is similar to the contrast of the granulation pattern, so that it is not straightforward to identify magnetic features except near the limb or at very high spatial resolution. The contrast can be enhanced if the observations are carried out in the cores of spectral lines, in particular if these lines are temperature sensitive. Most commonly used are the chromospheric cores of the Ca II H and K lines and wavelength bands dominated by lines of diatomic molecules, whose relatively low dissociation potential makes their spectra extremely temperature-sensitive. Examples are the G-band at around 430.5 nm dominated by spectral lines of the CH molecule or the CN band head near 388 nm [372, 373, 374]. Observations in these wavelength bands allow higher resolution to be obtained than with magnetograms since they can be carried out with wider filters (0.1–3 nm wide) rather than in the narrow bands necessary for magnetograms (< 0.01 nm), so that shorter exposure times are possible. The higher contrasts in spectral line cores suggest that the temperature enhancement in the upper photosphere and the chromosphere in magnetic elements is much stronger than in the lower photosphere.

The brightness in the Ca II K line core has been used as a proxy of magnetic brightening since the invention of the spectroheliograph, showing both the magnetic network and the active regions with high contrast. Recently, very high resolution Ca II K line observations have been made with the Dutch Open Telescope [375]. An example is shown (along with an image in the G band, which originates in the photosphere) in Figure 20. The sunspots are seen in both photospheric and chromospheric radiation, but are less readily visible in the latter. The plage, on the other hand, appears particularly bright in the chromosphere, and the network structure is also clearly discernible. Note that it is not always the same features that are most clearly visible in the chromosphere and in the photosphere.

With the advent of observations in the ultraviolet spectral range, further proxies for the magnetic field became available. These include in particular the He II line at 30.4 nm, which is recorded by the EUV Imaging Telescope (EIT) on board the SOHO spacecraft [376].

Besides on the inclination, $\mu = \cos\theta$ (where θ is the angle between the line of sight and the local vertical direction on the Sun), on the size of magnetic features and on wavelength, the exact value of the intensity contrast depends strongly on the
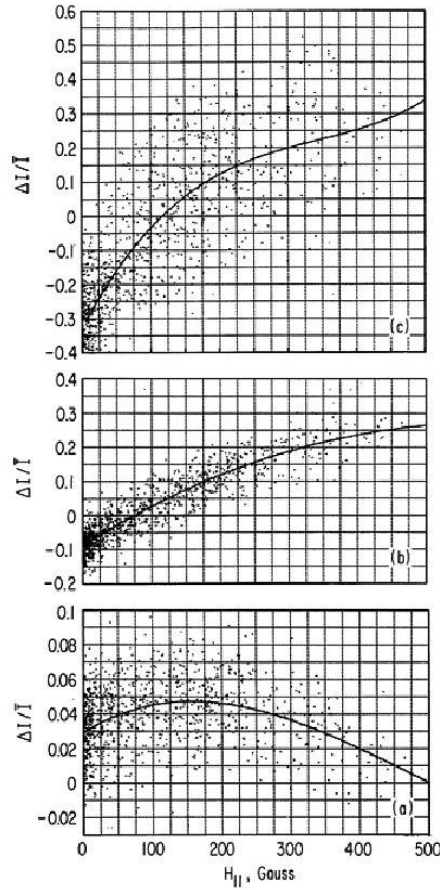
Figure 19. Brightness contrast $\Delta I/I$ of, from bottom to top, (a) the continuum, (b) the core of Fe I 525.02 nm, and (c) Ca II K vs. the magnetic field strength averaged over the spatial resolution element of the observations. The observations refer to active regions (from [368]).

spatial resolution of the observations. At high resolution, (e.g., in the G-band) the smaller magnetic features in the faculae break up into strings of small bright points or elongated features lying in the dark intergranular lanes. Moreover, at very high resolution, the size and shape of the bright structures changes with μ, so that it is even unclear if the same magnetic features are seen as bright structures at different μ values [377]. There are indications that bright features near the limb do not represent the same magnetic structures as bright points at larger μ values [367, 371]. High-resolution observations reveal that the tiny bright points disappear closer to the limb and are replaced by larger bright 'fans' that appear as if the walls of the granules behind the magnetic feature had brightened [377, 378] as shown in Figure 21. This figure also suggests a 3-D structure of the visible solar surface, with the granules lying higher than the intergranular lanes. The bright fan appearing behind magnetic elements results from the larger transparency of the latter in comparison to the non-magnetic atmosphere, so that the radiation comes from slightly deeper (and thus hotter) layers of the granule behind the magnetic element (see Sect. 7.5).
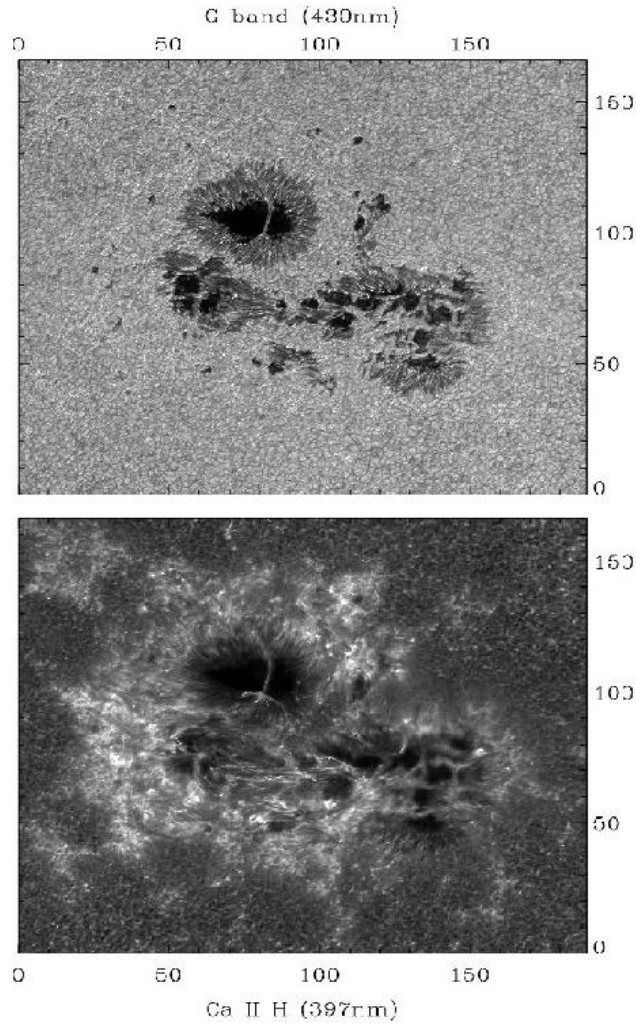
Figure 20. AR 10375 imaged with the Dutch Open Telescope in the G-band (upper frame) and the core of the Ca II H line (lower frame). Figure courtesy of P. Sütterlin and R.J. Rutten.

7.5. Models and numerical simulations

Almost all models of magnetic elements or, more generally, magnetic flux concentrations consider them to be some form of magnetic flux tube. Strictly speaking, this term is restricted to axially symmetric structures, but it is often used for magnetic flux concentrations in a more general sense. An exception are magnetic features displaying translational symmetry, which are sometimes also referred to as flux slabs. In the following we will refer to magnetic flux concentrations as flux tubes irrespective of their exact geometry. Basically, flux tubes are bundles of nearly parallel field lines whose cross section is bounded by a topologically simple closed curve. Often the field lines are considered to lie almost parallel to each other (and almost parallel to the 'axis' of the tube), although structures with a twisted field (sometimes called magnetic flux
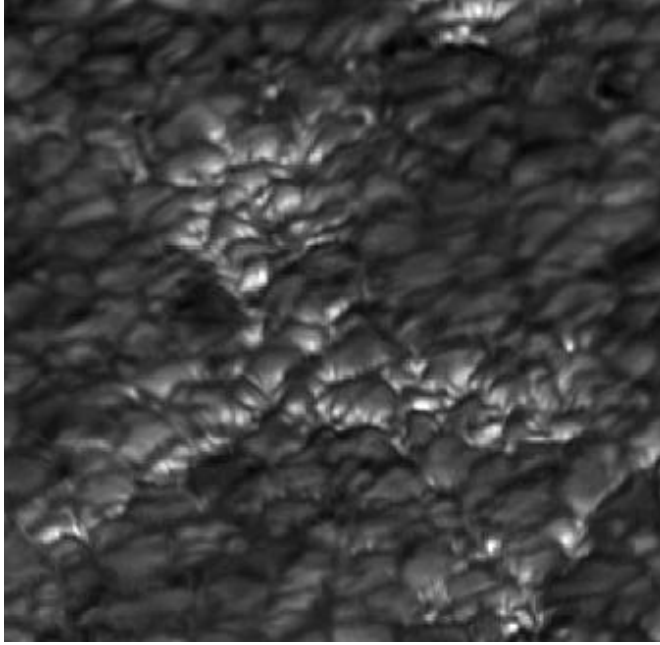
Figure 21. G-band image of a plage region observed at an inclination of $\cos\theta \approx 0.5$ with a spatial resolution of about 70 km (a tenth of a second of arc) at the Swedish Solar Telescope on La Palma (figure courtesy of V. Zakharov).

ropes) have also been considered in many investigations.

Flux-tube models of many types are known, differing in their level of generality. An adequate working description of magnetic elements that satisfies many currently available observations is provided by the thin-tube approximation [379, 380, 67]. A thin-tube model can be considered to be the solution that satisfies the MHD equations to lowest order in an expansion in radius (distance from the axis). Thus, the thin-tube approximation should be a good assumption for the smallest magnetic elements, but an increasingly poor representation of larger magnetic features. The approximation basically neglects magnetic curvature forces and the internal structure of the flux tube in the horizontal direction. The lateral force equilibrium is simply described by a balance of total pressure: $p_\mathrm{e} = p_\mathrm{i} + B^2/2\mu_0$, with the external gas pressure, p_e, being equal to the sum of the gas pressure in the flux tube, p_i, and the magnetic pressure. Consequently, the internal gas pressure of a flux tube with kG magnetic field in the solar atmosphere reaches only 10–30 % of the value in its surroundings at the same height.

In its simplest form the thin-tube approximation neglects temporal variations and, in addition to lateral pressure balance, assumes hydrostatic equilibrium along the field lines. Consequently, only the internal temperature profile as a function of height remains to be specified (apart from the total magnetic flux and the value of the field strength at an arbitrary height) in order to obtain a uniquely defined model of a thin flux tube. If the radial expansion is carried to second order, the approximation remains valid for somewhat thicker tubes [381, 382]. Other approaches include combinations of a potential field with a boundary current sheet [383] or a full solution of the magnetostatic equations for an axially symmetric flux tube [384].

Comprehensive 3-D radiation MHD simulations (see below) suggest that horizontal pressure balance is satisfied in the strong-field magnetic features to a high degree, so that for many purposes a thin tube (or slender slab) is a good approximation of magnetic elements. In addition, models based upon the thin-tube approximation also satisfy a number of observational constraints. A major success has been the explanation of the centre-to-limb variation of the continuum contrast of faculae (at least as measured at a spatial resolution of the order of a Mm on the Sun). Owing to the strong evacuation of the tube, the surface of optical depth unity (the visible surface) drops by 100–200 km within the flux tube, similar to the Wilson depression in sunspots. The temperature of the solar gas increases rapidly with depth, so that the 'side walls' of the flux tube between the external and the internal levels of optical depth unity tend to be rather hot and thus bright. Since the depression of the visible surface is largely independent of the flux tube size, the ratio of width to depth of the depression depends strongly on the diameter of the magnetic feature. This is illustrated in Figure 17. The hot walls of narrow flux tubes are only seen if they are located relatively close to the centre of the solar disc. At larger inclinations, the backward wall gets hidden. For broader tubes this happens only much closer to the solar limb [385, 386]. This simple geometrical concept qualitatively explains the centre-to-limb variation of the continuum contrast [367, 371]. The details seen in the highest resolution data, such as the bright fan behind magnetic elements near the limb require more detailed models [387, 388, 389].

A number spectro-polarimetric observations can also be explained by relatively simple models. As the gas pressure drops with height approximately at an exponential rate, the magnetic field strength drops with $\sqrt{p}$ and, to allow magnetic flux conservation, the cross sectional area increases as $1/\sqrt{p}$. Observations of Stokes V profiles of Zeeman-sensitive spectral lines in the infrared and of chromospheric lines are consistent with such gradients of the field strength [390]. The field strengths observed in lines formed at different heights also support this model [337, 342]. The expansion of the flux tubes, combined with their location in downflow lanes also provides a natural explanation of the combination of asymmetric and unshifted Stokes V profiles [391, 320].

The models discussed so far do not include an energy equation and thus do not possess any predictive power for the thermal or dynamic structure of magnetic elements. In order to reproduce such observations (e.g. line weakening or G-band contrasts) and to obtain a better understanding of the physical processes acting in and around magnetic elements, one has to carry out MHD simulations including a proper description of radiative transfer. Similarly, static or stationary models have no predictive power regarding the high field strengths of the concentrated magnetic features. In order to understand the large observed values the formation process of flux tubes must be modeled.

Closer to reality than the thin-tube approximation are 2-D MHD models of flux slabs, either with [392, 393] or without imposed mirror symmetry [394]. In the former case, the solution quickly reaches a nearly stationary state, in the latter case it turns out to be very dynamic, with the flux tube swaying to and for as it is buffeted by the nearby granules.

3-D simulations of solar convection have been very successfully carried out [395, 396]. These simulations are fully compressible and take into account non-gray radiative transfer and a realistic equation of state. They reproduce a wide variety of observations [397, 398]. Similarly realistic 3-D MHD simulations of magneto-
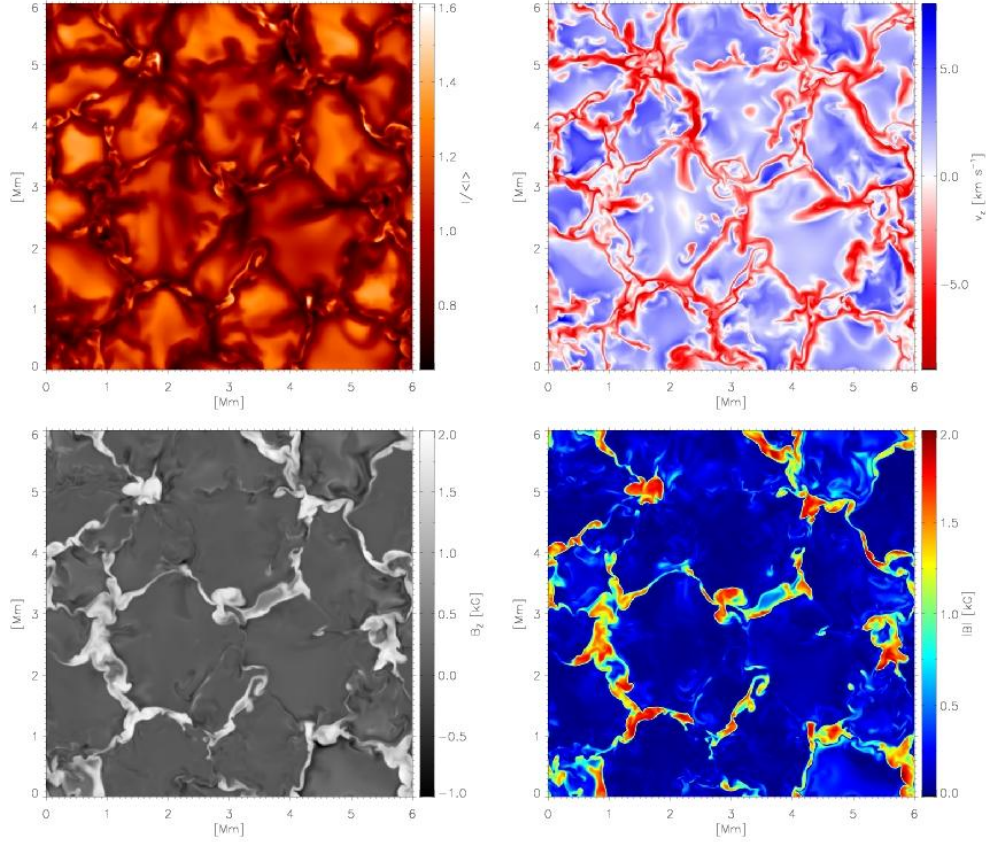
Figure 22. Snapshot of brightness (upper left), vertical component of the velocity field (upper right), vertical component of the magnetic field (lower left), and magnetic field strength (lower right) at the height of the (corrugated) solar surface deduced from a 3-D radiation MHD simulation covering a region of 6×6 Mm on the solar surface [404]. The horizontally averaged vertical magnetic field strength is 200 G. The correspondence between the color scale and the physical quantity it represents can be deduced from the colour bars on the right of each panel.

convection have also been run for some time [399, 400]. Such simulations now reproduce critical observations in detail [401, 402, 403, 404].

Figure 22 shows a snapshot of a simulation which was started with an initially homogeneous and unipolar field of 200 G [402, 404]. The magnetic field rapidly becomes concentrated in the dark downflowing intergranular lanes within the convective turnover time of the granules. Values of over 2000 G are commonly reached in the flux concentrations, in good agreement with the observations. In addition to these strong fields, a weak field is also found everywhere in the simulation box. The probability distribution function of the field strength has a peak at around zero (very weak are present mainly above the granules) and drops off towards higher field strengths. If the magnetic flux in the domain is small (e.g., an initial field of 10 G), then the field strength drops almost exponentially (in agreement with observations in the infrared [346]), although flux concentrations with kG field elements are still present. This corresponds to the situation in the quiet Sun, which is best reproduced by a mixed-polarity field with about 20 G average vertical field strength [405]. As

the vertical magnetic flux in the simulation box is increased, a hump appears in the distribution function of magnetic field strength at kG field strengths. This indicates an increasingly large proportion of strong fields, which are mainly found in horizontally elongated structures located along the downflow lanes (see Figure 22).

At values of the average flux density at the solar surface beyond roughly 200 G, the properties of the convection are strongly affected by the magnetic field. The granules become smaller and more stable (compare with [406]), the downflow within the magnetic features is quenched, with downflows now being concentrated at their edges. This quenching of the downflow is clearly visible in Figure 22 at locations of strong field. Also well visible is that the magnetic elements brighten, producing thin, bright ribbons surrounded by the darker intergranular gas, very similar to what is observed in high resolution continuum images. This enhanced brightness is caused by radiation flowing into the evacuated magnetic feature from the sides (through the hot walls). In realistic simulations, the flow of the radiative flux is followed [404] and shown to behave according to the hot-wall model [385].

The (Wilson) depression of the visible surface in small magnetic flux concentrations leads to an increase in the solar surface area, so that the elements act like leaks in the solar surface and lead to a brightening of the Sun as a whole. This excess radiation extracts energy from the gas in the convection zone. Owing to the high effective thermal conductivity brought about by convective mixing, a part of the deficit is distributed through the whole convection zone, so that a net increase in the total solar energy flux results [301, 302].

The gas in the magnetic features is not entirely optically thin and a part of the strong influx of radiation into a magnetic element is absorbed, especially in the mid-photospheric layers. The absorbed radiation heats up the gas in the magnetic element, so that at equal optical depth the magnetic features become hotter than the surroundings, leading to the ionization of neutral species (i.e. to the weakening of lines of neutral atomic species) and the dissociation of molecules. This qualitatively explains the enhanced brightness of magnetic elements at particular wavelengths (e.g. in spectral line cores) and in particular spectral bands (G-band and other spectral bands populated by molecular spectral lines).

Quantitative and stringent tests of the simulations can be made by computing spectral lines or whole spectral regions for each horizontal grid point of the simulation domain. In the case of the high contrast G-band, approximately 300 CH and atomic lines are computed for each horizontal grid point. The similarity with properties of observed features is striking [407, 408]. The bright fan-like structures seen in facular regions near the limb are also well reproduced by such simulations [387, 388]. This suggests that the simulations contain much of the relevant physics necessary to describe the thermal structure of the photospheric layers of magnetic elements. However, more tests, i.e. comparisons with observational data, in particular with sensitive spectro-polarimetric diagnostics, are needed in order to probe other aspects of the simulations.

The simulations show the ceaseless movement of the magnetic features as they are buffeted around by the granulation. The concentrated magnetic flux moves along the downflow lanes, carrying out something close to a random walk as granules are born, evolve, and disappear. It becomes difficult to identify individual magnetic features and, in particular, to determine lifetimes, since there is a constant transfer of flux between them as concentrations of magnetic flux wax and wane. If features of opposite polarity are close together, these dynamics leads to flux cancellation and to a steady

reduction of the magnetic flux in the simulation box, if no additional flux enters it from outside.

Considering that the photospheric magnetic field forms the footpoints of the coronal loops, one of the effects of this permanent motion is that the field lines in the corona, which are pulled along by the dynamic photospheric field, become braided. As a consequence, tangential discontinuities and current sheets form, where the stored magnetic energy can be released or dissipated [409, 410, 411] (see Sect. 8). It is evident from the simulations that spatial scales below even the best resolution reachable by current observations play an important role in this process.

7.6. Oscillations and waves

Magnetic elements support various wave modes, most of which have mainly been studied theoretically. The observational evidence for flux-tube waves has been limited to low amplitude oscillations, mainly at a period of five minutes [412, 413], although in one case a shorter period oscillation has been reported [414]. It has been argued that the observational evidence is so limited because the magnetic features are spatially unresolved. If multiple magnetic features, each supporting an oscillation at a different phase, are present in the resolution element, then the various oscillation signals at least partly cancel. The interest in the study of such waves is driven by their potential contribution to chromospheric and coronal heating.

Basically, there are three wave modes in a slender flux tube: a slow magnetosonic mode called the tube wave, a transversal kink wave, and a torsional Alfvén wave. In a flux tube with sound speed c_s, Alfvén speed $c_A = B/\sqrt{\mu_0 \rho_i}$, internal gas density ρ_e, and external density ρ_e, the three modes travel at the tube speed c_t, the kink speed, c_k, and the Alfvén speed [379, 67], respectively, with

$$c_t^2 = \frac{c_s^2 c_A^2}{c_s^2 + c_A^2}, \quad c_k^2 = \left(\frac{\rho_i}{\rho_i + \rho_e} \right) c_A^2 . \tag{7.3}$$

The Alfvén wave has no cutoff, so that any torsional oscillation excited in a flux tube propagates while kink and longitudinal modes propagate only at frequencies above their respective cutoff values [67, 415]. Studies of the excitation of such waves generally concentrate on the effect of stochastic perturbations in the surroundings of the flux tube [416, 417], which is similar to the excitation mechanism for the solar global oscillations. In both cases, the perturbations are due to convection. The waves differ in their propagation characteristics. The longitudinal tube waves are affected by radiative damping [418] and easily form shocks with energy dissipation [419, 420]. The kink modes are far less susceptible to damping and dissipation, while Alfvén waves are not damped and easily reach the corona. Most accessible to observations are the longitudinal waves [421, 422, 423] and these are the only ones for which positive observational detections exist [414, 413, 412]. In order to detect the other wave modes, the flux tubes need to be resolved near the solar limb, which is even harder than at disk centre since due to foreshortening even more magnetic elements are present in a given angular resolution element. In the case of torsional waves, individual magnetic elements need to be completely resolved.

7.7. Internetwork and turbulent fields

Magnetic fields in the interiors of supergranules outside active regions were dubbed internetwork fields, in order to distinguish them from the more readily detectable

network fields [424, 364, 425]. The magnetic flux of a typical internetwork feature is about 10^{16} Mx, which is 1–2 orders of magnitude smaller than the flux of a typical magnetic element in the network. However, the emergence rate of internetwork elements is so large that the total magnetic flux emerging in the form of the internetwork field per unit of time is estimated to be two orders of magnitude larger than the rate of flux emergence in the small (ephemeral) bipolar regions that regenerate the network [14]. Internetwork elements emerge inside the supergranules and move with the horizontal flow to the downflow lanes, where they merge or cancel with other internetwork features or with network elements [426]. They have an estimated average lifetime of around 2 hours, which is an order of magnitude lower than the estimated lifetime of the network flux.

A controversy surrounds the intrinsic field strength of internetwork features. Whereas observations of infrared lines indicate low intrinsic field strength of below 500 G [323, 346], recent measurements using visible lines [347, 348] suggest that the field strengths are mostly in the kG range or are a mixture of weak and strong fields [427]. It is at present unclear whether both types of observations are simply showing fields populating different parts of a single, broad field-strength distribution [428], or if there is a problem with one of the diagnostics.

Besides the relatively well studied internetwork fields a truly turbulent component of the field has long been proposed. Field lines belonging to this component are tangled on a very small scale, reaching to below the spatial resolution of current observations. While initial searches using the Zeeman effect remained unsuccessful in detecting such a field, they did provide upper limits [429]. More recent work has concentrated on using the Hanle effect, which can detect weak fields even in the presence of an isotropic distribution of magnetic field directions [430, 431, 432, 433, 434]. These measurements suggest that a turbulent field of a few tens of Gauss may be present, although the exact value (lying between 10 and 60 G) is still unclear. Recently, it has been proposed on the basis of the Hanle effect of atomic and molecular lines that even much more flux is hidden in the form of a turbulent field [435].

The origin of this turbulent field is at present completely open, with the same mechanisms being discussed as for the internetwork field. The MHD simulations indicate that the distinction into different types of magnetic features is artificial and they all are part of a single distribution of field strengths. As the average field strength increases, the spatial distribution and associated properties of the field gradually change, from a turbulent field to flux tubes.

7.8. Influence of magnetic features on solar irradiance

The total irradiance of the Sun (i.e., its radiative flux integrated over wavelength, as measured above the Earth's atmosphere), is known to vary on all time scales observed so far [436]. At the short end of the scale, at around minutes to hours, the variability is dominated by the convection (mainly granulation) and the acoustic oscillations, which contribute mostly at around 5 minutes. At longer time scales reaching up to the solar cycle different causes of the irradiance have been proposed. These include changes in the Sun's internal thermal structure, R-modes [437], a toroidal, subsurface field [438, 439] and the magnetic field at the solar surface [440, 441]. The variability of the surface magnetic features as the dominant source of the observed irradiance variations has been steadily gaining ground and is now well established. The most developed models include the effects of both dark sunspots (and pores) as well as of
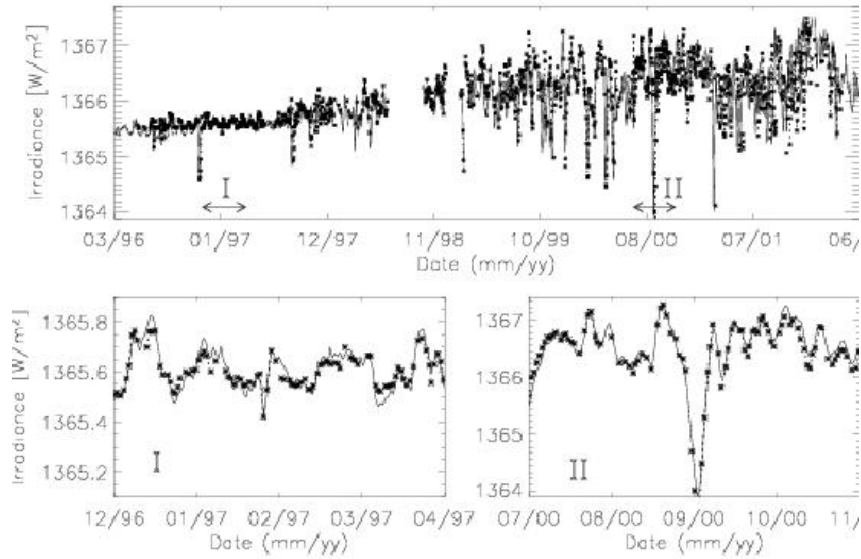
Figure 23. Total solar irradiance measured by the VIRGO instrument on SOHO (solid line) and synthesized from models of solar magnetic features and MDI magnetograms (stars). The top panel shows the period between 1996 and 2002, while the lower panels show shorter stretches on an expanded scale (from [442].)

bright magnetic elements. The spectra resulting from empirical model atmospheres describing each type of feature are computed and the spatial locations of the features (taken from magnetograms and continuum images) are also employed to synthesize the irradiance. The resulting synthetic irradiance agrees very well with the observed value [442, 443] (see Figure 23).

These investigations suggest that the surface magnetic field is responsible for over 90% of the Sun's total irradiance variations on time scales up to the solar cycle. Such models also explain the apparent paradox that the Sun is brightest at activity maximum when the number of dark sunspots its surface is largest. The magnetic elements forming faculae, each of which is rather inconspicuous in white light compared to sunspots, together cause a larger and, in particular, longer lasting brightening than sunspots do. This has partly to do with the fact that faculae cover a considerably larger area than sunspots. Also, the magnetic field composing sunspots decays into smaller elements, producing bright facular regions, which can survive considerably longer than the original sunspot. Finally, much of the excess emission from magnetic elements comes from the upper layers of the photosphere (see Sect. 7.4) and thus mainly contributes in the UV spectral range. Hence a significant fraction of the facular contribution to total irradiance is not visible to detectors with a wavelength sensitivity similar to the human eye.

8. The magnetic field in chromosphere and corona

The phenomena observed above the solar surface are so rich in variety (and so are the names given to them) that here we can only mention the most common and most

spectacular. Due to its dominance, the magnetic field in almost all cases is the key to the physics behind them.

The study of the magnetic field in the atmospheric layers above the photosphere however suffers from the fact that although it here exhibits a dominant influence it is difficult to measure. We will first review briefly from which techniques we draw our present knowledge about the chromospheric and coronal magnetic field, we then give a phenomenological overview of some typical structures inferred from these observations and discuss at the end some more fundamental aspects.

8.1. Measurement and modeling of the magnetic field

Imprints of the magnetic field above the solar surface are usually faint and can sometimes be observed only indirectly.

At radio frequencies below about 3 GHz thermal bremsstrahlung from free electrons in the upper chromosphere and lower corona can be observed by ground-based radio antennas. This radiation propagates in the source region at a frequency above the local plasma frequency in one of the two natural electromagnetic wave modes, the o- or x-mode, depending on its sense of circular polarization with respect to the local magnetic field direction. As the two modes are differently absorbed, the radiation which finally escapes the birefringent corona retains a finite polarization. The degree of polarization is to lowest order proportional to the magnetic field strength along the propagation direction in the source region [444]. Above active regions and sunspots with a strong magnetic field, the 3rd (occasionally even the 2nd) harmonic of the electron gyrofrequency exceeds the local plasma frequency and the corresponding gyro emission can escape the corona. The observed gyro harmonic frequencies are typically above 1 GHz and are directly proportional to the magnetic field strength in the source region (e.g., [445]).

At optical frequencies the emission lines from coronal ions are usually very faint because the plasma density is low and the emissivity roughly scales with the square of the density. In addition, the lines are extremely broadened due to a coronal temperature beyond 10^6 K for the emitting ions. The Zeeman effect is therefore difficult to detect and to be analyzed quantitatively to yield estimates for the magnetic field strength. The conditions are more favorable at chromospheric heights (e.g., [446]) or in prominences (e.g., [447]) where the plasma is cooler and more dense.

The possibilities to resolve the Zeeman line shift also improve at infrared wavelengths because the line splitting increases with λ^2 while the temperature broadening increases only linearly with the observing wavelength λ. For example, combined Zeeman and Hanle effect measurements of Ca I emissions at $\lambda = 850$ and 854 nm have been made above sunspots [448] and of the He I line at $\lambda = 1083$ nm above active regions [449, 450]. Form these spectro-polarimetric measurements the full magnetic field vector could be retrieved in the low chromosphere and near the base of the corona, respectively.

Successful attempts to detect the magnetic field in the hot corona above the limb have for a long time been restricted to the observation of resonance scattering of the forbidden line $\lambda = 530$ nm emitted by Fe XIV (e.g., [451]). The radiation is excited at the transition from an excited state with a life time which greatly exceeds the Larmor period imposed by the excited state's magnetic dipole moment. The observed orientation of the polarization axis of the scattered radiation then relates to the orientation of the coronal magnetic field perpendicular to the line-of-sight.

By a careful analysis of the Hanle effect together with Doppler shifts experienced by solar wind ions on the resonantly scattered O VI line at $\lambda = 103.2$ nm the magnetic field above the pole can be constrained to within a few G [452]. The longitudinal Zeeman effect has only recently been successfully detected in the corona, 0.15 R$_\odot$ above the limb for infrared emission lines from Fe XIII at $\lambda = 1075$ and 1080 nm [453]. Other infrared lines which are useful for coronal Zeeman and Hanle effect observations are currently investigated [454, 455, 456].

In spite of this recent progress our present knowledge of the magnetic field is still largely based on extrapolations from photospheric magnetograms where Zeeman and Hanle effect measurements are often routinely made from ground based observatories (e.g., the Wilcox Solar Observatory, WSO, near Stanford, the Synoptic Optical Long-term Investigation of the Sun, SOLIS, at Kitt Peak, the Vacuum Tower Telescope, VTT, and the Heliographic Telescope for Solar Magnetic and Instability Studies, THEMIS, on Teneriffe) and from space (Michelson Doppler Imager, MDI, on board the SoHO spacecraft and the facilities on the upcoming Solar-B satellite).

Quasi-static extrapolations of the photospheric field into the corona are usually justified by the drastic change of the role the magnetic field plays in the dynamics of the photosphere on the one hand and in the corona on the other hand. The magnetic flux which emerges from the solar surface is tightly anchored in the highly conducting, massive and high β photosphere and is there pushed around at a typical speed of 1 kms^{-1}. In the low β corona magnetic forces dominate and force imbalances are transmitted along the magnetic field with an Alfvén speed of about 1000 kms^{-1}. The line-tied coronal field therefore immediately adjusts to the boundary flux imposed in the photosphere while the photosphere hardly reacts due to its large inertia to occasional rapid processes in the corona. However the height region sandwiched between photosphere and corona, the chromosphere and transition region is much more complex than many of the extrapolation models suggest and the impact of the Sun's lower atmosphere on these models has not yet been fully assessed.

To accomplish the extrapolation, different approximations to the full set of MHD equations governing the magnetic field in the corona are used. In its simplest form, the corona is assumed to be current-free and Gauss' theorem is used to obtain a potential field (or Laplace field) approximation of the coronal magnetic field which matches the observed normal component on the solar surface and some reasonable outflow boundary condition which mimics the solar wind impact on the field at a distance of 1-2 R$_\odot$ above the solar surface (e.g., [457])

In the low corona, the small value of β allows us to neglect pressure and gravity forces to lowest order, so that in a stationary corona the Lorentz-force $\mathbf{j} \times \mathbf{B}$ must approximately vanish. This requires $\mathbf{j} = \alpha \mathbf{B}$ for some yet unknown scalar α. The vanishing divergence of the current density $\mathbf{j}$ has the consequence that α must be constant along any given field line, $(\mathbf{B} \cdot \nabla) \alpha = 0$.

The coefficient α has the dimension of an inverse length and $1/\alpha$ can be visualized as the distance over which coronal currents induce perturbations in $\mathbf{B}$ of the same order as the potential field strength. Values of $|\alpha| \lesssim 10$ R$_\odot^{-1}$ have been inferred from, e.g., vector magnetograph measurements [458, 459].

The force-free approximation however it is intrinsically nonlinear and if based on boundary information alone, its calculation is a highly ill-posed problem (see discussion in, e.g., [460, 461]). For this reason, a "light" force-free version is often employed where α is reduced to a global constant (e.g., [462]; so-called linear force-free (or Taylor field, [463]) which has its own physical significance as will be discussed in chapter 8.7 below).
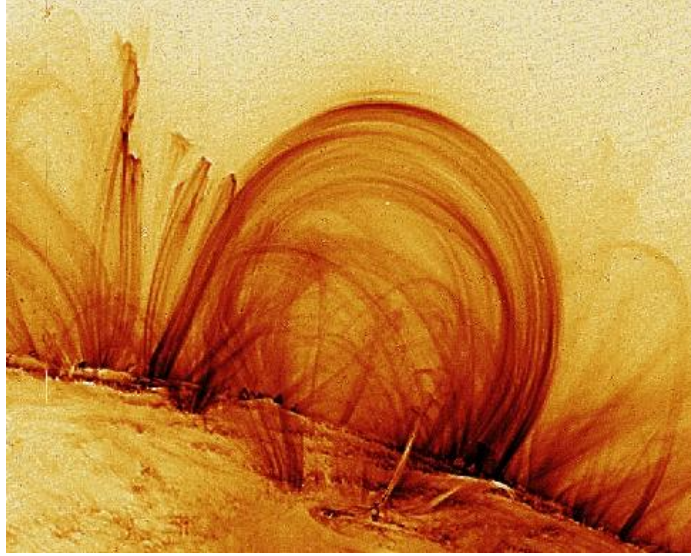
Figure 24. Highly structured loops above the limb taken in EUV from the TRACE satellite. The loops could be viewed as materialized magnetic field lines. The TRACE telescope today yields the highest spatial resolution for these type of images.

Besides, it is not quite obvious which boundary data is necessary and sufficient for a unique nonlinear force-free field extrapolation. The invariance of α along the field lines, for example, has the consequence that the overall flux conservation $\int_S B_r d^2x$ $= 0$ normal to the solar surface S is replaced by the much stricter requirement that for every value of α the differential flux $\int_{dS(\alpha)} B_r d^2x$ must vanish. Here $dS(\alpha)$ is the differential subsurface of S where α assumes a given value. Even more constraints exist (see, e.g., [464, 465]) and various numerical methods have been proposed to solve the force-free field boundary value problem [466, 467, 468, 469, 470, 471, 472].

Full MHD models are required if the outer parts of the corona are to be included where β approaches unity. Quasistationary solutions can either be obtained by relaxation [473, 474] or from solving a variational problem (e.g., [475]).

With the advent of space missions like Yokhoh, the Solar and Heliospheric Observatory (SoHO) and the Transition Region and Coronal Explorer (Trace) high resolution images with high cadence rates became available from coronagraphs, UV and X-ray cameras. Their data show the radiation from plasma which has risen from hot spots in the chromosphere upwards along individual field lines and thus trace out thin magnetic flux tubes in the corona . As an example Fig. 24 displays loops above the limb observed by the TRACE satellite. The images of these loops therefore tell us much about the topology of the coronal field and the changes it undergoes by quasi-static line-tying and also when the field configuration becomes eruptive (see the recent review [476]). The image data now are available with both high spatial and temporal resolution so that quantitative 3D reconstructions from the observed 2D projections are being attacked to verify magnetic field extrapolations from surface magnetograms.
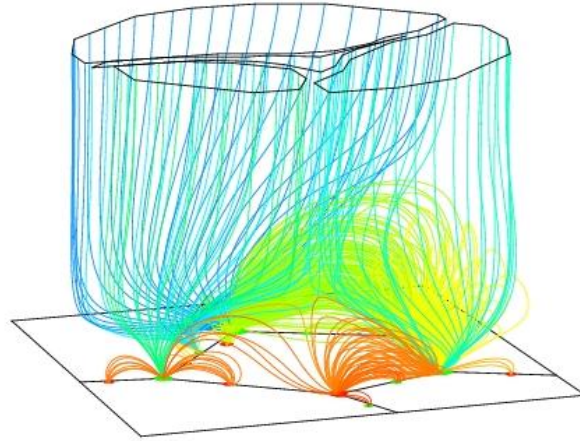
Figure 25. Magnetic field above a set of magnetic elements located at the edge of supergranule cells (lines on the solar surface). Part of the field lines open to the corona while the carpet field connects elements of different polarity flux on the surface. The field lines are calculated from a potential field model.

8.2. Chromospheric network, canopy and carpet

As described in chapters 3 and 7, the magnetic flux which emerges from the photosphere is not distributed smoothly over the solar surface but highly concentrated in small flux elements. The upper photosphere and chromosphere form a relatively cool layer up to a height of several 1000 km above the visible surface where the plasma density and pressure decrease with a scale height of only a few 100 km. As a result the flux elements in turn widen their horizontal cross section (see Fig. 18)to keep the pressure balance with the surrounding plasma. Eventually, individual flux tubes are bound to merge with flux of equal polarity or bend into magnetic arches to connect to flux elements of opposite polarity as sketched in Fig. 25.

The horizontal fields at the bottom of the 'wine glasses' and of the lowest arches and formed this way above the supergranulation cells constitute the magnetic canopy. Observations have shown that in the quiet chromosphere the flux tube expansion is relatively gentle, the filling factor is small so that the flux tubes merge only in the chromosphere and form a canopy base at about 1000 km above the photosphere. In active regions the magnetic filling factor is enhanced beyond 50% in the upper photosphere [237]. Consequently, neighboring flux tubes merge already in the photosphere [342]. In sunspots, this expansion is so rapid, that the formation of a layer of horizontal fields occurs already in the mid photosphere.

Some observations yield evidence for a particularly rapid expansion of the magnetic field in the lower chromosphere leading to the formation of a nearly horizontal field canopy at a height of roughly 800 km above τ=1, cf. [477, 478, 479, 480]. It has been shown that magnetic canopies at these heights can be produced if the chromosphere is very inhomogeneous in temperature, with hot flux tubes and cool gas in between them [481]. The necessary inhomogeneity of the chromospheric plasma was proposed by [482, 483] and [484]. Recent observations of CO molecular emissions
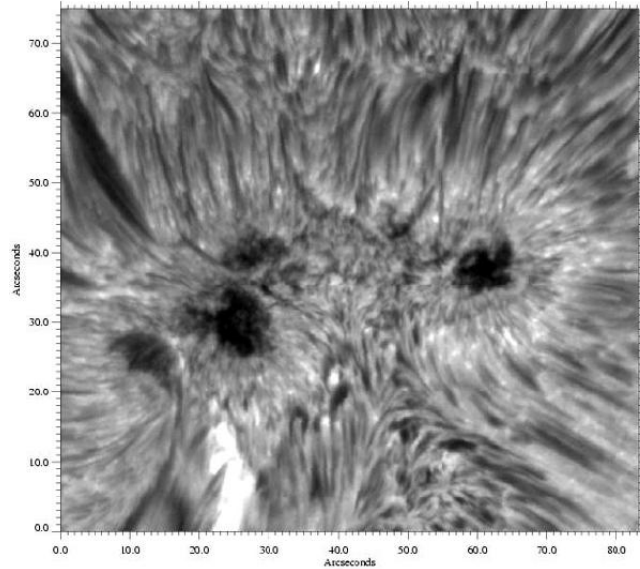
Figure 26. Hα image taken by B. de Pontieu with the Swedish Vacuum Solar Telescope (SVST). The dark elongated fibrils are radially arranged around a group of small sunspots indicating strongly diverging field lines emanating from the sunspots

in the infrared seem to confirm this highly structured lower chromosphere [485]. The plasma β is just at the verge between values $\gg 1$ in the photosphere to $\ll 1$ in the upper chromosphere. Hence, the canopy fields may have some influence to thermally insulate the plasma and to sustain the temperature inhomogeneity.

Magnetic arches above the canopy up to the height of the transition region typically span larger horizontal distances of several 10^4 km and more. These field structures make up the magnetic carpet [486]. Again, temperature and plasma density and flow vary enormously among these flux tubes. Cool chromospheric material and hot coronal plasma may lie side by side with neighboring magnetic arches separated only by some 10^3 km [487]. Images taken in Hα disclose the horizontal direction of these arches and hence of the predominant horizontal field direction in this height by the orientation of fibrils at the edges of plages and in the neighborhood of filaments. In these images fibrils are visible as elongated dark threads (see Fig. 26).

The distinction between the lower chromospheric internetwork plasma, the canopy as the lowest magnetic layer and the carpet field above is not very precise and has been critizised [488] since even the internetwork region is not entirely field free (see chapter 7.7). Hence, with smaller flux elements being taken account of, Fig. 25 would have to be extended by a large number of low flux magnetic connections to the surface area inside the supergranulation cells.

8.3. Coronal holes and plumes

Coronagraph observations reveal a striking inhomogeneity of the Sun's corona and demonstrate the enormous influence the magnetic field has in structuring the Sun's
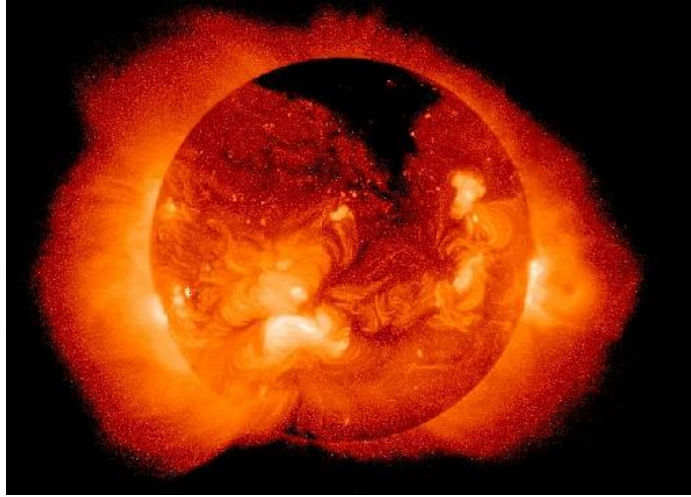
Figure 27. Bright magnetically closed coronal regions in an X-ray image of the Sun from the YOHKOH spacecraft. The dark polar regions are coronal holes from which the magnetic field escapes into the heliosphere.

atmosphere. An extended part of the solar surface, about 20-30%, is covered by coronal holes. These are surface regions which are magnetically connected to the outer heliosphere [489, 490, 491, 492, 493]. A local dominance of photospheric flux elements of one polarity provides a net field of about 10 G or more at the coronal base which feeds the open flux.

There is no containment of plasma possible on these open field lines but the plasma is blown away from the Sun along the open field lines to feed the fast solar wind [494]. Already down at the coronal base blue shifts of as much as $\simeq 3$ kms^{-1} have been observed [495]. The plasma density on these field lines is therefore reduced by almost an order of magnitude compared to regions in the corona which are permeated by magnetically closed field lines [496]. The reduction in density reaches down to the base of the corona. Since emission intensities in X-ray and EUV lines roughly scale with the plasma density squared, coronal holes are clearly distinguishable by the lack of X-ray and EUV emission (see Fig. 27).

The flux imbalance in a coronal hole not only controls the net magnetic flux that can effectively penetrate the chromosphere and transition zone but also influences the height, length and hence temperature of the resulting closed field arcades. The larger and hotter loops are found strongly underrepresented in the coronal hole relative to the quiet Sun, while shorter and cooler loops are almost equally present in both regions. This additionally contributes to the darkening of coronal hole areas [497]. Only for emission lines formed at temperatures below about $7 \, 10^5$ K, the intensity difference between coronal holes and the closed-field quiet Sun regions appear less pronounced [498, 499].

Another indicator of coronal hole regions on the solar surface are observations of the chromospheric He I 1083 nm line made regularly at Kitt Peak Observatory. This line appears brighter in coronal holes than on closed field line regions. The physics behind this radiation process is, however, very complex.

The shape and distribution of coronal holes on the Sun's surface changes
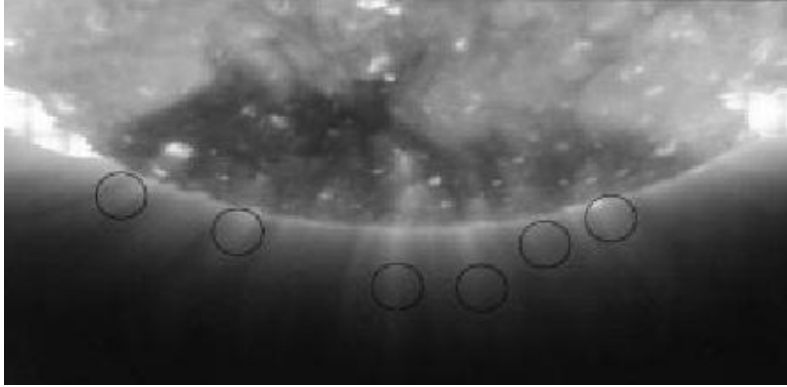
Figure 28. Polar plumes over the Sun's southern coronal hole during times of low solar activity. The almost radially extended density striations outline the direction of the open magnetic field from the south pole. (from [502]).

drastically during the 11-year's activity cycle. At activity minimum coronal holes are concentrated at high latitudes and cover, with opposite magnetic polarity, the polar caps of the Sun almost entirely down to about a latitude of 50° - 60°. The coronal whole then occupies about 20% of the solar surface with an average magnetic flux density of 5-10 G [493]. The latitudinal average flux density below 50° cancels to less than a Gauss [500].

At activity maximum, coronal holes are distributed in patches all over the solar surface, sometimes linked by "narrow coronal hole channels" to one of the polarities of a larger bipolar region. These channels sometimes extend over a good fraction of $R_\odot$ and may also cross the equator. Relations between the coronal hole shape and the lowest multipole moments of the magnetic surface field during solar maximum have been derived by [501]

A large fraction of the open magnetic flux at these times escapes from active regions and their neighborhood. The enhanced field strength in these areas is compensated by a smaller overall coronal hole area of only 5-10% of the solar surface [493], so that the open flux is remarkable stable over the solar cycle.

At solar minimum some magnetic flux tubes which emerge out of a coronal hole are visible against the dark background sky in coronagraphs or EUV images as polar plumes. These are occasional field aligned plasma striations with a life time of several days. The photospheric origin of plumes is newly emerged small bipolar flux [503] which reconnects with the background coronal hole field. The reconnection seems to provide the heating needed to support the enhanced density inside the plume flux tube. Enhancements by a factor 5 and more with respect to the coronal hole background density have been observed [504]. The plasma outflow speed into the solar wind from plumes, however, seems to be reduced [505, 495].

8.4. Active regions and loops

The brightest objects in EUV and soft X-rays images of the Sun are active regions. They are associated with strong magnetic bipolar regions on the Sun's surface. These regions form within a few days as massive amounts of magnetic flux break through the solar surface. They are irregularly shaped, sometimes arranged in groups but
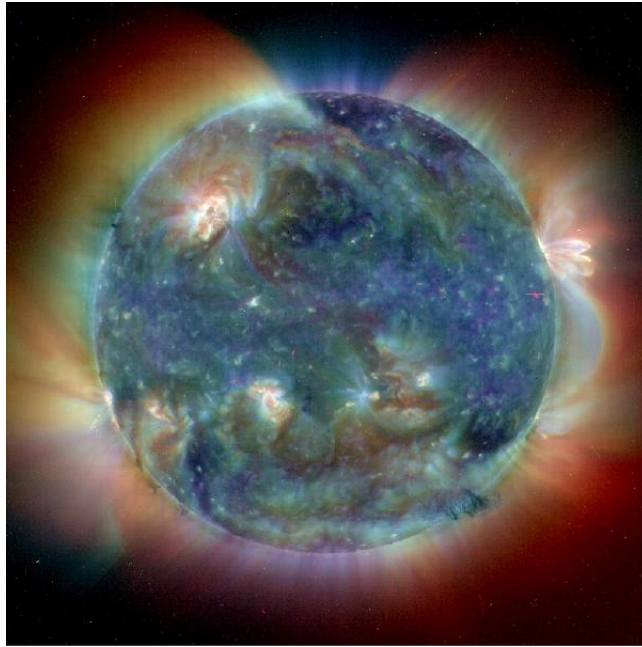
Figure 29. Bright active regions in the EUV image taken by the EIT instrument of the SoHO spacecraft. The image is actually a composite of images taken at three different wavelengths (17.1, 19.5 and 28.4 nm) and superposed in blue, green and red. The solar surface background appears dark because the continuum radiation from the cool surface at these wavelengths is well below the emission from the hot coronal loops. On the Sun's limb active regions loops are distinctly visible.
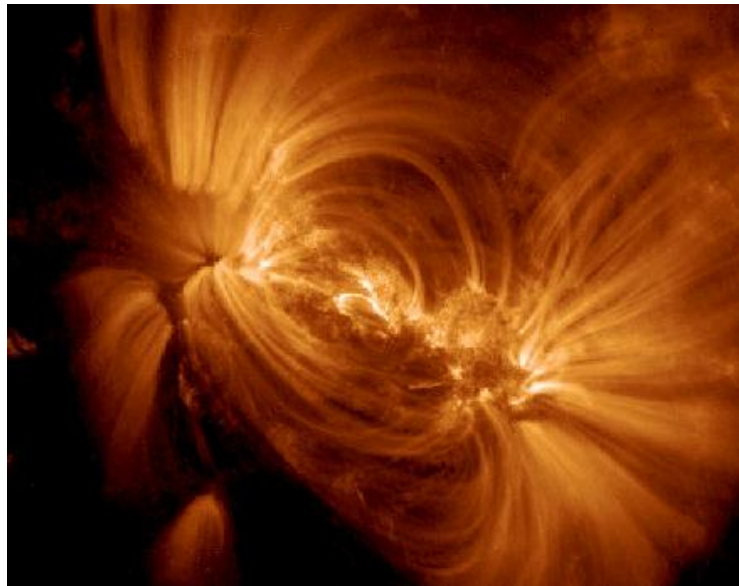
Figure 30. Details of bright loops above an active bipolar region seen in EUV wavelengths by the TRACE spacecraft.

they are always arranged in the same longitudinal order ("Hale's Law", see 3.2.2). Magnetic flux densities of up to 100 G and more can be reached in the lower corona above a strong bipolar region. The lifetime of active regions may extend over many solar rotations though they start to diffuse after one or two weeks which gently reduces the flux density and the overall (absolute) flux that can build up in the lower corona. Differential rotation together with the diffusion also causes a characteristic deformation of the active region towards the end of its life time (see Fig. 1).

Flux tubes emerging from an active region are filled with plasma which is markedly hotter than elsewhere in the Sun's atmosphere and makes them distinctly visible in EUV images (Fig. 30) as loops which magnetically connect the opposite polarities of the bipolar region. Which physical mechanism provides the heating energy is still an active area of research. The enhanced density scale height on flux tubes rooted in active regions makes them distinctly visible in EUV and soft X-rays and also in optical emissions from ions which form at temperatures well above 10^6 K. An example is the forbidden green corona line at $\lambda = 530$ nm emitted from Fe XIV. Positive correlations between the emissivity at various wavelengths and the field strengths at the foot points of the respective field line have been derived by several authors [506, 507, 508]. Hence there is strong evidence that the magnetic field is an important ingredient in the heating mechanism for coronal loops.

Comparisons of extrapolation models (see chapter 8.1) of the coronal magnetic field with the observed shapes of field lines in EUV images help to estimate the electric current strengths which flows along these field lines. Especially in active regions these currents may be appreciable and lead to marked deviations of the shape of observed loops and their models based on a potential field [509, 510, 511, 512, 513]. A substantial current was also found by [514] when they tried to match their field extrapolation to the loops observed by [449] near a young active region.

Loops visible in EUV images which emerge from active regions appear astonishingly thin even though simple field extrapolation predicts a widening of the flux tube's cross section with height (see Fig. 24 and discussion by [515]). An explanation for this observation might be that at lower heights the emitting flux tubes are so thin in diameter that they cannot be resolved and the widening of the cross section therefore remains undetected. Also, unresolved fragmented bundles of emitting loops ("multithreads") of different temperature and density have been proposed to explain the non-isothermal emission observed from these loops [516, 517, 518]. As an alternative explanation a twist of the thin flux tubes has been suggested [519, 520, 515]. This requires a field-aligned current which induces a toroidal magnetic field and a magnetic curvature force which then keeps the flux tube concentrated on a small cross section like in a plasma pinch device in the laboratory. Simulations have shown that as the current increases, the loop axis also rises, and eventually becomes distorted off the loop plane into an S-shape. Finally, Mikic et al. found that the loop is driven kink unstable if the number of turns over the whole loop length exceeds about 2.4 [519, 520].

In soft X-rays and less pronounced in EUV, the expected S-shape deformation of bright loops is indeed observed ("sigmoids"; see, e.g., [521, 522]). The sense of the S reflects the sign of α or of the current helicity density $\mathbf{j} \cdot \mathbf{B}$ [523] on the respective magnetic flux rope. This sign has been found to be almost unique on either hemisphere but reversed with respect to the other hemisphere ("hemispheric helicity law"; [524, 525]). Why the S-shape for EUV loops is not as apparent as for X-ray loops is not clear. The former are usually lower, shorter and therefore may be
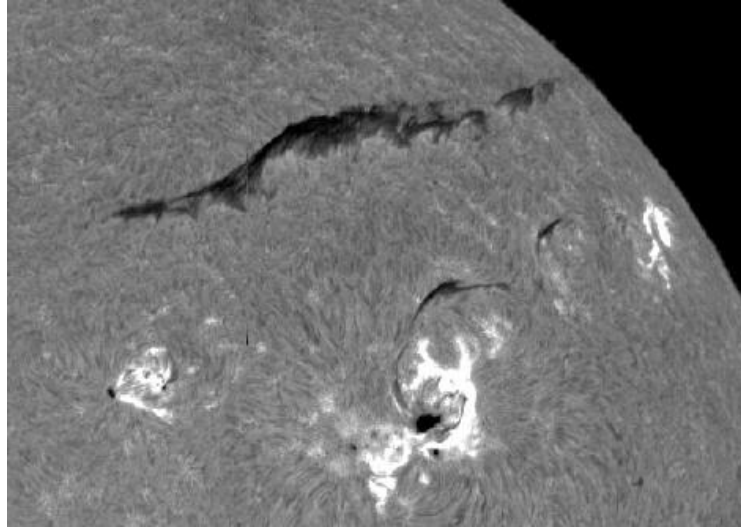
Figure 31. Dark filament lying above the surface of the Sun in an image taken at the emission line of Hα by the Big Bear Solar Observatory (BBSO). The cool filament material absorbs the Hα radiation from the surface so that they appear dark on the solar disk. Closer to the equator, a bright active region with smaller filaments in the neighborhood

more stable against an S-shape distortion than the higher reaching X-ray loops.

8.5. Filaments and helmet streamers

Regions of opposite polarity of the radial magnetic field in the lower corona are separated by a neutral line where the vertical magnetic flux at the coronal base changes sign. Often, especially in the vicinity of active regions and sunspots, filaments are stretched out above the neutral line. A filament is a vertical sheet of cool and high density plasma with temperature of about 10^4 K hovering some 10^4 to 10^5 km above the photosphere. Often they stretch out horizontally over 10^5 km and more. Due to their high density, the filament material is optically thick. On the disk, filaments therefore absorb the solar surface emissions so that they appear dark (Fig. 31). When observed above the limb, their dense plasma intensively scatters the solar radiation so that they are seen as bright prominences. A good account on the observational facts about filaments can be found in [526] and [527]. Depending on the activity of the neighborhood, filaments also show some activity but in general they are remarkably stable and resistant to nearby perturbations. Filaments originally formed above the neutral line between the poles of a bipolar active region often survive the active region as a quiescent prominence by weeks. The more astonishing is that many filaments sometimes disappear after days and weeks of quiescence in a sudden eruption within a few hours.

Closer inspection in the wings of Hα and in EUV Doppler shifts reveal a considerable, presumably field-aligned mass flow. The fact that the filament mass does not simply rain down onto the solar surface can only be attributed to magnetic fields which suspend the plasma against gravity. Also, their apparent stability on the one hand and the vigor of their eruption on the other hand are evidence of an energetic magnetic field system which extends far beyond the visible filament.

Hanle effect measurements of the magnetic field that permeates the dense, cool prominence material reveal flux densities of 5-10 G for quiescent prominences but may locally reach up to 100 G in more active ones [447, 526]. The field inside the filament is found to be almost horizontally oriented with a considerable component elongated along the filament axis, i.e., along the neutral line underneath. Leroy, Bommier and coworkers found an average angle of the filament magnetic field with respect to the neutral line of 40±30 degrees [447]. The component perpendicular to the neutral line was in the vast majority of cases found in opposition to the polarity of photosphere below ("inverse polarity law"). Also the orientation of the field component along the neutral line was found to be systematic ("chirality law"): if $\hat{\mathbf{p}}$ denotes the horizontal unit vector normal to the neutral line in normal-polarity direction (i.e., from magnetic "+" to "−") and $\hat{\mathbf{z}}$ the vertical unit vector then the field component along the neutral line is always in direction of $\hat{\mathbf{p}} \times \hat{\mathbf{z}}$ in the northern hemisphere ("dextral") and in $-\hat{\mathbf{p}} \times \hat{\mathbf{z}}$ direction in the southern hemisphere ("sinistral"). The rules for two components of the field inside the filament seem to hold independent of the solar cycle and can be expressed in brief as $\mathbf{B}_{\text{filament}} = a\hat{\mathbf{p}} + b\hat{\mathbf{p}} \times \hat{\mathbf{z}}$ where a and b have the same order of magnitude with $a < 0$ ("polarity law") and $b > 0$ or < 0 on the northern or southern hemisphere, respectively.

(b) t=430
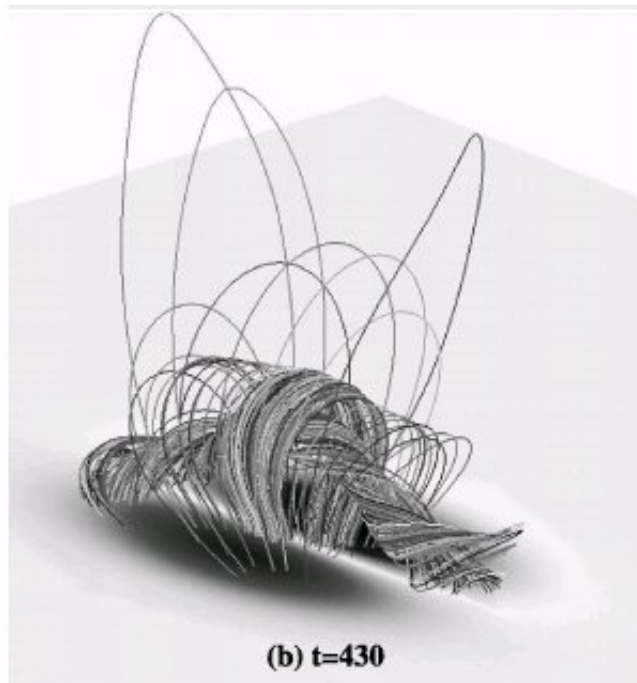
Figure 32. Field lines of the numerical model for a filament [528]. The shading on the ground denotes the surface field strength. Note the central helical flux tube enclosed by an outer arcade field.

The simplest field topology which properly connects the photospheric field and the field observed inside the filament is originally due to Kuperus and Raadu [529] and has been further extended to 3D by numerous authors (e.g., [530, 528, 531]). Fig. 32 displays the field configuration assumed to exist in the vicinity of a filament.
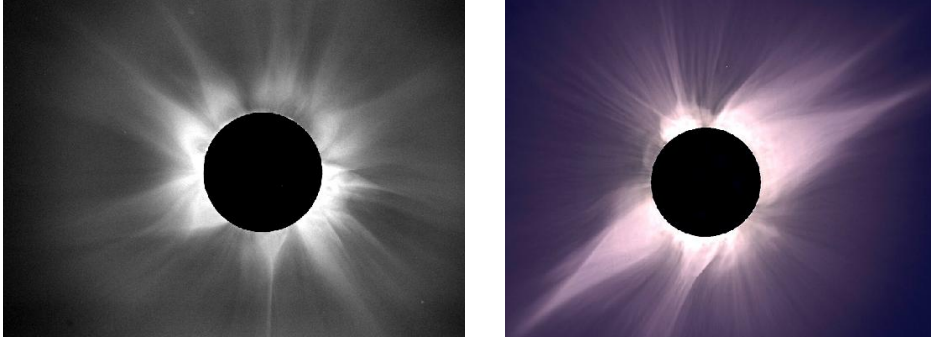
Figure 33. White light coronagraph images of the solar eclipses 1980 (left) and 1991 (right). In the right image helmet streamers extend out to beyond three R$_\odot$ in all directions at times of high solar activity 1980 while they are more concentrated at lower latitudes during times of more moderate activity as on the left example (images courtesy of the High Altitude Observatory).

It involves a twisted magnetic flux rope, stretched along the neutral line, which gives the necessary support to the cool filament plasma in the upwardly curved pockets of the helical field [532]. In these heights, the horizontal $\hat{\mathbf{p}}$ component of the magnetic field, belonging to the flux rope, is directed in inverse polarity direction. At the bottom of the flux rope closer to the surface, this field component eventually has switch to normal polarity and the field components in a plane normal to the neutral line describe a saddle point. The location of these saddle points for all planes along the flux rope are referred to as the "x-line". Hence the filament material is thought to reside above the x-line at the bottom of the flux tube in a height where the magnetic field is about horizontal and is directed in inverse polarity direction, as observed.

The twist of the flux rope relates the observed geometrical chirality to the more physical current helicity density $\mathbf{j} \cdot \mathbf{B}$. With the above model, dextral filaments would have a flux rope with negative current helicity, sinistral filaments need positive current helicity. This way, the chirality law also agrees with the hemispheric helicity rule for the sigmoid distortion of X-ray loops mentioned in the previous section. In fact, the surface current helicity density observed by vector magnetographs in active regions and sunspots where the field intensity is strong enough to be reliably measured shows a clear dominance of the sign expected from the helicity rule on either hemisphere independent of the solar cycle [533, 459].

Also other observed features like the orientation of the filament barbs (see the filament 'legs' in Fig. 31) and the horizontal field orientation derived from fibrils (Fig. 26) in the filament channel comply with the above general hemispheric chirality or helicity rule (e.g., [524, 534]).

The filament magnetic field model also complies with the general orientation found for coronal X-ray arcades which span the neutral line at heights well above a filament [535]. The magnetic arcade field often continues outwards to more than a solar radius. Limb observations with coronagraphs of the corona above a neutral line reveal, if seen head-on, a helmet streamer above the polarity inversion separated from the filament by a cavity of depleted plasma density (see Fig. 33). The cavity may reach out above the Sun's surface for a fraction of $R_\odot$ while the tip of the helmet streamer extends to 2 $R_\odot$ or more. The cavity and the inner edge of the helmet streamer show the concave shape which we expect from the magnetic field lines of an arcade above a

neutral line. The outer edge of the helmet streamer, in contrast, is straightened out into interplanetary space and joins into the heliospheric current sheet. Coronagraph observations with Lasco/SoHO show that these cusps may be the source region for the dense, slow solar wind [536]. At times of small coronal activity, the streamers extend almost two-dimensionally in azimuthal direction and cover the lower heliomagnetic latitudes ("streamer belt"). Whether the helmet streamer magnetic field possesses a significant longitudinal component along the neutral line underneath like the filament, a feature which seems to be present in according MHD models [473], has not yet been observed.

While the Kuperus-Raadu flux rope magnetic field topology for the filament is widely accepted, there is still a debate about how the flux rope is formed, what gives this configuration its stability and how the stable field configuration may turn into a filament eruption within hours. For the genesis of filaments shear motion of the field line foot points along the neutral line with either flux cancellation (e.g., [537, 538, 539, 530, 540]) or emergence of properly wound flux (e.g., [524, 541, 542, 543, 522]) have been considered. Least understood, however, is the eruption process. It often starts with a slow rise of the filament and the arcade field a few hours before both are rapidly lifted upwards (see Fig. 34). Following the eruption, a set of loops across the neutral line are left behind which brighten in EUV and X-rays ("post-flare loops", see Fig. 36). The chromosphere at their feet on either side of the neutral line starts to radiate intensively in Hα ("two-ribbon flare"). More observational details and also conceptual ideas about filament eruptions have been collected by, e.g., [544].

Tens of Minutes to an hour after the eruption coronagraphs reveal large parts of the overlying helmet being blown away into the heliosphere as a coronal mass ejection (CME). In many cases the quiescent three-part structure, i.e., filament - cavity - helmet, is maintained in the ejecta. Often the filament material, distinctly visible in coronagraph observations, displays the helically twisted structure of the original filament flux rope (see Figs. 35 and 37) The imprint of this helical structure can still be observed in-situ at 1 AU in the magnetic clouds into which the CME evolves as it propagates into the heliosphere [545, 546, 547, 548].

The few phenomenological facts presented so far convincingly demonstrate the overwhelming role of the magnetic field in the Sun's atmosphere. For the remaining part of this chapter we would like to turn the logic around: given the dominance of the magnetic field in the corona, one can derive certain characteristics or constraints of coronal processes. Again due to lack of space we can touch only few of the issues discussed in the present literature.

8.6. Magnetic surfaces and null points

The magnetic field induces a structure into space: the high mobility of charged particles parallel to the field compared to their perpendicular mobility brings points on the same field line into a physical neighborhood even though they may geometrically be far apart.

In laboratory plasma devices with some symmetry imposed by the boundaries of the plasma chamber, field lines may ergodically cover whole surfaces. These magnetic surfaces are then spanned locally by the divergence-free fields $\mathbf{B}$ and $\mathbf{j}$ and can be labeled by the local plasma pressure p since $\nabla p = -\mathbf{j} \times \mathbf{B}$ is normal to these surfaces. In the force-free limit when the pressure p becomes negligible, surfaces $\alpha = \mathrm{const}$ can
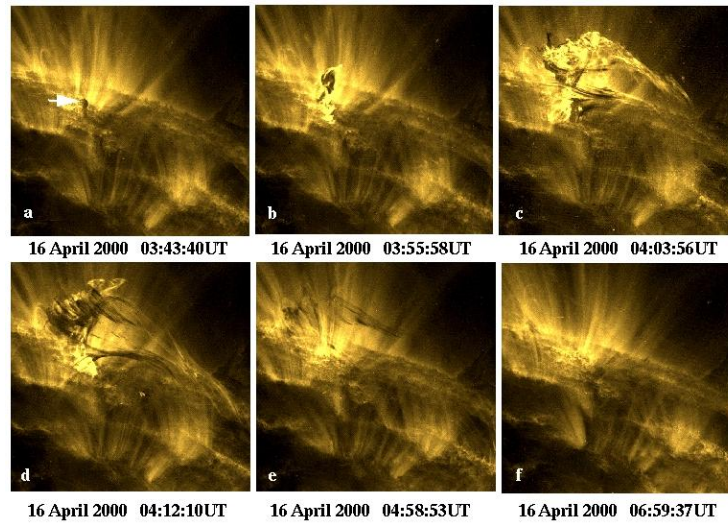
Figure 34. Eruption of a small filament observed by TRACE. The initial location of the filament is at the tip of the arrow in the first panel.

Figure 35. Cool filament material just after eruption carried high up into the corona by magnetic forces as observed by the EIT instrument on board SoHO.

play a similar role. Since α is constant along a field line, any α contour on the solar surface maps to a surface in a force-free field corona. These nested surfaces are an important concept if, e.g., we want to define what exactly we mean by a flux tube or flux rope. It is possible however at least for some regions of the corona, that the flux distribution on the solar surface is so heterogeneous and the related magnetic surfaces
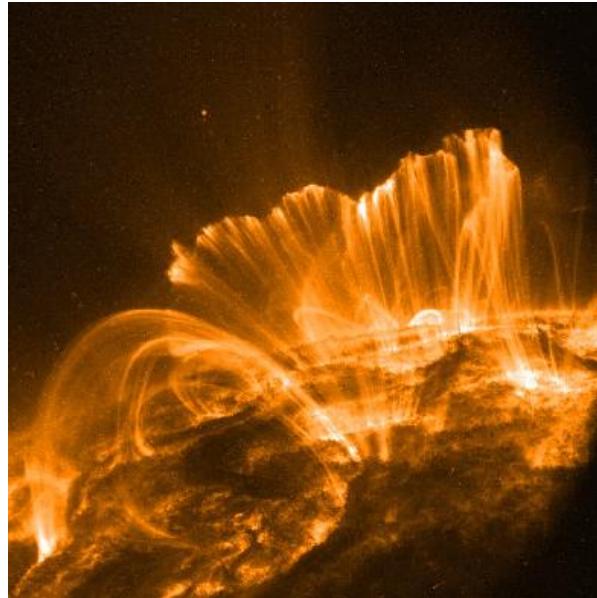
Figure 36. Post-flare loops arranged in an arcade crossing the magnetic neutral line. The EUV image was taken by the TRACE spacecraft
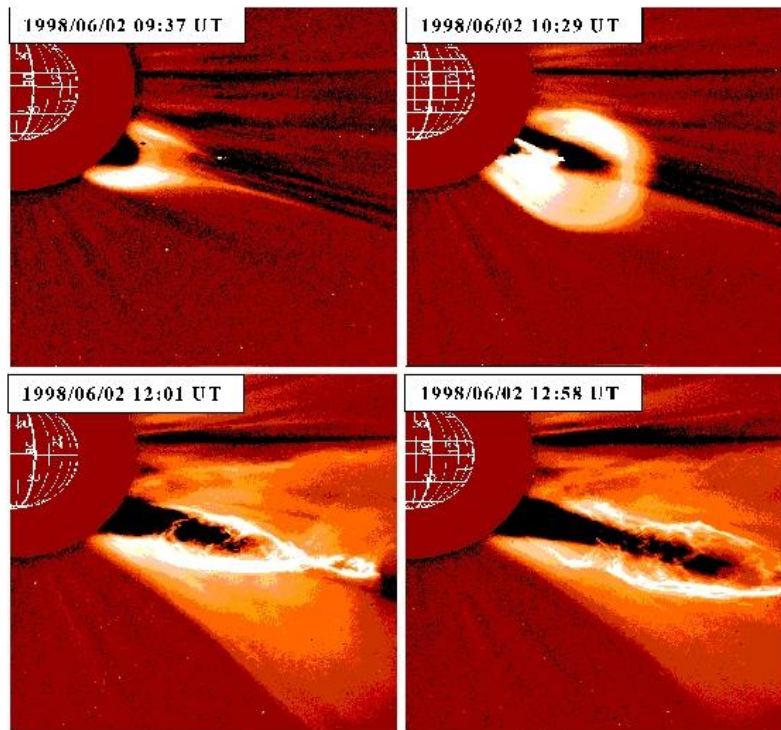
Figure 37. Sequence of images showing the eruption of coronal mass into the heliosphere observed by the LASCO coronagraph on board the SoHO spacecraft.

are so eroded that constant-α contours and surfaces are no longer useful.

Another concept to order magnetic-field-permeated, 3D space is by topological connectivity. Provided we can separate the surface flux in an enumerable set of localized flux elements, field lines which connect the same source elements may be defined a flux tube. Obviously, the surfaces of these flux regions are particularly prone to reconnection. Especially those points, where the magnetic field vanishes have been found to be critical for the stability of the magnetic configuration [549]. In a 2D geometry, the x-lines as they exist below a filament flux rope, are the preferred site of reconnection. In a 3D magnetic field configuration, however, it turns out that lines of vanishing magnetic field strength are structurally unstable: a slight random change in the field components dissolves a $|B|$=0 line into a number of individual $|B|$=0 points. Only these $|B|$=0 points ("null points") are stable since small changes in any field component make the point move but do not destroy it. Magnetic null-points have therefore attracted quite some attention recently [550, 551, 552, 484].

Obviously, the way we defined flux tubes above, a null-point has to lie on the surface of a flux tube. The field in its neighborhood can be approximated by the first term of its Taylor expansion $\mathbf{B}= (\partial\mathbf{B}/\partial\mathbf{x}) \cdot (\mathbf{x} - \mathbf{x}_0)$ and is therefore topologically determined by the Jacobian matrix $(\partial\mathbf{B}/\partial\mathbf{x})$. Its eigenvalues and associated eigenvectors determine the orientation of a fan plane and an orthogonal spine direction formed by field lines which pass close to the null point as sketched in Fig. 38 [550]. At larger distances from the null point, the field lines on the fan extend to a surface ("separatrix", as this surface separates differently connected flux regions), and the spine extends into a singular field line. The whole set of interwoven null points, fan surfaces and spines form what is often referred to as the skeleton of a magnetic field.

In the region near the null point energetic plasma may be locally trapped and isotropized because the mirror force prevents it from escaping both along the spine and, somewhat less effectively, along the fan. It has been found that the intersection line of fans of related null points, the so called separator, is particularly prone to reconnection (e.g., [549, 553, 554]). Priest and coworkers investigated systematically the changes of the skeleton of a potential field with respect to changes of surface magnetic elements (e.g., [555]). These topological changes indicate the state towards which a real plasma might want to relax. If this state is topologically different (i.e., has a different skeleton) from the original state, it can only be reached by reconnection taking place.

8.7. Energy and helicity of the coronal magnetic field

The energy output from the chromosphere and corona is considerable: about 1000 and 300 Wm^{-2} are the estimated mean outward energy flux density from the respective atmosphere layer of the quiet Sun [556, 557] into EUV and X-ray radiation, electron heat conduction and into the solar wind. Individual active regions and bright loops radiate locally up to 10^4 Wm^{-2} (e.g., [558, 559]). Large CMEs have been estimated to release up to 10^{26} J within minutes [560] which is comparable to the radiative loss of the whole corona during one or two days.

According to a concept promoted by Parker in a series of papers, (e.g., [561, 410]), large flares and CMEs are just the bottom end of eruptive processes on all scales which convert magnetic energy into heat and bulk plasma motion. The source of this energy is assumed to be the continuous motion of the foot points of magnetic field lines which
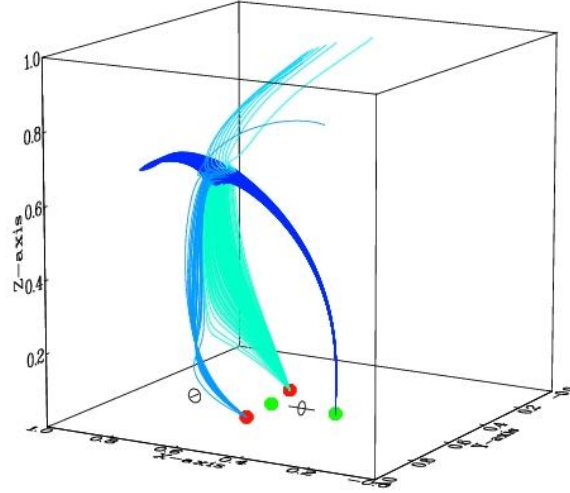
Figure 38. The magnetic field lines through the vicinity of a coronal null point (at $z \sim 0.6$) of the potential field due to four magnetic surface elements (full dots on the surface, the magnetic sign of the surface elements is color coded in red and green). The spine connects to the element on the right side and leaves the box on its left end. The two reversed polarity elements on the front and rear side lie on the curved fan surface. Two further null points in the photosphere are indicated by a small stick/disk which shows the orientation of their respective spine/fan. A fourth null point is located underneath the photospheric surface.

leads to a stretching and braiding of the coronal field. The energy flux induced by this surface motion is easily estimated if the frozen-in condition $\mathbf{E} = \mathbf{v} \times \mathbf{B}$ is used in the Pointing flux vector component normal to the solar surface. The resulting power transported through the solar surface is (here and below, subscripts h and r refer to the horizontal and radial components on the solar surface, respectively)

$$P_E = \frac{1}{\mu_0} \int\limits_{\text{photosphere}} \left(B_h^2 v_r - (\mathbf{B}_h \cdot \mathbf{v}_h) B_r \right) \, d^2x \qquad (8.1)$$

P_E has two terms which are the contributions from flux emergence/cancellation and from work done by line-tying against magnetic stress. Both terms are highly fluctuating and their averages are not straightforward to estimate. Parker argues that the line-tying term alone can yield the power necessary to explain the radiative output of the corona while the term due to flux emergence and cancellation rapidly changes sign and gives only a minor contribution to the energy balance. The contribution of the line-tying term can be estimated if we regroup the respective surface integration measure $B_r \, d^2x$ pairwise into the flux elements at the conjugate foot points of the closed flux tubes. With $B \simeq$ 1-10 G, and a mean foot point separation velocity of $\simeq$ 1 kms^{-1} we obtain the order of magnitude of the quiet Sun energy flux density.

Parker's key paradigm to explain the conversion of this energy input into coronal heat is the conjecture that even if the foot point motion has only moderate gradients, the magnetic field driven by it will eventually develop arbitrarily thin current sheets. These will probably dissipate intermittently in small reconnection events. Field lines which encounter a null point may play an important role in this development of current sheets. Their foot points are close to each other at one end but far separated at the

other so that they may well experience a distinctly different shear.

The emergence of new flux from below the photosphere (first term in the integrand of eq. 8.1) provides another source of current sheet formation. Indeed, many flares are observed to occur near young active regions [562, 563]. First direct evidence for the existence of a strong current sheet in the vicinity of newly emerged flux was obtained only recently [449].

Indeed short duration flares and explosive events are observed with a broad range of energies in EUV and X-rays. Their statistics shows an energy dependent occurrence rate of $f(E) \propto E^{-\eta}$ with $\eta \simeq 1.8$ - 2.6 [476, 564, 565, 566] down to energies of $E = 10^{17}$ J. An exponent η larger than 2 implies that the small energy flares contribute most to the heating of the corona. The total energy input into the corona would in this case depend on the minimum possible flare energy.

It is still controversial, however, whether these frequent, small-energy flares by themselves yield enough power to explain the heating of the corona entirely. Alternative and additional heating mechanisms involve continuous ohmic heating by DC currents (e.g., [567, 568, 411, 449]) and dissipation of waves (e.g., [569],chapter 3 of [570],[571, 572]). Some fraction of the free energy available in small scale flare events will probably be released by exciting one or more of the MHD wave modes. Wave activity and oscillations are observed in the chromosphere and corona in a broad range of frequencies. Spectral line broadening beyond the expected thermal width is often interpreted as due to high-frequency turbulent or wave induced plasma motion. Oscillations of the super-granular plasma with a 3-min period are a prominent feature in chromospheric Doppler shifts. In the corona, transverse Alfvénic loop oscillations at periods of 200-300 s (e.g., [573, 574]) and slow mode type compressional oscillations at even longer frequencies [575] have been observed. Their damping and hence their contribution to coronal heating is, however, still a matter of research [576]. Besides quasiperiodic variations, an increasing, seemingly random, dynamic variability is observed in EUV images, the finer the observational resolution. Some authors [577] take this as evidence that coronal heating occurs rather erratically and on small time scales.

Less controversial than the minimum flare energy is the maximum possible energy released in a large flare or CME. These major eruptions though they are highly dynamic in the corona are not able to change the magnetic flux distribution in the photosphere. A lower bound of the magnetic energy the corona will retain after the eruption therefore is the minimum magnetic energy state which complies with the surface boundary conditions. This state is given by the associated potential field. If in addition to the fixed surface field, we require a certain amount of relative helicity to remain in the corona, the minimum energy state is that of the respective constant-α force-free field (Taylor field, [463]). If in addition to the normal component of the boundary field we impose a connectivity map to the boundary, the nonlinear α force-free field which complies with this connectivity has the least magnetic energy (see [578, 579, 465, 580]).

The amount of energy which can be set free by a large flare is therefore limited by the energy difference of the field prior to the flare to the energy of one of the above minimum-energy fields for the same surface magnetic flux distribution. There is strong evidence that the eruptions are enabled by field line reconnection which alters the connectivity of the foot points. It has further been found that reconnection hardly changes the overall helicity [581, 582]. Field line reconnection is a rather local process while the helicity, e.g., of a flux tube, resides in its twist or, equivalently, in

the toroidal flux which in equilibrium is evenly spread out all along the flux tube. If flux tubes with different twist reconnect the toroidal flux from each of the reconnected ends redistributes along the newly formed tubes by means of Alfvén waves. The total helicity is almost conserved, but due to the mixing of toroidal flux the difference in helicity per unit length between the new flux tubes is less than the difference was between the old ones. Hence reconnection tends to equalize the helicity among the reconnecting flux tubes [582] and drives the plasma towards a constant-α state. The lowest energy state of the field above the solar surface we can expect on these grounds after a large flare will therefore be the linear force-free field. But even this is probably an underestimate because α will only be leveled out on those flux tubes which were involved in a reconnection process and not in the whole of the corona.

The above minimum energy estimates of the potential or linear force-free field can be calculated from the observed surface field B_r, using the extrapolation methods mentioned in chapter 8.1. An energy estimate of the actual field before the flare is much more of a problem. In principle it should be possible to obtain such an estimate by the virial $\int \mathbf{r} \cdot \mathbf{f} d^3 x$ (e.g., [465]) over the total force density $\mathbf{f}$ in the plasma. In the MHD approximation and conventional notation,

$$\mathbf{f} = \frac{1}{\mu_0}\mathbf{j} \times \mathbf{B} - \nabla p - \rho\frac{GM_\odot}{r^2}\hat{\mathbf{r}} - \rho(\mathbf{v} \cdot \nabla)\mathbf{v} \tag{8.2}$$

Inside a stationary corona, $\mathbf{f}$ should vanish and so should the virial, independent of where we place the origin of $\mathbf{r}$. With $\mathbf{r}$ at the Sun's center we obtain after partial integration

$$\frac{1}{2\mu_0}\int_{\text{corona}} B^2 \, d^3x \quad = \int_{\text{corona}} \left(\rho\frac{GM}{r} - 3p - \rho v^2\right) d^3x$$
$$+ \int_{\text{coronal boundaries}} \left(\frac{1}{2\mu_0}B^2\mathbf{r} - \frac{\mathbf{B}}{\mu_0}(\mathbf{B} \cdot \mathbf{r}) + p\mathbf{r} + \rho(\mathbf{v} \cdot \mathbf{r})\mathbf{v}\right) \cdot \mathbf{n} \, d^2x \tag{8.3}$$

The inner boundary of the corona is chosen as the coronal base at $r \simeq R_\odot$ where the non-magnetic forces are negligible and the surface normal $\mathbf{n}$ points towards the Sun's center. The contribution to the surface integral in (8.3) from the outer boundary of the corona is usually neglected. With $\mathbf{B}$ *sim* $\hat{\mathbf{r}}$ beyond r *sim* $2.5 \, R_\odot$, the integrand of the surface integral decreases in magnitude and changes sign as the solar wind $\mathbf{v}$ *sim* $v_r\hat{\mathbf{r}}$ increases beyond about the Alfvén speed. With these simplifications

$$\frac{1}{2\mu_0}\int_{\text{corona}} B^2 \, d^3x = \int_{\text{corona}} \left(\rho\frac{GM}{r} - 3p - \rho v^2\right) d^3x$$
$$+ \frac{R_\odot}{2\mu_0}\int_{\text{coronal base}} (B_r^2 - B_h^2) \, d^2x \tag{8.4}$$

remains which yields the magnetic energy in terms of the surface field and some minor non-magnetic contributions which may be neglected in a first approach.

The problem with eq. (8.4) is, however, that the magnetic surface field is mostly observed in the photosphere where the force-free condition may not yet hold and not at the coronal base [446, 461]. How errors in the surface observations, especially in B_h may seriously affect eq. (8.4) is discussed in [583]. Yet it is instructive to consider some consequences of eq. (8.4) more closely.

If the coronal magnetic energy is enhanced by line-tying as in eq. (8.1) we cannot expect a systematic change of B_r^2 to account for the increase in magnetic energy on the

right hand side of eq. (8.4). Consequently, B_h^2 in eq. (8.4) will have to decrease which we indeed observe as the rising of coronal loops with increasing shear. The maximum energy that can possibly be achieved is when $B_h \simeq 0$, i.e., when all field lines are stretched out almost radially into the heliosphere. However, this configuration is never reached because as B_h decreases with increasing energy, and so does the capability to pump further energy into the corona by line-tying according to eq. (8.1).

Hence, besides the lower energy bound given by the linear force-free field there is also an upper bound for the energy of a force-free coronal magnetic field which is represented by a field with all field lines open to the heliosphere ("Aly's conjecture"; [584, 585, 586]) A simple calculation shows that the energy of a field $\mathbf{B} = B_r(R_\odot)R_\odot^2\mathbf{r}/r^3$ (though this is not force-free; see, e.g. [585], for an exact construction of a force-free "all-open field lines" configuration) with a dipole boundary $B_r(R_\odot)$ has twice the energy of the Laplacian dipole field (similarly there is a factor $n+1$ for general multipoles). Roughly, we therefore expect a factor of about 2 or more between the upper and lower energy bounds. Depending on how close the actual magnetic energy approaches this upper limit an appreciable amount of the coronal magnetic field energy can in principle be released in large flares. It was pointed out by [541] that the gravitational forces on the filament and the helmet enhances the energy of the suspending magnetic field in eq. (8.4). If only part of the filament and helmet mass is expelled in a CME, the mass loading prior to a CME could act like the lid of a jack-in-the-box.

Estimates of the magnetic energy of active regions before and after a CME have been made by several authors for limited regions of the corona. [512] found a magnetic energy of 6.5 10^{24} J for an active region with an equivalent potential field energy of about 3.8 10^{24} J and an Aly-limit of 7.6 10^{24} J. [511] found the magnetic energy of an active region reduced from 8.4 10^{25} J to 5.7 10^{25} J after an eruption.

Besides energy, we have seen that helicity is another invariant of ideal MHD (see chapter 5.4). It also plays an important role in structuring the coronal magnetic field. Its original definition eq. (5.7), however, is useful only for a plasma bounded by magnetic surfaces. Only for these configurations is H independent of the gauge of the vector potential $\mathbf{A}$. For open systems such as the corona, the definition of helicity was generalized by [587] and [588] through the introduction of the relative helicity

$$H_r = \int (\mathbf{A} \cdot \mathbf{B} - \mathbf{A}_0 \cdot \mathbf{B}_0)\, d^3x \qquad (8.5)$$

which measures the helicity relative to a reference field $\mathbf{B}_0 = \nabla \times \mathbf{A}_0$. For H_r to be gauge invariant, $\mathbf{B}_0$ must satisfy the same normal boundary conditions as $\mathbf{B}$ and $\mathbf{A}_0$ the same tangential boundaries.

A conventional choice for $\mathbf{B}_0$ is the potential field for the boundary conditions given along with the Coulomb gauge for $\mathbf{A}_0$ and $(\mathbf{A}_0)_r = 0$ on the solar surface. With the frozen-in $\mathbf{E} = \mathbf{v} \times \mathbf{B}$ employed, a simple expression then results for the flow of relative helicity through the solar surface (see, e.g., [587, 589])

$$P_H = 2 \int_{\text{photosphere}} \left((\mathbf{A}_0 \cdot \mathbf{B}_h)v_r - (\mathbf{A}_0 \cdot \mathbf{v}_h)B_r \right)\, d^2x \qquad (8.6)$$

As in eq. (8.1) there are two separate contributions, one due to vertical motions and the second due to horizontal line-tying.

In a number of analytical and numerical investigations [590, 591, 592, 593] it was shown that random surface motion $\mathbf{v}_h$ is much less effective for the helicity transport

in eq. (8.6) than it is for the energy transport in eq. (8.1). Some amount of helicity is produced by the steady rotation of the Sun alone and is stored on the open field lines in the deformation of the interplanetary field into Parker's spiral [594]. The ordered, differential rotation of the Sun is capable of generating only a small part of the helicity expected to reside in the closed coronal field [590] and seems insufficient to explain the total helicity flux which is eventually released in CMEs [510, 545]. The only candidate left in eq. (8.6) for an effective production of relative helicity is the vertical convection term, i.e., the emergence of properly twisted flux.

In [591] the total helicity produced by the Sun during a solar cycle was estimated to be about 10^{47} Mx^2. Observational evidence that random line-tying has to be ruled out for helicity production can be found in the hemispheric asymmetry of the observed current helicity [533, 459], the chirality law of filaments (e.g., [534, 527]) and the sigmoid X-ray structures above active regions [521, 522]. Hence a major source of the coronal helicity has to be sought in the twist of emerging flux represented by the first term of the integrand in eq. (8.1) and partly in the motion of active regions which concentrate the majority of the surface flux [590, 595].

As the helicity cannot be dissipated by reconnection like the magnetic energy, the closed field line region of the corona can only keep its helicity in quasi-steady balance if helicity of opposite sign is exchanged across the hemispheres or if helicity is transported away by the magnetic clouds of CMEs. Estimates of the release of relative helicity during the major flare mentioned above range from 1.3 10^{42} to 0.7 10^{42} Mx^2 [511]. An active region was continuously observed and its helicity budget monitored for five solar rotations [509]. It was found that a major part of the helicity carried away by a series of CMEs, about 2 10^{42} Mx^2 each, must have been provided by uprising twisted magnetic flux.

9. The magnetic field in the heliosphere

The heliosphere is the only region where in-situ observations of the magnetic field have been made. The majority of observations were carried out by various space crafts in the plane of the ecliptic near 1 AU. However, the Helios 1 and 2 space crafts provided measurements as close a 0.29 AU [596], the Voyager 1 and 2 space crafts have explored the heliosphere out to almost 100 AU [597] and Ulysses scanned the magnetic field over the solar poles at a distance between 1.3 and 5.4 AU [598]. These measurements show that in the heliosphere, the magnetic field has lost its dominant role. Instead, the plasma β is back to the order of unity with a few exceptions like the interior of CME magnetic clouds or the inside of magnetospheres and β even increases further with distance from the Sun.

9.1. Heliospheric current sheet and Parker's spiral

The open magnetic flux which emanates from the coronal holes fills the whole space angle of 4π beyond about 3 R$_\odot$. As the coronal holes make up only about 20% of the solar surface at solar minimum and even less at maximum activity, the magnetic flux has to overexpand between the coronal base and ~ 3 R$_\odot$. The expansion of an open flux tube cross section in this height range compared to an r^{-2} expansion is defined as the flux tube's expansion factor. Its value usually exceeds 5 and may be up to 20 or more for magnetic flux close to the boundaries of a coronal hole [598].
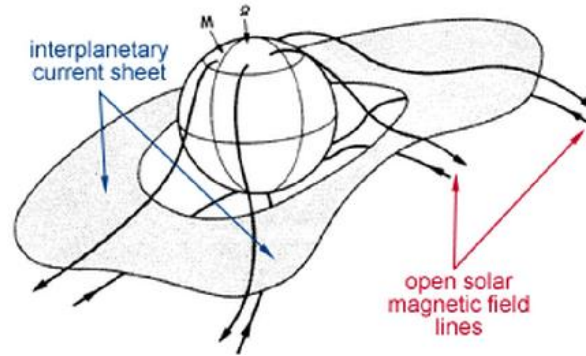
Figure 39. Sketch of the current sheet and how it is magnetically connected to the coronal helmet streamers. The cartoon is from J.T. Hoeksema, Stanford University)

The solar wind rapidly accelerates in this height region and helps to straighten out the field radially along the wind velocity direction. This produces the characteristic cusps of helmet streamers visible in coronagraph images. Empirically, a strong anti-correlation has been found between the asymptotic solar wind velocity in a flux tube and the expansion factor of its cross section in the corona [599, 600]. There is therefore evidence that the magnetic field has some control on the acceleration of the solar wind.

Beyond about 3 $R_\odot$ the inward and outward directed flux polarities are organized in two simply connected angular domains separated by an undulating, radially stretched heliospheric current sheet (HCS). Back on the Sun, this current sheet connects to the cusps of the helmet streamers which form above the meandering neutral line on the solar surface. Comparisons with space craft observations have shown that the position of the HCS can at most times be quite satisfactorily be modeled (e.g.,[601]) by simple potential field extrapolations of solar surface magnetograms. These models often employ a virtual sphere at about ~ 3 $R_\odot$ ("source surface") where as boundary condition a strictly radial field direction is imposed.

At solar activity minimum, the majority of the open solar magnetic flux emanates from polar coronal holes and the HCS within about 1AU is confined close to the solar equatorial plane. At activity maximum, the neutral line on the solar surface is rather erratic, open flux regions are spread out over the whole solar surface which causes the HCS to be considerably displaced from the heliographic equatorial plane. From Ulysses observations, it was concluded that the HCS at solar maximum is highly inclined and oriented almost perpendicular to the equatorial plane [602, 603, 604]. The enhanced ratio of quadrupole to dipole moment indicates that the HCS is also considerably warped [501]. Some authors [605] even argue for a more complex HCS geometry at solar maximum. They claim that at least occasionally even isolated reversed polarity cones may exist which would cause a second detached current sheet on the surface of the radial cone.

The straightening effect of the solar wind ensures, however, that the current sheet well below 1AU only warps azimuthally and is straightened in radial direction so that (within about 1 AU) it appears like a "ballerina skirt" (see Fig. 39), a term coined by Alfvén [606]. During late declining and minimum solar activity, the HCS is often approximated within less than 1 AU by a plane inclined with respect to the heliographic equator. Due to this inclination, the HCS intersects the ecliptic at least

twice. A space craft in the ecliptic plane should therefore see two (or an even number of) sector boundaries during one solar rotation where the heliospheric radial magnetic field component changes sign [607]. During maximum activity, HCS encounters were observed by Ulysses up the the highest latitudes of its orbit [602] (see Fig. 42).

In radial directions pointing well away from the HCS, the solar wind is accelerated within a fraction of 1 AU to a final speed of about 800 km s^{-1} ("fast solar wind"), more than 5 times the Alfvén velocity at 1 AU [608]. Observations of the Ulysses spacecraft show that beyond 1 AU and above 30° latitude there is relatively little variation in the fast solar wind speed. Close to the HCS, the plasma has a larger density and the final solar wind speed only reaches about 400 - 600 km s^{-1} ("slow solar wind") [609, 610]. Density irregularities carried away by the dense, slow wind can be observed in coronagraph image sequences out to about 30 R$_\odot$ [536, 611] and by radio scintillation measurements to even larger distances. These observations also show that the slow solar wind originates from the cusps of the helmet streamers and perhaps also from their lateral boundaries.

For distances beyond 3 R$_\odot$ and in regions unperturbed by the HCS the radial magnetic field component B_r must decline as r^{-2} in order to ensure flux conservation. Similarly, the radial mass flux ρv_r must on average decrease as r^{-2} to maintain a stationary solar wind outflow. However, while their feet are still anchored on the Sun, heliospheric field lines will eventually be deformed by the rotation of the Sun and thus create an azimuthal field component. Parker [612] and Weber and Davis [613] gave a first description of the stationary, azimuthally symmetric heliospheric background field which results from this deformation. In the Sun's rotating frame the solar wind velocity and magnetic field vectors must be parallel in order to keep the field stationary. Hence,

$$(v_\phi - \Omega r \cos\theta)B_r = v_r B_\phi \tag{9.1}$$

where Ω is the Sun's rotation rate of $\sim 2\pi/(27 \text{ days})$, θ denotes the heliographic latitude and index ϕ the azimuthal component. The azimuthal velocity v_ϕ will turn out to be practically negligible and is determined from the conservation of angular momentum

$$\frac{\rho v_r}{r}\frac{\partial}{\partial r}rv_\phi - \frac{B_r}{\mu_0 r}\frac{\partial}{\partial r}rB_\phi = 0 \tag{9.2}$$

which can readily be integrated to

$$r\left(v_\phi - \frac{B_r B_\phi}{\mu_0 \rho v_r}\right) = L(\theta) \tag{9.3}$$

where L is a constant along the field line. Upon elimination of v_ϕ from (9.1) and (9.3) we obtain for the azimuthal component of the magnetic field

$$B_\phi = \frac{B_r}{rv_r}\left(L(\theta) - \Omega r^2 \cos\theta\right)\left(1 - (\frac{B_r^2}{\mu_0 \rho v_r^2})\right)^{-1} \tag{9.4}$$

The field line deflection $\phi_B = \text{atan}(B_\phi/B_r)$ ("Parker angle") from the radial direction can only increase smoothly with distance from the Sun if the singularity $B_r^2 = \rho v_r^2$ in (9.4) is resolved by a simultaneous vanishing of the numerator. The distance at which this condition is met, i.e., where v_r is the (radial) Alfvén velocity, is $r = r_A$ ("Alfvénic critical distance"). The critical distance has an important physical meaning: since the solar wind is superalfvénic for $r > r_A$, no inward propagating Alfvén waves can ever pass this barrier. The condition for smooth field lines at r_A

therefore determines the integration constant L to $\Omega r_A^2 \cos\theta$ and hence the angular momentum carried away by the solar wind. In situ measurements of the heliospheric field and the solar wind speed between 0.3 and 1 AU together with equation (9.3) gave values for the Alfvén critical distance of $r_A \simeq 10\text{-}14$ $R_\odot$ [614, 615]. With these parameters, a deflection for the Parker angle of $\phi_B \simeq 45°$ is obtained at about 1 AU.

The conservation of the radial invariants of the solar wind parameters have been tested extensively in in-situ observations because they may be extrapolated to distances where measurements have not yet been made. The radial magnetic flux constant $r^2 B_r$ has a typical magnitude of 3 - 4 nT AU^2 and is found to be, apart from fluctuations, independent of latitude except of course for the sign change across the HCS [615, 616, 617]. The mean magnetic pressure therefore seems in perfect lateral balance. Fig. 41 shows the sign flip of $r^2 B_r$ at the HCS of an otherwise flat latitude profile. The variation of $r^2 B_r$ with solar activity is only about 1 nT AU^2 with the largest values at the decline phase of the activity cycle [617]. This temporal stability of $r^2 B_r$, being a direct measure of the Sun's open magnetic flux, is surprising because the total unsigned flux through the solar surface varies by as much as 80% during the solar cycle [618]. An explanation was offered by [619] which allows magnetic field line reconnection of open flux only with closed flux tubes. This is sufficient to feed the solar wind and redistribute open flux during the course of a solar cycle, however, it does not change the amount of open flux.

Also, the mean mass flux $r^2 \rho v_r$ has been found from Ulysses observations to be almost independent of heliographic latitude. A median value of $\sim 2.5\ 10^{12}$ amu m/s AU^2 at all latitudes and in fast and slow solar wind regions was found from the Ulysses in situ observations [609]. Measurements of Lyα radiation scattered at neutral interstellar H atoms which penetrated into the heliosphere, however, can only be reconciled with a decrease of the average mass flux by a about 30 % at latitudes above 40°[620].

For distances $r \gg r_A$ where $B_r^2/\mu_0\rho \ll v_r^2$ we obtain from (9.4) another approximate constant along a heliospheric field line, $r v_r B_\phi$ which should coincide with $-\Omega B_r r^2 \cos\theta$. The latter is a constant provided the field line stays at a constant latitude θ. For the Parker spiral angle ϕ_B this yields

$$\tan\phi_B = \frac{B_\phi}{B_r} = -\frac{\Omega}{v_r} r \cos\theta \qquad (9.5)$$

which is the same expression we obtain from (9.1) if the vanishingly small v_ϕ component is neglected. Comparisons of both expressions for ϕ_B in (9.5) using Ulysses data showed good average agreement (see Fig. 42, [621, 604]). The statistics, however, are obscured by fluctuations in the various field and flow components so that the results depend on the method of averaging. For example, [616] claim to have observed somewhat less tightly wound field lines at high latitudes during Ulysses' first polar passage than Parker's model would predict.

9.2. CIRs, transients and turbulence

Parker's spiral model, however, can only be a first order stationary approximation to a very dynamic heliospheric field and flow configuration. The fact that the HCS is embedded in a slow, dense solar wind compared to the fast, light wind inside the sector regions will eventually cause to destabilize the HCS the more it is inclined with respect to the heliographic equator. The spiral structure of the field causes an analogous folding of the HCS surface. Fast wind streams will penetrate into the
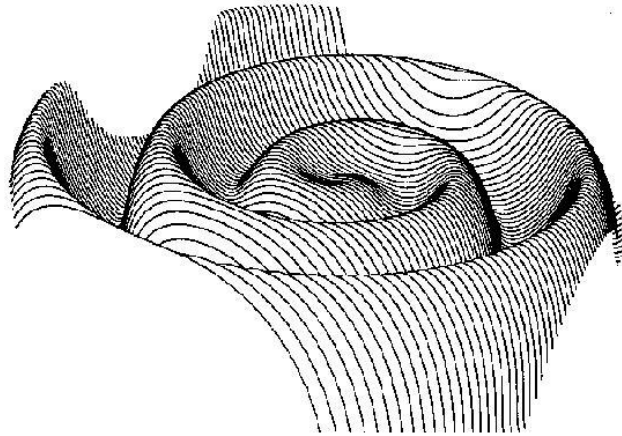
Figure 40. Deformation of the HCS up to a distance of about 12 AU. Close to the Sun, the HCS is approximated by a plane inclined by 15° with respect to the heliographic equator. With increasing distance from the Sun, the latitude of the inclined HCS is preserved along the Parker spiral characteristics (from [622]).
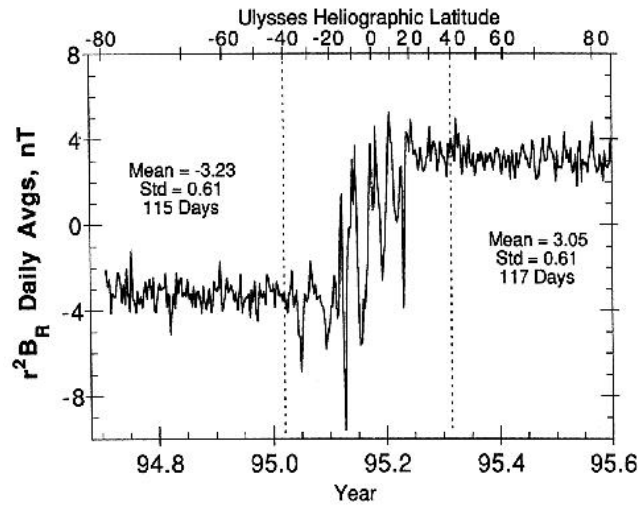
Figure 41. Radial heliospheric field component scaled to 1AU vs. observation time along the Ulysses trajectory from the south to north pole (from [616]). Between -40 and 40° of latitude the HCS was repeatedly crossed.

equatorial plane where the HCS is displaced off to higher latitudes. As the solar wind flow is practically radial, the fast wind sector will eventually run into the slow current sheet ahead.

The fact that the solar wind plasma is frozen into the spiraling magnetic field prevents the fast wind from penetrating the slow wind region. Instead, the less tightly wound fast solar wind leaves a rarefaction region behind and compress the warped current sheet ahead, forming a corotating interaction region (CIR). The dependence of the CIR formation on the initial coronal and HCS boundary state has been reviewed
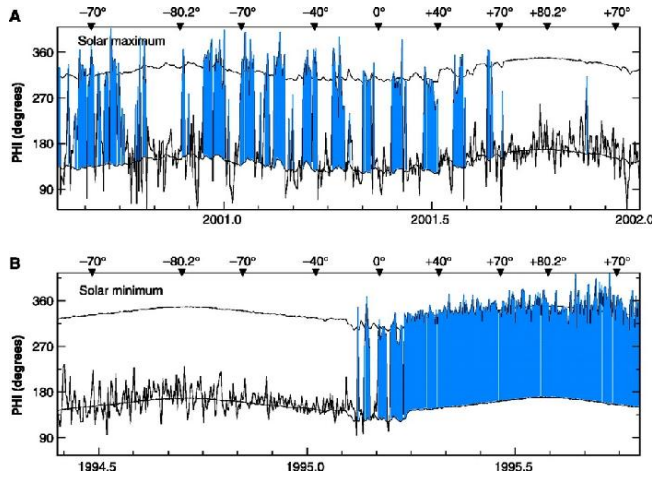
Figure 42. Azimuthal deflection angle of the heliospheric magnetic field from the radial direction vs. observation time along the Ulysses trajectory (from [604]). The top and bottom panel show maximum and minimum solar activity conditions, respectively. The smooth curves represent the angle as derived from Parker's model (rhs of 9.5), the fluctuating curve represents the measured ratio atan B_ϕ/B_r. It flips between sectors of inward (angles around 100) and outward directed (angles around 300) field whenever the heliospheric HCS is crossed.

by [623], a general overview can be found in [624].

Typically, CIRs form at 1 AU and beyond as this is the distance where the Parker spiral angle becomes significant. Beyond about 3 AU, the compression of the CIR becomes so strong that a pair of shocks is formed on either side: a fast mode shock at the front side which accelerates the slow plasma ahead and a reverse shock on the back side which decelerates the fast wind from behind. Simulations show how CIRs are deformed through interaction with the solar wind [625, 626]. These calculations demonstrate also that the wings of the reverse shock can propagate to much higher latitudes than correspond to the initial tilt of the HCS thus explaining an initially puzzling observation of the Ulysses spacecraft [627].

At even larger distances from the Sun, the CIR surfaces steepen and merge. Whenever a merged CIR passed by the Voyager 1 spacecraft observed between 14 an 18 AU quasiperiodic magnetic field enhancements by a factor 3-4 with periods around 26-days [628]. To the extent that CIRs overtake each other and interact they diminish in number [597] at distances beyond ~ 30 AU. Beyond this distance, the solar rotation period cannot be found anymore in the magnetic field fluctuations.

Besides the corotating heliospheric field pattern described so far, the in-situ field observations display a large amount of transient and turbulent perturbations. Most prominent are transient magnetic clouds which originate from coronal mass ejections. They propagate away from the Sun with speeds ranging from several 100 to 1200 km/s. In most cases, the speed of the clouds has at least the speed of the ambient solar wind [629]. If this speed exceeds that of the ambient solar wind by more than the Alfvén velocity, a fast mode shock forms on its front side. At high latitudes the CME clouds were also observed to rapidly expand due to excess magnetic pressure inside so that both a forward and reverse shock may form [630, 631]. Another consequence of the cloud's expansion is a drastic reduction of the particle pressure and plasma β in its interior so that we may expect the field inside the cloud to relax towards a force-free

equilibrium (see, however [632]).

A common magnetic field signature of a CME passing a space craft is the rotation of the meridional field components as expected from the passage of a giant helical flux rope. As we pointed out in chapter 8 the sense of rotation of the flux rope is determined by the helicity of the associated magnetic cloud. In a number of studies, it was indeed possible to identify the origin of the CMEs back on the Sun's surface and it was found that in these cases the sense of rotation corresponds to the helicity of the original filament and hence on the hemisphere, from where it was ejected [633, 547, 546].

A comprehensive 3D model of CME clouds is still under debate. Field observations of space crafts only yield point measurements which are often interpreted under the assumption that the perturbation is convected radially away from the Sun. It is still unclear, how far the CME cloud extends azimuthally and whether or how it is magnetically connected to the Sun. Bi-directional electron streams parallel and anti-parallel to the magnetic field are often observed inside the cloud. They are usually taken as evidence that the respective field line is still connected to the corona at both ends. However, also a complete lack of electron streams has occasionally been seen, which is interpreted as the presence of a field line rooted with both feet in the outer heliosphere [634, 624]

A numerical simulation of a CME and its propagation through the heliosphere is a formidable task. Purely hydrodynamical computations already show the complicated interaction of a CME with the fast and slow solar wind regimes in the background and its subsequent distortion [635, 636]. Including the magnetic field in these computations poses a real challenge. Even the background balance between magnetic field and solar wind are difficult to model numerically [637]. First steps to follow the CME release process and its propagation have in an MHD model recently been started (e.g., [638, 632, 639]). These calculations reproduce the gross features observed. The magnetic cloud of fast CMEs in these simulations, however, does not seem to evolve to a near force-free flux rope but is found to be considerably distorted by the solar wind plasma it runs into.

Another permanent feature of heliospheric observations are turbulent magnetic field fluctuations. Large amplitude, almost incompressible transverse Alfvén waves are observed whenever space crafts enter the fast solar wind [640]. Ulysses high latitude observations show that the relative transverse field variance $< \delta \mathbf{B}_\perp^2 > / < B^2 >$ increases with latitude from 0.1 almost linearly to ~ 0.3 at $40°$ latitude [641]. These waves are therefore well in the non-linear regime.

The resulting radial evolution of the Alfvénic turbulence has been investigated by a number of authors. A comprehensive review was given by [642]. The wave power spectra measured by the Helios space crafts between 0.3 and 1 AU show a gradual decline from a power law index of -1 towards Kolmogorov's inertial range index -5/3 with increasing distance from the Sun [643]. The interaction of this turbulence with the solar wind has been modeled by a number of authors. [644] assume an initial Alfvénic wave power spectrum emitted from the solar surface and evolve the spectrum by a non-linear cascade of wave energy to higher frequencies. The wave energy is absorbed at the high frequency end of the cascade by proton cyclotron absorption as proposed by [645]. This absorption provides the necessary acceleration and heating to drive fast solar wind. Other authors consider in their models the solar wind velocity shear and beyond ~ 10 AU energetic pickup ions (see below) as an additional source for the Alfvénic turbulence [646, 647]. The observed turbulent magnetic field fluctuation levels could thus be explained out to ~ 50 AU

9.3. The distant heliosphere

Observations of scattered Lyα radiation originating from the Sun and nearby stars show that our heliosphere is surrounded by a partially ionized interstellar cloud of mainly hydrogen gas (e.g., [648, 649]). The interaction of this cloud which constitutes the local interstellar medium (LISM) of our heliosphere with the solar wind has been thoroughly reviewed [650]. The LISM cloud drifts relative to the heliosphere causing its ionized component to be deflected at the heliospheric front side boundary while the cloud's neutral component can freely enter the heliosphere. Roughly where the solar wind ram pressure equals the LISM dynamic and thermal pressure, a reverse termination shock stops the solar wind and decelerates it into a hot, subsonic flow with increased density. Inside the region beyond the termination shock, the heliosheath, the solar plasma is deflected away into the heliotail and stretched out into the downstream direction of the LISM flow. The LISM plasma, on the other hand, has to flow around this obstacle and is swept away around the outer boundary of the heliosheath into the heliotail. The contact discontinuity between the heliosheath solar wind plasma on the inside and LISM plasma on the outside is called the heliopause.

Until a 2004, estimates of the stand-off distance of the termination shock ranged somewhere between about 90 and 200 AU. Voyager 1, advancing with ~ 3.5 AU/y in about the LISM upstream direction passed it in December 2004 at about 94 AU while the decreasing solar wind pressure in the declining phase of the solar cycle made the shock front move inwards towards the Sun [651]. Unfortunately, the failure of the plasma detector on board Voyager 1 makes it somewhat difficult to observe the plasma compression at the termination shock directly. However a pile-up of the almost azimuthal magnetic field, tangential to the shock front, could clearly be detected from the noisy field measurements. The field enhancement was from about 0.03 nT, still very close to Parker's predictions, on the upstram side to about 0.1 nT downstram of the termination shock. A puzzle in the observations is why the frequent flips of the azimuthal field polarity, reflecting the transitions between the inward and outward heliospheric field sectors (see Fig. 42), completely ceased after the termination shock had been passed.

Before the passage to the termination shock, our knowledge about the boundaries of the heliosphere were entirely based on HD and MHD models which extrapolate the observed solar wind quantities downstream and vary the LISM parameters within meaningful ranges (see [650] and references therein). These models, however, suffer greatly the uncertainties of unknown LISM parameters.

The only parameter known with sufficient accuracy is the relative speed of the LISM cloud of $v_{\mathrm{LISM}} \simeq 26$ km/s and the direction of this flow. This value has both been inferred from the Lyα observations (e.g., [652]) and from in-situ measurements of the neutral helium, a minor constituent of the cloud which penetrates the heliosphere [653]. The temperature estimates of ~ 8000 K are already uncertain so that it is not quite clear whether the LISM flow is sub- or supersonic. In the latter case, a bow shock is required in front of the heliopause to decelerate the LISM plasma to subsonic speeds and allow its deflection around the heliopause. Depending on the H/He composition the estimate of 8000 K yields a sound speed of about 10 km/s and hence a supersonic LISM flow. A possible cosmic ray component in the LISM plasma could, however, enhance the sound speed [650].

In particular the strength and orientation of the local interstellar magnetic field are rather uncertain. Typical model assumptions for the field strength are of the order

of 0.1-0.3 nT [654]. A typically assumed H^+ density of 0.2 cm^{-3} yields an Alfvén velocity of about 10 km/s. Hence both, the sonic and the Alfvénic Mach numbers of the LISM flow are of the order of unity so that numerical models show substantial differences if LISM temperature and magnetic field strength and direction is varied [655, 656]. A stronger field compresses the heliopause further inwards, an oblique field direction may cause a marked asymmetry of the shape of the heliopause.

Which influence the magnetic field from outside the heliosphere may have has to await more precise estimates of its strength and direction. The magnetic field which reaches the heliospheric boundary from the inside is much better known. Extrapolating Parker's spiral field to large distances suggests that the magnetic field regains its dominance again in the outer heliosphere. The field direction eventually becomes almost entirely azimuthal and the field pressure decreases as $B^2 \simeq B_\phi^2 \simeq r^{-2}$. This has indeed been observed out to 80 AU with slight deviations due to solar cycle and solar wind speed variations but else in fair agreement with Parker's model [657]. Assuming a constant solar wind speed v_r, the conservation of the radial mass flow causes the plasma density to decay as $\simeq r^{-2}$ and an adiabatic solar wind pressure would then decline with $p^{-2\gamma}$ for a polytropic index γ. Hence, $\beta \sim p/B^2 \sim r^{-2(\gamma-1)}$ should decrease with distance r for an index $\gamma > 1$.

However, with decreasing (thermal) solar wind density a new source of particles becomes important beyond about 15 AU: pick-up ions ionized by charge exchange from the interstellar neutral hydrogen of the LISM cloud which penetrates the heliosphere. In the direction from the Sun towards the heliospheric stagnation point these hydrogen atoms acquire a speed of $v_r + v_{\text{LISM}}$ in the frame of the solar wind. Once ionized, they become frozen to the solar wind and gyrate about the azimuthal magnetic field direction with an energy of some keV. The pickup distribution rapidly isotropizes and the ions pass some of their energy to the thermal solar wind plasma. This additional source of heating can be observed by a reduced temperature decrease beyond about 25 AU [658]. The result is an increase rather than a decrease of β with further distance from the Sun to values well above unity at the termination shock [650, 654].

Another consequence of the pickup ions is the mass loading of the solar wind. Momentum conservation should then decelerate the wind, and Parker's spiral should wind more tightly according to (9.5). There is, however, also a diamagnetization effect due to the large magnetic moment of the gyrating pickup ions [659]. The fact that B_ϕ is found in reasonable agreement with Parker's model and an undecelerated wind [657] suggests that the two effects may compensate.

The negligible role of the solar wind magnetic field in the distant heliosphere has led many researchers to neglect it altogether in their simulations of the heliosphere, with only few exceptions [660, 661]. Upstream of the termination shock the solar wind is decelerated and heated to be subsonic, the azimuthal magnetic field B_ϕ piles up, as is observed by Voyager 1, and is, especially near the stagnation point, compressed towards the heliopause ("Axford-Cranfield effect"). This may locally lead to a considerable field strength, however, the temporal variations of the solar wind and the polarization reversals with the solar cycle probably destroy this effect to a large degree [654].

In addition, the termination shock location is my no means stationary. Voyager observations suggest that the shock front was moving inward at the time of the passage. It was shown in model simulations that the front can move within a solar cycle by as much as 10 AU [662, 663]. The remains of CIRs and CMEs will additionally shake the heliosheath continuously and reconnection of the heliosheath magnetic field with the

reversed polarity solar wind field or with the LISM field may lead to a further erosion of the magnetic field in the heliosheath.

10. Outlook

The magnetic field plays a role in almost all parts of solar physics, so that the study of the Sun's magnetism has wide-ranging implications. Some of the main results concerning the solar magnetic field have been presented, or at least mentioned in this review. Many more have become victims of the limited space and the aim of the authors to present an overview spiced with a few examples, rather than a complete compilation. In any case, however important the compilation or presentation of past achievements may be, for the scientist working at the coal face of solar magnetic field research, the progress we hope to make in the near and mid-term future is by far the more interesting. Such progress is driven not so much by the open, unanswered questions, of which there are many, including some very basic ones. Rather, the main driver is the availability of new tools. These include new space instruments, ground-based telescopes and associated post-focus instruments, but also new codes, (numerical) techniques and computers.

In the following we point out some of the requirements for making progress and list some of the new tools that have either recently become available, or are planned for the near to mid-term future. We follow roughly the same order as the sections of this review, starting with the large-scale structure of the magnetic field and ending with the magnetic field in the heliosphere.

The risk of such an endeavour is that unforeseen developments can change the course of the field very significantly, making even a carefully written outlook quickly obsolete.

10.1. Large scale structure of the magnetic field

The observation of global magnetic field patterns is far less demanding than the detailed study of individual features in that high spatial resolution is not a prerequisit. This is offset, however, by the need for long uninterrupted time series of as many useful quantities as possible.

A point that cannot be overstressed is the need for coherent synoptic full-disk data sets of constant high quality. Only with the help of such data can the dynamo be constrained with sufficient accuracy. Such data often appear routine and it may not seem worth the effort to continue to gather them over decades and ideally even centuries. However, such data invariably pay rich scientific dividents in the end. For example, the sunspot numbers data set, one of the longest running scientific time series, is one of the most studied time series in any field of science and even today keeps revealing fresh insights when analysed with new techniques. In fact, it has become almost standard practice to apply any newly developed technique for time series analysis to the sunspot number record.

A negative example are the sunspot area and position measurements carried out by the Royal Greenwich Observatory. These are important not just for constraining the solar dynamo, but also for the reconstruction of solar irradiance. Unfortunately, contributions to this homogeneous data set ended in 1976, just 2 years before the radiometer on the NIMBUS-7 satellite revealed the systematic variability of the solar

irradiance. The absence of this overlap still poses problems to researchers attempting to extend the irradiance record further back in time.

On a shorter time scale, the regular magnetograms provided by ground-based observatories, such as the Spectropolarimeter (SPM), on Kitt Peak and from space by the Michelson Doppler Imager (MDI) on the Solar and Heliospheric Observatory (SOHO) have made an immense difference to studies of the large scale magnetic field. However, these data still suffer from some shortcomings. One is the lack of vector magnetic field measurements since all these instruments only record the longitudinal magnetic field component. Another is the insufficient accuracy and often the relatively low spatial resolution of the data. Finally, the coverage of the solar poles is extremely poor.

Projects that will address these shortcomings are in different stages of development. The SOLIS instrument on Kitt Peak, which has recently started operation, will provide regular vector magnetograms of the full solar disk in addition to other interesting observables for many years. The HMI instrument on the Solar Dynamics Observatory (SDO) has a similar aim, but is planned to provide data at a higher resolution and a high cadence (but possibly with lower sensitivity). Not just the regular coverage and the magnetic vector provided by these instruments is important, but also the enhanced polarimetric sensitivity, needed to reliably determine the transverse field components. Such an enhanced sensitivity also allows weak fields (e.g. internetwork fields) to be followed, which are only imperfectly rendered by current synoptic magnetograms. Finally, the solar poles will be studied by the Visible light Imager and Magnetograph (VIM) on the Solar Orbiter mission of ESA.

10.2. The solar interior

Most of the work dealing with the magnetic field in the solar interior has been theoretical in nature and the basic unanswered question is how the solar dynamo works, i.e., how the Sun's magnetic field is generated. Although dynamo theory has made significant progress over the last decades, some basic questions remain unanswered.

There is no generally accepted model of the solar dynamo. The relative importance of dynamo action in the overshoot layer/tachocline and a more distributed dynamo in the bulk of the convective zone remains unclear, particularly so concerning the origin of the turbulent magnetic field in the near-surface layers. While large-scale numerical simulations so far has not shown solar-like results, there is hope that the rapid progress in computational power will allow us to reach a more relevant parameter regime in the next decade or two. Reynolds numbers realistic for the solar plasma, however, are and will for long be beyond computational capabilities.

The biggest drawback for dynamo theory, however, is the lack of observational information about the structure and evolution of the magnetic field in the solar interior.

Another point that has so far not been adequately addressed in the context of dynamo theory is the description of the magnetic flux concentrations with superequipartion fields in the Sun's interior. The interaction of these flux tubes with sub-surface flows is expected to be markedly different from that of a more diffuse fields.

The possibility to measure magnetic fields reliably in the solar interior would be revolutionary. Local helioseismology has this capability in principle, but so far it has not been possible to unambiguously distinguish between magnetic effects on p-modes

and other influences, such as thermal inhomogeneities.The theoretical work needed is demanding and it is not possible to predict if and when sufficiently reliable results will be obtained to run such applications. In addition, the observational input for the inversion calculations may also turn out to be difficult to supply: to discriminate between different effects on wave propagation, data with a low signal-to-noise ratio obtained after long time integration may be required.

10.3. The solar photosphere: magnetic elements and sunspots

Most evident and pressing is the need to study the magnetic field at a higher spatial resolution than currently achievable. Even the best images and measurements available today show structure at the resolution limit. Furthermore, 3-D numerical MHD simulations of plage or quiet Sun also predict considerable magnetic fine structure below the spatial resolution of current observations. Higher spatial resolution observational data are needed in order to test whether structures visible in the simulations are also present on the Sun. A clever choice of spectral diagnostics can overcome a part of the disadvantages of limited spatial resolution, but cannot replace high spatial resolution data.

Currently, the highest spatial resolution photospheric magnetic data are being provided by the Swedish Solar Telescope (SST) on the island of La Palma, thanks to a careful design and the use of adaptive optics. In the coming years, a number of new instruments will provide competition, starting in 2006 with the Solar-B spacecraft. Although the theoretical resolution of Solar-B is only half that of the SST, the constant conditions provided by space are a distinct advantage for observations aiming at, e.g., the evolution of the magnetic field. The Sunrise balloon-borne observatory is expected to combine the theoretical resolution of the SST (an even higher resolution will be achieved in the UV) with the near absence of seeing enjoyed in the stratosphere. On the ground, the Gregor telescope on the island of Tenerife, the New Solar Telescope (NST) at Big Bear Observatory, and in the more distant future the Advanced Technology Solar Telescope (ATST) should push the spatial resolution limit even further.

We expect that progress will not come from higher spatial resolution alone. For the study of weak magnetic fields (features with low magnetic flux), a higher polarimetric accuracy (lower noise level) is just as important. In the Sun's photosphere the magnetic field does not only occur in the form of magnetic flux concentrations, but also in a more irregular or "turbulent" state, which is a subject of intense current studies Additional work is needed to reliably determine the amount of flux in this state of the magnetic field, its structure and distribution, evolution and origin. Since the field is weak, a high polarimetric sensitivity, as provided, e.g., by the Zürich Imaging Polarimeter (ZIMPOL) is needed, in particular in combination with high spatial resolution.

In addition, observations in different spectral bands (or spectral lines) provide the possibility of determining the height dependence of magnetic parameters, particularly in combination with state-of-the-art inversion techniques. The determination of the 3-D structure of the magnetic field obtained by combining high spatial resolution maps with the vertical stratification deduced from spectral information will, we believe, become a regularly used observational tool in the future.

Spectacular results are also expected from novel techniques and data, such as those obtained with the VIM instrument proposed Solar Orbiter, which will allow stereoscopic measurements of magnetic features when combined with data obtained

in Earth orbit or from the ground.

Theory has taken immense strides to go beyond simple models aiming mainly to identify physical processes towards realistic descriptions of the complex magnetic structures found on the Sun. 3-D radiative MHD simulations of quiet Sun and plage regions are showing a remarkable similarity with high resolution observations. Detailed comparisons suggest a need for denser grids (which is not surprising, given that the Reynolds numbers achieved by the simulations are still orders of magnitude smaller than the solar values). A denser grid requires larger computational resources, which are one limiting factor for progress in this field.

Just as exciting, e.g. for the study of sunspots, are the possibilities opened up by considering larger domains and running longer time series. In contrast to magnetic elements, models of sunspots have so far been severely limited. Models describing complete sunspots are restricted to assuming axial symmetry and to parameterising many of the key physical processes acting in them, while models that treat such processes explicitly are localised to a small region inside a sunspot (e.g., a piece of the umbra or penumbra). Therefore, one of the main aims of an MHD simulation covering a large domain is to simulate a complete sunspot. The simulation of small-scale magnetic elements would also greatly benefit from a larger computational domain, since it would allow their interaction with meso- and supergranulation to be followed, thus bringing the study of solar magnetic fine structure a step closer to the study of the global evolution of the magnetic field.

10.4. The upper atmosphere: chromosphere and corona

The very structure of the solar chromosphere is the subject of intense debate and this uncertainty also extends to the magnetic field. The main bone of contention is whether or not the quiet chromosphere harbours low-lying magnetic canopies (a uniquely chromospheric phenomenon), such as those seen in active regions. Observations of chromospheric fields now possible at the Canary Island Observatories will certainly provide exciting new results. In order to resolve this question, a high signal-to-noise ratio is expected to play a stronger role than the highest spatial resolution possible.

None of the planned space instrumentation foreseen for the near future has a chromospheric polarimetry channel in it. However, there are at least two new ground based instruments, TIP2 (the upgrade of the Tenerife Infrared Polarimeter) at the Vacuum Tower Telescope on Tenerife and SPINOR at the Vacuum Tower on Sacramento Peak, that are providing such data.

One reason why chromospheric structure still is rather enigmatic has to do with the difficulties posed by the chromosphere to modellers. A plasma β on the order of unity, the presence of shock waves and supersonic flows, the need for partial-redistribution NLTE (for typical chromospheric lines such as the H and K lines of Ca II), ionisation and recombination time scales larger than dynamical time scales, etc., all combine to make the life of the modeller difficult. However, there is no way around extending the successful 3-D simulations from the photosphere to the chromosphere. First attempts still neglect some of the physics, but this is one direction in which there is a strong need to go. As far as the magnetic field is concerned, it is already instructive in a first step to extrapolate the field from the photosphere (either from simulations or high spatial resolution observations) into chromospheric layers.

The main hinderance to more rapid progress in coronal physics is that the structure, dynamics and thermodynamics of the corona are dominated by the magnetic

field, which, however, can only be measured in a rather rudimentary way in these layers. Up to now, with the exception of radio measurements (see below), coronal studies have relied either on extrapolations of the magnetic field from the photosphere, or (more commonly) on the use of proxies such as the spatial distribution of intensity of transition region lines, or loops visible in coronal radiation.

The premier technique for measuring the coronal magnetic field has so far been radio observations, which can provide maps of the magnetic field strength, but do not in general allow the full magnetic vector to be measured. This is unfortunate, since in the corona the magnetic field becomes very inhomogeneous in direction, but relatively homogeneous in strength. The configuration of the field determines whether such important processes as magnetic reconnection can take place or not.

Maps of the magnetic field strength obtained from radio data have in the past often suffered from either low spatial and/or temporal resolution, or a sparse coverage of the Fourier plane (in the case of interferometrically obtained data). The introduction of a dedicated array (FASR) should help to significantly improve coronal magnetic field measurements with radio techniques.

At the same time, new techniques for coronal magnetic field measurements are currently being developed and studied, which might overcome some of the shortcomings of radio measurements. They include longitudinal magnetograms made in (coronagraphically imaged) infrared coronal lines, the utilization of the Hanle effect in EUV lines (for a future application in space), and using the Zeeman effect in the HeI 10830 Å triplet for vector magnetic field measurements near the coronal base. Each technique has its advantages and disadvantages and none gives a complete picture of the coronal field. While the Zeeman effect in IR coronal lines may remain limited to measuring the longitudinal field owing to the limited signal strength, the HeI 10830 Å triplet does not sample the hot coronal gas directly, and the Hanle effect in EUV lines has not been studied sufficiently to determine its full promise or the pitfalls.

One generic reason why no single technique will be able to provide anything near a complete picture of the coronal field is that the coronal gas is optically thin. However, a tomographic reconstruction of the coronal magnetic field is probably possible if longitidinal Zeeman and transverse Hanle observations are combined – another field where a substantial theoretical effort is needed.

A further complication is that gas at many different temperatures is intermingled. Therefore, measurements in a diagnostic line sensitive to gas within a certain temperature range show only the part of the field embedded in that gas. Neighbouring field lines may host gas at a very different temperature that may be accessible only at another wavelength and/or with another technique. It is likely that, on the medium to long term, different diagnostics and techniques will have to be combined to get a proper view of the coronal field. Extrapolations from photospheric magnetic field measurements will remain an integral part of the arsenal of techniques for studying coronal fields. However, in future such extrapolations and proxies will be increasingly supplemented, augmented and tested by direct measurements. For example, the extrapolated field can give a hint of the height to which a certain measurement refers.

Highly dynamic phaenomena in the corona, like eruptions and coronal mass ejections, which are very probably triggered by the coronal magnetic field, have attracted great interest in the past and our understanding of these phaenomena has improved enormously in the recent decade, both by observations with, e.g., the Yohkoh, SoHO and TRACE instruments and by improved MHD modelling. Predictions of individual events are still a challenge though. Again, a problem is

that our knowledge of the magnetic field at the site of the eruption is still too limited to discern the sequence of physical processes of an eruption in detail.

10.5. The heliosphere

Our knowlegde of the magnetic field in the heliosphere is probably better than in many other regions of our solar system. From the very beginning, the importance of the magnetic field was recognized and almost all space missions were equipped with magnetometers. In-situ measurements have been complemented with sophisticated MHD simulations, so that the basic understanding of the magnetic field in the region between 0.3 and 5 AU is quite advanced.

Owing to the vanishing divergence of the magnetic field, an extrapolation of the heliospheric field closer to the Sun is possible to some extent. Yet, the region inward of 0.3 AU, where the corona fades out into the solar wind, is little understood. With MHD models of the corona and inner heliosphere we can roughly map the solar surface magnetic field to the heliosphere and relate in situ satellite observations with their sources on the Sun. This magnetic mapping has so far assumed the field to be stationary and dynamical aspects of the connection between the coronal and heliospheric magnetic field are not clear yet. It is in this region below 0.3 AU where the solar wind is accelerated to a super-Alfvénic speed and CMEs sometimes to speeds well above 1000 km/s. The magnetic field almost certainly plays a key role in these acceleration processes but a widely accepted, physically sound explanation is still lacking. The Solar Orbiter mission will hopefully shed some light onto this region.

The heliosphere is highly dynamic. CMEs and interaction regions are complex phaenomena which could only partially be disclosed by in-situ observations. Here, MHD simulations have greatly improved our understanding of their three-dimensional plasma structure and magnetic field and how they are shaped in interaction with the background solar wind while they propagate outwards through the heliosphere. The STEREO mission will, for the first time, attempt to follow CMEs by means of optical obervations out to 1 AU. Even though only the plasma density enhancements of the CME cloud will be visible, we will also learn much about the magnetic field configuration of the cloud. Certainly, these observations will give new constraints and inspiration to refined MHD simulations of the propagation process.

Until recently, our knowledge about the distant heliosphere and its interaction with the local interstellar medium (LISM) was almost entirely due to MHD models which use our present knowledge about the inner heliosphere as boundary values. This situation has drastically changed since the Voyager 1 probe has crossed the termination shock. The new and unique in-situ observations of the heliosheath plasma will considerable constrain future MHD models. As the LISM magnetic field plays only a minor role in these models, it will have to be seen, how much the interstellar field value and direction can be constrained by these observations. New missions like the Heliopause Probe especially devoted to explore the outer heliospheric boundaries are considered and may yield more precise observations than those from the Voyager spacecrafts. But a lot of patience is required here. It will take at least 25 years until the next generation of space crafts will reach the termination shock.

References

[1] E. N. Parker. *Cosmical magnetic fields: Their origin and their activity.* Oxford, Clarendon Press; New York, Oxford University Press, p. 858, 1979.

[2] R. Schwenn and E. Marsch. *Physics of the inner heliosphere I. Large-Scale phenomena.* Springer-Verlag, Berlin, Germany, 1990.

[3] R. Schwenn and E. Marsch. *Physics of the inner heliosphere II. Particles, waves and turbulence.* Springer-Verlag, Berlin Heidelberg New York., also Physics and Chemistry in Space, volume 21; 2, 1991.

[4] C. J. Schrijver and C. Zwaan. *Solar and stellar magnetic activity.* Cambridge University Press, 2000.

[5] K. G. Strassmeier et al. Proceedings of the 1st Potsdam Thinkshop on Sunspots and Starspots. *Astronomische Nachrichten*, 323:155 ff, 2002.

[6] S. V. Berdyugina. Starspots: A Key to the Stellar Dynamo. *Living Rev. Solar Phys.*, LRSP-2005-8:http://solarphysics.livingreviews.org, 2005

[7] J.-F. Donati. Imaging the magnetic topologies of cool active stars. In H.M.J. Boffin, D. Steeghs, J. Cnypers (Eds.), *Astronomography, Indirect Imaging Methods in Observational Astronomy*, pages 207ff, Lecture Notes in Physics 573, Springer-Verlag, Berlin, 2001.

[8] S. K. Solanki and Y. C. Unruh. Spot sizes on Sun-like stars. *Monthly Not. Royal Astron. Soc.*, 348:307–315, 2004.

[9] M. Schüssler and S. K. Solanki. Why rapid rotators have polar spots. *Astron. Astrophys.*, 264:L13–L16, 1992.

[10] C. J. Schrijver and A. M. Title. On the formation of polar spots in Sun-like stars. *Astrophys. J.*, 551:1099–1106, 2001.

[11] G. Bond, B. Kromer, J. Beer, R. Muscheler, M. N. Evans, W. Showers, S. Hoffmann, R. Lotti-Bond, I. Hajdas, and G. Bonani. Persistent solar influence on North Atlantic climate during the holocene. *Science*, 294:2130–2136, 2001.

[12] J. D. Haigh. Modelling the impact of solar variability on climate. *Journal of Atmospheric and Terrestrial Physics*, 61:63–72, 1999.

[13] K. L. Harvey and C. Zwaan. Properties and emergence of bipolar active regions. *Sol. Phys.*, 148:85–118, 1993.

[14] H. J. Hagenaar, C. J. Schrijver, and A. M. Title. The properties of small magnetic regions on the solar surface and the implications for the solar dynamo(s). *Astrophys. J.*, 584:1107–1119, 2003.

[15] A. R. Choudhuri. *The physics of fluids and plasmas : an introduction for astrophysicists.* Cambridge University Press, Cambridge, 1998.

[16] R. B. Leighton. Transport of Magnetic Fields on the Sun. *Astrophys. J.*, 140:1547, 1964.

[17] N. R. Sheeley. The flux-transport model and its implications. In K. L. Harvey, editor, *The Solar Cycle*, pages 1–13, San Francisco: Astronomical Society of the Pacific Conf. Series 27, 1992

[18] Y. M. Wang and N. R. Sheeley. The rotation of photospheric magnetic fields: A random walk transport model. *Astrophys. J.*, 430:399–412, 1994.

[19] Y.-M. Wang. Cyclic Magnetic Variations of the Sun. In R. A. Donahue and J. A. Bookbinder, editors, *Cool Stars, Stellar Systems, and the Sun*, page 131, San Francisco: Astronomical Society of the Pacific Conf. Series 154, 1998

[20] I. Baumann, D. Schmitt, M. Schüssler, and S. K. Solanki. Evolution of the large-scale magnetic field on the solar surface: A parameter study. *Astron. Astrophys.*, 426:1075–1091, 2004.

[21] D. V. Hoyt and K. H. Schatten. Group sunspot numbers: A new solar activity reconstruction. *Sol. Phys.*, 179:189–219, 1998.

[22] C. Fröhlich and J. Lean. The sun's total irradiance: Cycles, trends and related climate change uncertainties since 1976. *Geophys. Res. Lett.*, 25:4377–4380, 1998.

[23] C. Fröhlich. Solar Irradiance Variability. In J. Pap et al., editor, *Solar Variability and its Effect on Climate*, page 97, Geophysical Monograph 141, (Washingthon, DC: American Geophysical Union), 2004.

[24] C. N. Arge, E. Hildner, V. J. Pizzo, and J. W. Harvey. Two solar cycles of nonincreasing magnetic flux. *J. Geophys. Res. (Space Physics)*, 107, A1 16-1, 2002.

[25] J. A. Eddy. The Maunder Minimum. *Science*, 192:1189–1202, 1976.

[26] R. Tapping. Solar activity indices. In P. Murdin, editor, *Encyclopedia of Astronomy and Astrophysics*, page 2470, Bristol & London, 2000. Institute of Physics & Nature Publishing Group.

[27] E. W. Maunder. Distribution of sun-spots in heliographic latitude, 1874-1913. *Mon. Not. R.*

Astron. Soc., 74:112, 1913.

[28] G. E. Hale and S. B. Nicholson. The Law of Sun-Spot Polarity. *Astrophys. J.*, 62:270, 1925.

[29] R. F. Howard. Axial tilt angles of sunspot groups. *Sol. Phys.*, 136:251–262, 1991.

[30] R. Howe, J. Christensen-Dalsgaard, F. Hill, R. W. Komm, R. M. Larsen, J. Schou, M. J. Thompson, and J. Toomre. Dynamic Variations at the Base of the Solar Convection Zone. *Science*, 287:2456–2460, 2000.

[31] J. G. Beck, L. Gizon, and T. L. Duvall. A New Component of Solar Dynamics: North-South Diverging Flows Migrating toward the Equator with an 11 Year Period. *Atrophys. J. Lett.*, 575:L47–L50, 2002.

[32] R. Howard and B. J. Labonte. Surface magnetic fields during the solar activity cycle. *Sol. Phys.*, 74:131–145, 1981.

[33] R. Howe, J. Christensen-Dalsgaard, F. Hill, R. W. Komm, R. M. Larsen, J. Schou, M. J. Thompson, and J. Toomre. Deeply Penetrating Banded Zonal Flows in the Solar Convection Zone. *Astrophys. J.*, 533:L163–L166, 2000.

[34] S. V. Vorontsov, J. Christensen-Dalsgaard, J. Schou, V. N. Strakhov, and M. J. Thompson. Helioseismic Measurement of Solar Torsional Oscillations. *Science*, 296:101–103, April 2002.

[35] M. Schüssler. The solar torsional oscillation and dynamo models of the solar cycle. *Astron. Astrophys.*, 94:L17, 1981.

[36] H. C. Spruit. Origin of the torsional oscillation pattern of solar rotation. *Sol. Phys.*, 213:1–21, 2003.

[37] O. R. White. The Solar Spectral Irradiances from X-ray to Radio Wavelengths. In J. M. Pap, C. Fröhlich, H. S. Hudson, and S. K. Solanki, editors, *The Sun as a Variable Star: Solar and Stellar Irradiance Variations*, page 45. Cambridge: Cambridge Univ. Press, 1994.

[38] G. C. Reid. Solar Variability and the Earth's Climate: Introduction and Overview. *Space Sci. Rev.*, 94:1–11, 2000.

[39] A. Larkin, J. D. Haigh, and S. Djavidnia. The Effect of Solar UV Irradiance Variations on the Earth's Atmosphere. *Space Sci. Rev.*, 94:199–214, 2000.

[40] A. Belov. Large Scale Modulation: View From the Earth. *Space Sci. Rev.*, 93:79–105, 2000.

[41] N. Marsh and H. Svensmark. Cosmic Rays, Clouds, and Climate. *Space Sci. Rev.*, 94:215–230, 2000.

[42] I. G. Usoskin, S. K. Solanki, M. Schüssler, K. Mursula, and K. Alanko. Millennium-Scale Sunspot Number Reconstruction: Evidence for an Unusually Active Sun since the 1940s. *Physical Review Letters*, 91:211101, 2003.

[43] I. G. Usoskin, K. Mursula, S. Solanki, M. Schüssler, and K. Alanko. Reconstruction of solar activity for the last millennium using ^{10}Be data. *Astron. Astrophys.*, 413:745–751, 2004.

[44] S. K. Solanki, I. G. Usoskin, B. Kromer, M. Schüssler, and J. Beer. Unusual activity of the Sun during recent decades compared to the previous 11,000 years. *Nature*, 431:1084–1087, October 2004.

[45] J. Beer. Long-term indirect indices of solar variability. *Space Sci. Rev.*, 94:53–66, 2000.

[46] G. A. Bazilevskaya. Observations of Variability in Cosmic Rays. *Space Sci. Rev.*, 94:25–38, 2000.

[47] W. Gleissberg. A long-periodic fluctuation of the sun-spot numbers . *The Observatory*, 62:158–159, 1939.

[48] G. Wagner, J. Beer, J. Masarik, R. Muscheler, P. W. Kubik, W. Mende, C. Laj, G. M. Raisbeck, and F. Yiou. Presence of the solar de Vries cycle (~205 years) during the last ice age. *Geophys. Res. Let.*, 28:303, 2001.

[49] A. N. Peristykh and P. E. Damon. Persistence of the Gleissberg 88-year solar cycle over the last ~12,000years: Evidence from cosmogenic isotopes. *J. Geoph. Res.*, 108, A1 1-1, 2003

[50] M. Schüssler. Axisymmetric alpha-squared-dynamos in the Hayashi-phase. *Astron. Astrophys.*, 38:263–270, 1975.

[51] L. L. Kitchatinov, M. Jardine, and A. Collier Cameron. Pre-main sequence dynamos and relic magnetic fields of solar-type stars. *Astron. Astrophys.*, 374:250–258, 2001.

[52] H. C. Spruit. Dynamo action by differential rotation in a stably stratified stellar interior. *Astron. Astrophys.*, 381:923–932, 2002.

[53] M. J. Thompson, J. Christensen-Dalsgaard, M. S. Miesch, and J. Toomre. The Internal Rotation of the Sun. *A&AR*, 41:599–643, 2003.

[54] L. Mestel and N. O. Weiss. Magnetic fields and non-uniform rotation in stellar radiative zones. *Mon. Not. R. Astron. Soc.*, 226:123–135, 1987.

[55] P. Charbonneau and K. B. MacGregor. Angular Momentum Transport in Magnetized Stellar Radiative Zones. II. The Solar Spin-down. *Astrophys. J.*, 417:762, 1993.

[56] G. Rüdiger and L. L. Kitchatinov. The slender solar tachocline: a magnetic model. *Astron.*

Nachr., 318:273, 1997.

[57] K. B. MacGregor and P. Charbonneau. Angular Momentum Transport in Magnetized Stellar Radiative Zones. IV. Ferraro's Theorem and the Solar Tachocline. *Astrophys. J.*, 519:911–917, 1999.

[58] P. Garaud. Dynamics of the solar tachocline - I. An incompressible study. *Mon. Not. R. Astron. Soc.*, 329:1–17, 2002.

[59] E. N. Parker. Kinematical hydromagnetic theory and its application to the low solar photosphere. *Astrophys. J.*, 138:552–575, 1963.

[60] N. O. Weiss. The expulsion of magnetic flux by eddies. *Proc. Roy. Soc. London, Ser. A*, 293:310–328, 1966.

[61] E. N. Parker. Stellar fibril magnetic systems. I - Reduced energy state. *Astrophys. J.*, 283:343–348, 1984.

[62] A. Brandenburg, I. Procaccia, and D. Segel. The size and dynamics of magnetic flux structures in magnetohydrodynamic turbulence. *Physics of Plasmas*, 2:1148–1156, 1995.

[63] M. Schüssler. On the structure of magnetic fields in the solar convection zone. In *The Hydromagnetics of the Sun*, pages 67–76. (Nordwijk, NL: European Space Agency), ESA SP-220, 1984.

[64] M. Schüssler. Magnetic flux tubes and the solar dynamo. In K. Tsinganos, editor, *Solar and astrophysical magnetohydrodynamic flows*, page 17, Dordrecht, 1996. Kluwer Academic Publishers.

[65] C. Zwaan. On the Appearance of Magnetic Flux in the Solar Photosphere. *Sol. Phys.*, 60:213, 1978.

[66] C. Zwaan. The evolution of sunspots. In J. H. Thomas and N. O. Weiss, editors, *Sunspots. Theory and Observations*, pages 75–100, Dordrecht, 1992. Kluwer Academic Publishers.

[67] H. C. Spruit. Equations for thin flux tubes in ideal MHD. *Astron. Astrophys.*, 102:129–133, 1981.

[68] A. Ferriz-Mas and M. Schüssler. Instabilities of magnetic flux tubes in a stellar convection zone. I. Equatorial flux rings in differentially rotating stars. *Geophys. Astrophys. Fluid Dyn.*, 72:209–247, 1993.

[69] E. N. Parker. The Formation of Sunspots from the Solar Toroidal Field. *Astrophys. J.*, 121:491, 1955.

[70] E. N. Parker. The generation of magnetic fields in astrophysical bodies. X - Magnetic buoyancy and the solar dynamo. *Astrophys. J.*, 198:205–209, 1975.

[71] F. Moreno-Insertis. Rise times of horizontal magnetic flux tubes in the convection zone of the sun. *Astron. Astrophys.*, 122:241–250, 1983.

[72] H. C. Spruit and A. A. van Ballegooijen. Stability of toroidal flux tubes in stars. *Astron. Astrophys.*, 106:58–66, 1982.

[73] A. Ferriz-Mas and M. Schüssler. Instabilities of magnetic flux tubes in a stellar convection zone. I. Equatorial flux rings in differentially rotating stars. *Geophys. Astrophys. Fluid Dyn.*, 72:209–247, 1993.

[74] A. Ferriz-Mas and M. Schüssler. Instabilities of magnetic flux tubes in a stellar convection zone. II. Flux rings outside the equatorial plane. *Geophys. Astrophys. Fluid Dyn.*, 81:233–265, 1995.

[75] S. M. Tobias, N. H. Brummell, T. L. Clune, and J. Toomre. Pumping of Magnetic Fields by Turbulent Penetrative Convection. *Astrophys. J.*, 502:L177, 1998.

[76] S. B. F. Dorch and Å. Nordlund. On the transport of magnetic fields by solar-like stratified convection. *Astron. Astrophys.*, 365:562–570, 2001.

[77] U. Ziegler and G. Rüdiger. Box simulations of rotating magnetoconvection. Effects of penetration and turbulent pumping. *Astron. Astrophys.*, 401:433–442, April 2003.

[78] W. P. Abbett, G. H. Fisher, Y. Fan, and D. J. Bercik. The Dynamic Evolution of Twisted Magnetic Flux Tubes in a Three-dimensional Convecting Flow. II. Turbulent Pumping and the Cohesion of Ω-Loops. *Astrophys. J.*, 612:557–575, 2004.

[79] M. Schüssler and M. Rempel. Structure of the magnetic field in the lower convection zone. In A. Wilson, editor, *From Solar Min to Max: Half a Solar Cycle with SOHO*, page 499, (Nordwijk, NL: ESTC, European Space Agency), 2002

[80] D. J. Galloway and N. O. Weiss. Convection and magnetic fields in stars. *Astrophys. J.*, 243:945–953, 1981.

[81] A. A. van Ballegooijen. The overshoot layer at the base of the solar convective zone and the problem of magnetic flux storage. *Astron. Astrophys.*, 113:99–112, 1982.

[82] M. Schüssler. Stellar dynamo theory. In J. O. Stenflo, editor, *Solar and Stellar Magnetic Fields: Origins and Coronal Effects*, volume 102, page 213, Dordrecht, 1983. Kluwer

Academic Publishers.

[83] M. Rempel. Overshoot at the base of the solar convection zone: a semianalytical approach. *Astrophys. J.*, 607:1046–1067, 2004.

[84] F. Moreno-Insertis, M. Schüssler, and A. Ferriz-Mas. Storage of magnetic flux tubes in a convective overshoot region. *Astron. Astrophys.*, 264:686–700, 1992.

[85] M. Rempel, M. Schüssler, and G. Tóth. Storage of magnetic flux at the bottom of the solar convection zone. *Astron. Astrophys.*, 363:789–799, 2000.

[86] J. G. Wissink, D. W. Hughes, P. C. Matthews, and M. R. E. Proctor. The three-dimensional breakup of a magnetic layer. *Mon. Not. R. Astron. Soc.*, 318:501–510, 2000.

[87] Y. Fan. Nonlinear Growth of the Three-dimensional Undular Instability of a Horizontal Magnetic Layer and the Formation of Arching Flux Tubes. *Astrophys. J.*, 546:509–527, 2001.

[88] M. Schüssler and A. Ferriz-Mas. Magnetic flux tubes and the dynamo problem. In A. Ferriz-Mas and M. Nunez, editors, *Advances in Nonlinear Dynamos*, pages 123–146, London, 2003. Taylor & Francis.

[89] D. J. Acheson. Instability by magnetic buoyancy. *Sol. Phys.*, 62:23–50, 1979.

[90] K. S. Cline, N. H. Brummell, and F. Cattaneo. On the Formation of Magnetic Structures by the Combined Action of Velocity Shear and Magnetic Buoyancy. *Astrophys. J.*, 588:630–644, 2003.

[91] Y. Fan and G. H. Fisher. Radiative Heating and the Buoyant Rise of Magnetic Flux Tubes in the Solar interior. *Sol. Phys.*, 166:17, 1996.

[92] F. Moreno-Insertis, M. Schüssler, and K. Glampedakis. Thermal properties of magnetic flux tubes. I. Solution of the diffusion problem. *Astron. Astrophys.*, 388:1022–1035, 2002.

[93] P. Caligari, F. Moreno-Insertis, and M. Schüssler. Emerging flux tubes in the solar convection zone. 1: Asymmetry, tilt, and emergence latitude. *Astrophys. J.*, 441:886–902, 1995.

[94] Y. Fan. Magnetic Fields in the Solar Convection Zone. *Living Reviews in Solar Physics*, LRSP-2004-1:http://solarphysics.livingreviews.org, 2004.

[95] A. R. Choudhuri and P. A. Gilman. The influence of the Coriolis force on flux tubes rising through the solar convection zone. *Astrophys. J.*, 316:788–800, 1987.

[96] A. R. Choudhuri. The evolution of loop structures in flux rings within the solar convection zone. *Sol. Phys.*, 123:217–239, 1989.

[97] Y. Fan, G. H. Fisher, and A. N. McClymont. Dynamics of emerging active region flux loops. *Astrophys. J.*, 436:907–928, 1994.

[98] M. Schüssler, P. Caligari, A. Ferriz-Mas, and F. Moreno-Insertis. Instability and eruption of magnetic flux tubes in the solar convection zone. *Astron. Astrophys.*, 281:L69, 1994.

[99] S. D'Silva and A. R. Choudhuri. A theoretical model for tilts of bipolar magnetic regions. *Astron. Astrophys.*, 272:621, 1993.

[100] F. Moreno-Insertis, P. Caligari, and M. Schüssler. Active region asymmetry as a result of the rise of magnetic flux tubes. *Sol. Phys.*, 153:449–452, 1994.

[101] P. Caligari, M. Schüssler, and F. Moreno-Insertis. Emerging Flux Tubes in the Solar Convection Zone. II. The Influence of Initial Conditions. *Astrophys. J.*, 502:481, 1998.

[102] P. A. Gilman and R. Howard. Rotation rates of leader and follower sunspots. *Astrophys. J.*, 295:233–240, 1985.

[103] G. H. Fisher, Y. Fan, D. W. Longcope, M. G. Linton, and A. A. Pevtsov. The Solar Dynamo and Emerging Flux - (Invited Review). *Sol. Phys.*, 192:119–139, 2000.

[104] M. Schüssler. Magnetic buoyancy revisited - Analytical and numerical results for rising flux tubes. *Astron. Astrophys.*, 71:79–91, 1979.

[105] T. Emonet and F. Moreno-Insertis. The Physics of Twisted Magnetic Tubes Rising in a Stratified Medium: Two-dimensional Results. *Astrophys. J.*, 492:804, 1998.

[106] Y. Fan, E. G. Zweibel, M. G. Linton, and G. H. Fisher. The Rise of Kink-Unstable Magnetic Flux Tubes in the Solar Convection Zone. *Astrophys. J.*, 505:L59, 1998.

[107] S. B. F. Dorch, V. Archontis, and Å. Nordlund. 3D simulations of twisted magnetic flux ropes. *Astron. Astrophys.*, 352:L79–L82, 1999.

[108] Y. Fan, E. G. Zweibel, M. G. Linton, and G. H. Fisher. The Rise of Kink-unstable Magnetic Flux Tubes and the Origin of delta-Configuration Sunspots. *Astrophys. J.*, 521:460–477, 1999.

[109] W. P. Abbett, G. H. Fisher, and Y. Fan. The Effects of Rotation on the Evolution of Rising Omega Loops in a Stratified Model Convection Zone. *Astrophys. J.*, 546:1194–1203, 2001.

[110] Y. Fan, W. P. Abbett, and G. H. Fisher. The Dynamic Evolution of Twisted Magnetic Flux Tubes in a Three-dimensional Convecting Flow. I. Uniformly Buoyant Horizontal Tubes. *Astrophys. J.*, 582:1206–1219, 2003.

[111] F. Moreno-Insertis. The motion of magnetic flux tubes in the convection zone and the subsurface origin of active regions. In *NATO ASI Proc. 375: Sunspots. Theory and Observations*, page 385, Dordrecht, 1992. Kluwer Academic Publishers.

[112] A. Eff-Darwich and S. G. Korzennik. A new upper limit to the temporal variation of the rotation rate of the tachocline between 1994 and 2002. In H. Sawaya-Lacoste, editor, *Local and Global Helioseismology: the Present and Future*, page 267, (Nordwijk, NL: European Space Agency), ESA SP-517, 2003

[113] F. Moreno-Insertis, P. Caligari, and M. Schüssler. "Explosion" and Intensification of Magnetic Flux Tubes. *Astrophys. J.*, 452:894, 1995.

[114] M. Rempel and M. Schüssler. Intensification of Magnetic Fields by Conversion of Potential Energy. *Astrophys. J.*, 552:L171–L174, 2001.

[115] M. Ossendrijver. The dynamo layer in solar-type stars. *Astron. Nachr./AN*, 326:166–169, 2005.

[116] K. Petrovay. What makes the sun tick? - the origin of the solar cycle. In A. Wilson, editor, *The Solar Cycle and Terrestrial Climate*, page 3, (Noordwijk, NL: European Space Agency), ESA SP-463, 2000

[117] M. Ossendrijver. The solar dynamo. *A&AR*, 11:287–367, 2003.

[118] P. Charbonneau. Dynamo Models of the Solar Cycle. *Living Reviews in Solar Physics*, LRSP-2005-2:http://solarphysics.livingreviews.org, 2005.

[119] H. K. Moffatt. *Magnetic field generation in electrically conducting fluids.* Cambridge University Press, 1978.

[120] F. Krause and K. H. Rädler. *Mean-field magnetohydrodynamics and dynamo theory.* Oxford: Pergamon Press, 1980.

[121] T. G. Cowling. The magnetic field of sunspots. *Mon. Not. R. Astron. Soc.*, 94:39–48, 1933.

[122] M. Núñez. The decay of axisymmetric magnetic fields: a review of Cowling's theorem. *SIAM Review*, 38:553–564, 1996.

[123] W. M. Elsasser. Induction Effects in Terrestrial Magnetism Part I. Theory. *Phys. Rev.*, 69:106–116, 1946.

[124] D.J. Ivers and R.W. James. Antidynamo theorems for non-radial flows. *Geophys. Astrophys. Fluid Dyn.*, 40:147, 1988.

[125] M.R.E. Proctor. An extension of the Toroidal Theorem. *Geophys. Astrophys. Fluid Dyn.*, 98:235–240, 2004.

[126] E. N. Parker. The Generation of Magnetic Fields in Astrophysical Bodies I. The Dynamo Equations. *Astrophys. J.*, 162:665–673, 1970.

[127] H. Yoshimura. Solar-cycle dynamo wave propagation. *Astrophys. J.*, 201:740–748, 1975.

[128] L. L. Kitchatinov. Do dynamo-waves propagate along isorotation surfaces? *Astron. Astrophys.*, 394:1135–1139, 2002.

[129] G. Rüdiger and L. L. Kitchatinov. Alpha-effect and alpha-quenching. *Astron. Astrophys.*, 269:581–588, 1993.

[130] Ya. B. Zel'dovich. The magnetic field in the two-dimensional motion of a conducting turbulent fluid. *Sov. Phys. JETP*, 4:460, 1957.

[131] L. L. Kitchatinov and G. Rüdiger. Magnetic-field advection in inhomogeneous turbulence. *Astron. Astrophys.*, 260:494–498, 1992.

[132] A. Brandenburg, I. Tuominen, A. Nordlund, P. Pulkkinen, and R. F. Stein. 3-D simulation of turbulent cyclonic magneto-convection. *Astron. Astrophys.*, 232:277–291, 1990.

[133] M. Ossendrijver, M. Stix, and A. Brandenburg. Magnetoconvection and dynamo coefficients:. Dependence of the alpha effect on rotation and magnetic field. *Astron. Astrophys.*, 376:713–726, 2001.

[134] M. Ossendrijver, M. Stix, A. Brandenburg, and G. Rüdiger. Magnetoconvection and dynamo coefficients. II. Field-direction dependent pumping of magnetic field. *Astron. Astrophys.*, 394:735–745, 2002.

[135] G. B. Field, E. G. Blackman, and H. Chou. Nonlinear alpha-Effect in Dynamo Theory. *Astrophys. J.*, 513:638–651, 1999.

[136] N. Kleeorin, K. Kuzanyan, D. Moss, I. Rogachevskii, D. Sokoloff, and H. Zhang. Magnetic helicity evolution during the solar activity cycle: Observations and dynamo theory. *Astron. Astrophys.*, 409:1097–1105, 2003.

[137] S. I. Vainshtein and F. Cattaneo. Nonlinear restrictions on dynamo action. *Astrophys. J.*, 393:165–171, 1992.

[138] W. V. R. Malkus and M. R. E. Proctor. The macrodynamics of alpha-effect dynamos in rotating fluids. *J. Fluid Mech.*, 67:417–443, 1975.

[139] A. Phillips, J. Brooke, and D. Moss. The importance of physical structure in solar dynamo

models. *Astron. Astrophys.*, 392:713–727, 2002.

[140] J. Brooke, D. Moss, and A. Phillips. Deep minima in stellar dynamos. *Astron. Astrophys.*, 395:1013–1022, 2002.

[141] A. Nordlund, A. Brandenburg, R. L. Jennings, M. Rieutord, J. Ruokolainen, R. F. Stein, and I. Tuominen. Dynamo action in stratified convection with overshoot. *Astrophys. J.*, 392:647–652, 1992.

[142] A. Brandenburg, R. L. Jennings, Å. Nordlund, M. Rieutord, R. F. Stein, and I. Tuominen. Magnetic structures in a dynamo simulation. *J. Fluid Mech.*, 306:325–352, 1996.

[143] P. A. Gilman and J. Miller. Dynamically consistent nonlinear dynamos driven by convection in a rotating spherical shell. *Astrophysical Journal and Supplement Series*, 46:211–238, 1981.

[144] P. A. Gilman. Dynamically consistent nonlinear dynamos driven by convection in a rotating spherical shell. II - Dynamos with cycles and strong feedbacks. *Astrophysical Journal and Supplement Series*, 53:243–268, 1983.

[145] G. A. Glatzmaier. Numerical simulations of stellar convective dynamos. II - Field propagation in the convection zone. *Astrophys. J.*, 291:300–307, April 1985.

[146] A. S. Brun. On the interaction between differential rotation and magnetic fields in the Sun. *Sol. Phys.*, 220:333–344, 2004.

[147] A. S. Brun, M. S. Miesch, and J. Toomre. Global-Scale Turbulent Convection and Magnetic Dynamo Action in the Solar Envelope. *Astrophys. J.*, 614:1073–1098, 2004.

[148] M. S. Miesch. Large-Scale Dynamics of the Convection Zone and Tachocline. *Living Reviews in Solar Physics*, LRSP-2005-1:http://solarphysics.livingreviews.org, 2005.

[149] S. Childress and A. D. Gilbert. *Stretch, Twist, Fold: The Fast Dynamo; Lecture Notes in Physics, Vol. 37 .* Springer Berlin, Heidelberg, New York, 1995.

[150] F. Cattaneo. On the origin of magnetic fields in the quiet photosphere. *Astrophys. J.*, 515:L39–L42, 1999.

[151] S. Boldyrev and F. Cattaneo. Magnetic-Field Generation in Kolmogorov Turbulence. *Phys. Rev. Lett.*, 92(14):144501, 2004.

[152] A. A. Schekochihin, N. E. L. Haugen, A. Brandenburg, S. C. Cowley, J. L. Maron, and J. C. McWilliams. The Onset of a Small-Scale Turbulent Dynamo at Low Magnetic Prandtl Numbers. *Atrophys. J. Lett.*, 625:L115–L118, 2005.

[153] Y. Ponty, P. D. Mininni, D. C. Montgomery, J.-F. Pinton, H. Politano, and A. Pouquet. Numerical Study of Dynamo Action at Low Magnetic Prandtl Numbers. *Physical Review Letters*, 94(16):164502, 2005.

[154] A. Brandenburg, W. Dobler, and K. Subramanian. Magnetic helicity in stellar dynamos: new numerical experiments. *Astronomische Nachrichten*, 323:99–122, 2002.

[155] A. Brandenburg. The Inverse Cascade and Nonlinear Alpha-Effect in Simulations of Isotropic Helical Hydromagnetic Turbulence. *Astrophys. J.*, 550:824–840, 2001.

[156] A. Brandenburg, E. G. Blackman, and G. R. Sarson. How magnetic helicity ejection helps large scale dynamos. *Adv. Space Res.*, 32:1835–1844, 2003.

[157] A. Brandenburg and K. Subramanian. Strong mean field dynamos require supercritical helicity fluxes. *Astronomische Nachrichten*, 326:400–408, 2005.

[158] B. C. Low. Coronal mass ejections, magnetic flux ropes, and solar magnetism. *J. Geophys. Res.*, 106:25141–25164, 2001.

[159] A. Brandenburg. The Case for a Distributed Solar Dynamo Shaped by Near-Surface Shear. *Astrophys. J.*, 625:539–547, May 2005.

[160] G. Rüdiger and R. Arlt. Physics of the solar cycle. In A. Ferriz-Mas and M. Nunez, editors, *Advances in Nonlinear Dynamos*, pages 147–194, London, 2003. Taylor & Francis.

[161] M. Schüssler and D. Schmitt. Theoretical models of solar magnetic variability. In J. et al. Pap, editor, *Solar Variability and its Effect on Climate*, page 33, Geophysical Monograph 141, (Washingthon, DC: American Geophysical Union), 2004.

[162] D. Schmitt. An alpha-omega-dynamo with an alpha-effect due to magnetostrophic waves. *Astron. Astrophys.*, 174:281–287, 1987.

[163] A. Ferriz-Mas, D. Schmitt, and M. Schüssler. A dynamo effect due to instability of magnetic flux tubes. *Astron. Astrophys.*, 289:949–956, 1994.

[164] A. Brandenburg and D. Schmitt. Simulations of an alpha-effect due to magnetic buoyancy. *Astron. Astrophys.*, 338:L55–L58, 1998.

[165] D. Schmitt. Dynamo action of magnetostrophics waves. In *Advances in Nonlinear Dynamos*, Eds. A. Ferriz-Mas and M. Núñez Jiménez, Taylor & Francis, London, 2002

[166] K. S. Cline, N. H. Brummell, and F. Cattaneo. Dynamo Action Driven by Shear and Magnetic Buoyancy. *Astrophys. J.*, 599:1449–1468, 2003.

[167] M. Dikpati and P. A. Gilman. Analysis of hydrodynamic stability of solar tachocline latitudinal

differential rotation using a shallow-water model. *Astrophys. J.*, 551:536–564, 2001.

[168] G. Rüdiger and A. Brandenburg. A solar dynamo in the overshoot layer: cycle period and butterfly diagram. *Astron. Astrophys.*, 296:557, 1995.

[169] E. N. Parker. A solar dynamo surface wave at the interface between convection and nonuniform rotation. *Astrophys. J.*, 408:707–719, 1993.

[170] S. M. Tobias. Diffusivity Quenching as a Mechanism for Parker's Surface Dynamo. *Astrophys. J.*, 467:870, 1996.

[171] P. Charbonneau and K. B. MacGregor. Solar Interface Dynamos. II. Linear, Kinematic Models in Spherical Geometry. *Astrophys. J.*, 486:502, 1997.

[172] J. A. Markiel and J. H. Thomas. Solar interface dynamo models with a realistic rotation profile. *Astrophys. J.*, 523:827–837, 1999.

[173] Y.-M. Wang, N. R. Sheeley, and A. G. Nash. A new solar cycle model including meridional circulation. *Astrophys. J.*, 383:431–442, 1991.

[174] M. Dikpati. Solar magnetic fields and the dynamo theory. *Advances in Space Research*, 35:322–328, 2005.

[175] H. W. Babcock. The topology of the Sun's magnetic field and the 22-year cycle. *Astrophys. J.*, 133:572, 1961.

[176] R. B. Leighton. A magneto-kinematic model of the solar cycle. *Astrophys. J.*, 156:1, 1969.

[177] A. R. Choudhuri, M. Schüssler, and M. Dikpati. The solar dynamo with meridional circulation. *Astron. Astrophys.*, 303:L29, 1995.

[178] B. R. Durney. On a Babcock-Leighton dynamo model with a deep-seated generating layer for the toroidal magnetic field. *Sol. Phys.*, 160:213–235, 1995.

[179] M. Dikpati and P. Charbonneau. A Babcock-Leighton flux transport dynamo with solar-like differential rotation. *Astrophys. J.*, 518:508–520, 1999.

[180] D. Nandy and A. R. Choudhuri. Toward a mean field formulation of the Babcock-Leighton type solar dynamo. I. α-coefficient versus Durney's double-ring approach. *Astrophys. J.*, 551:576–585, 2001.

[181] M. Küker, G. Rüdiger, and M. Schultz. Circulation-dominated solar shell dynamo models with positive alpha-effect. *Astron. Astrophys.*, 374:301–308, 2001.

[182] G. A. Guerrero and J. D. Muñoz. Kinematic solar dynamo models with a deep meridional flow. *Monthly Not. Royal Astron. Soc.*, 350:317–322, 2004.

[183] P. Charbonneau, C. St-Jean, and P. Zacharias. Fluctuations in Babcock-Leighton Dynamos. I. Period Doubling and Transition to Chaos. *Astrophys. J.*, 619:613–622, 2005.

[184] M. Dikpati and P. A. Gilman. Flux-transport dynamos with α-effect from global instability of tachocline differential rotation: A solution for magnetic parity selection in the Sun. *Astrophys. J.*, 559:428–442, 2001.

[185] K. Petrovay and A. Kerekes. The effect of a meridional flow on Parker's interface dynamo. *Monthly Not. Royal Astron. Soc.*, 351:L59–L62, July 2004.

[186] M. Dikpati, P. A. Gilman, and K. B. MacGregor. Constraints on the Applicability of an Interface Dynamo to the Sun. *Astrophys. J.*, 631:647–652, 2005.

[187] P. Charbonneau and M. Dikpati. Stochastic fluctuations in a Babcock-Leighton model of the solar cycle. *Astrophys. J.*, 543:1027–1043, 2000.

[188] S. M. Tobias. Grand minimia in nonlinear dynamos. *Astron. Astrophys.*, 307:L21, 1996.

[189] J. Beer, S. Tobias, and N. Weiss. An active sun throughout the maunder minimum. *Sol. Phys.*, 181:237–249, 1998.

[190] M. Küker, R. Arlt, and G. Rüdiger. The Maunder minimum as due to magnetic Lambda-quenching. *Astron. Astrophys.*, 343:977–982, 1999.

[191] D. Moss and J. Brooke. Towards a model for the solar dynamo. *Mon. Not. R. Astron. Soc.*, 315:521–533, 2000.

[192] P. Hoyng. Turbulent transport of magnetic fields - Part Two - The role of fluctuations in kinematic theory. *Astron. Astrophys.*, 171:357, 1987.

[193] P. Hoyng. Turbulent transport of magnetic fields. III - Stochastic excitation of global magnetic modes. *Astrophys. J.*, 332:857–871, 1988.

[194] P. Hoyng. Helicity fluctuations in mean field theory: an explanation for the variability of the solar cycle? *Astron. Astrophys.*, 272:321, 1993.

[195] P. Hoyng. Is the solar cycle timed by a clock? *Sol. Phys.*, 169:253–264, 1996.

[196] A. J. H. Ossendrijver, P. Hoyng, and D. Schmitt. Stochastic excitation and memory of the solar dynamo. *Astron. Astrophys.*, 313:938–948, 1996.

[197] P. Charbonneau, G. Blais-Laurier, and C. St-Jean. Intermittency and Phase Persistence in a Babcock-Leighton Model of the Solar Cycle. *Atrophys. J. Lett.*, 616:L183–L186, 2004.

[198] J. P. Legrand and P. A. Simon. A two-component solar cycle. *Sol. Phys.*, 131:187–209, 1991.

[199] D. Schmitt, M. Schüssler, and A. Ferriz-Mas. Intermittent solar activity by an on-off dynamo. *Astron. Astrophys.*, 311:L1, 1996.

[200] W. Dobler. Stellar dynamos - theoretical aspects. *Astronomische Nachrichten*, 326:254–264, January 2005.

[201] G. Mathys, S. K. Solanki, and D. T. Wickramasinghe, editors. *Magnetic Fields Across the Hertzsprung-Russell Diagram*, San Francisco: Astronomical Society of the Pacific Conf. Series 248, 2001

[202] S. S. Vogt and G. D. Penrod. Doppler Imaging of spotted stars - Application to the RS Canum Venaticorum star HR 1099. *Publ. Astron. Soc. Pac.*, 95:565–576, 1983.

[203] M. Semel. Zeeman-Doppler imaging of active stars. I - Basic principles. *Astron. Astrophys.*, 225:456–466, 1989.

[204] S. L. Baliunas, R. A. Donahue, W. H. Soon, J. H. Horne, J. Frazer, L. Woodard-Eklund, M. Bradford, L. M. Rao, O. C. Wilson, Q. Zhang, W. Bennett, J. Briggs, S. M. Carroll, D. K. Duncan, D. Figueroa, H. H. Lanning, T. Misch, J. Mueller, R. W. Noyes, D. Poppe, A. C. Porter, C. R. Robinson, J. Russell, J. C. Shelton, T. Soyumer, A. H. Vaughan, and J. H. Whitney. Chromospheric variations in main-sequence stars. *Astrophys. J.*, 438:269–287, 1995.

[205] B. Montesinos and C. Jordan. On Magnetic Fields, Stellar Coronae and Dynamo Action in Late Type Dwarfs. *Mon. Not. R. Astron. Soc.*, 264:900, 1993.

[206] G. E. Hale. On the probable existence of a magnetic field in sun-spots. *Astrophys. J.*, 28:315–347, 1908.

[207] J. H. Thomas and N. O. Weiss. The theory of sunspots. In J. H. Thomas and N. O. Weiss, editors, *Sunspots: Theory and Observations*, pages 3–59. Kluwer, NATO ASI, C 375, 1992.

[208] B. Schmieder, J. C. del Toro Iniesta, and M. Vázquez (Eds.), *1st Advances in Solar Physics Euroconference: Advances in the Physics of Sunspots*. Kluwer, Dordrecht, 1997.

[209] S. K. Solanki. Sunspots: An overview. *Astron. Astrophys. Rev.*, 11:153–286, 2003.

[210] M. Sobotka, P. N. Brandt, and G. W. Simon. Fine structure in sunspots. I. Sizes and lifetimes of umbral dots. *Astron. Astrophys.*, 328:682–688, 1997.

[211] A. Tritschler and W. Schmidt. Sunspot photometry with phase diversity. II. Fine-structure characteristics. *Astron. Astrophys.*, 388:1048–1061, 2002.

[212] U. Grossmann-Doerth, W. Schmidt, and E. H. Schroeter. Size and temperature of umbral dots. *Astron. Astrophys.*, 156:347–353, 1986.

[213] M. Sobotka, P. N. Brandt, and G. W. Simon. Fine structure in sunspots. II. Intensity variations and proper motions of umbral dots. *Astron. Astrophys.*, 328:689–694, 1997.

[214] H. Socas-Navarro, V. M. Pillet, M. Sobotka, and M. Vázquez. The Thermal and Magnetic Structure of Umbral Dots from the Inversion of High-Resolution Full Stokes Observations. *Astrophys. J.*, 614:448–456, 2004.

[215] G. B. Scharmer, B. V. Gudiksen, D. Kiselman, M. G. Löfdahl, and L. H. M. Rouppe van der Voort. Dark cores in sunspot penumbral filaments. *Nature*, 420:151–153, 2002.

[216] L. H. M. Rouppe van der Voort, M. G. Löfdahl, D. Kiselman, and G. B. Scharmer. Penumbral structure at 0.1 arcsec resolution. I. General appearance and power spectra. *Astron. Astrophys.*, 414:717–726, 2004.

[217] E. Wiehr and G. Stellmacher. Velocity and magnetic field fluctuations in penumbral fine-structures. *Astron. Astrophys.*, 225:528–532, 1989.

[218] T. J. Bogdan, P. A. Gilman, I. Lerche, and R. Howard. Distribution of sunspot umbral areas - 1917-1982. *Astrophys. J.*, 327:451–456, 1988.

[219] I. Baumann and S. K. Solanki. On the size distribution of sunspot groups in the Greenwich sunspot record 1874-1976. *Astron. Astrophys.*, 443:1061–1066, 2005.

[220] M. N. Gnevyshev. On the nature of solar activity. *Izvestiya Glavnoj Astronomicheskoj Observatorii v Pulkove*, 16:36, 1938.

[221] M. Waldmeier. *Ergebnisse und Probleme der Sonnenforschung, 2. Aufl.* Geest und Porting, Leipzig, 1955.

[222] F. Meyer, H. U. Schmidt, P. R. Wilson, and N. O. Weiss. The growth and decay of sunspots. *Monthly Not. Royal Astron. Soc.*, 169:35–57, 1974.

[223] K. Petrovay and F. Moreno-Insertis. Turbulent erosion of magnetic flux tubes. *Astrophys. J.*, 485:398–408, 1997.

[224] R. Keppens and V. Martinez Pillet. The magnetic structure of pores and sunspots derived from advanced Stokes Polarimeter data. *Astron. Astrophys.*, 316:229–242, 1996.

[225] M. G. Adam. An observational examination of models for sunspot magnetic field configurations. *Sol. Phys.*, 125:37–44, 1990.

[226] B. W. Lites and A. Skumanich. Stokes profile analysis and vector magnetic fields. V - The

magnetic field structure of large sunspots observed with Stokes II. *Astrophys. J.*, 348:747–760, 1990.

[227] S. K. Solanki, I. Rüedi, and W. Livingston. Infrared lines as probes of solar magnetic features. V - The magnetic structure of a simple sunspot and its canopy. *Astron. Astrophys.*, 263:339–350, 1992.

[228] S. K. Mathew, A. Lagg, S. K. Solanki, M. Collados, J. M. Borrero, S. Berdyugina, N. Krupp, J. Woch, and C. Frutiger. Three dimensional structure of a regular sunspot from the inversion of IR Stokes profiles. *Astron. Astrophys.*, 410:695–710, 2003.

[229] T. Hewagama, D. Deming, D. E. Jennings, V. Osherovich, G. Wiedemann, D. Zipoy, D. L. Mickey, and H. Garcia. Solar magnetic field studies using the 12 micron emission lines. II - Stokes profiles and vector field samples in sunspots. *Astrophysical Journal and Supplement Series*, 86:313–332, 1993.

[230] M. Landolfi and E. L. Degl'Innocenti. Magneto-optical effects and the determination of vector magnetic fields from Stokes profiles. *Sol. Phys.*, 78:355–364, 1982.

[231] E. Landi Degl'Innocenti. Magneto-optical effects and the interpretation of linearly polarized intensity distributions observed with a vector magnetograph. *Sol. Phys.*, 63:237–245, 1979.

[232] C. Westendorp Plaza, J. C. del Toro Iniesta, B. Ruiz Cobo, V.M. Martínez Pillet, B. W. Lites, and A. Skumanich. Optical tomography of a sunspot. II. Vector magnetic field and temperature stratification. *Astrophys. J.*, 547:1130–1147, 2001.

[233] S. K. Solanki and H. U. Schmidt. Are sunspot penumbrae deep or shallow? *Astron. Astrophys.*, 267:287–291, 1993.

[234] H. U. Schmidt. Sunspots. *Geophys. Astrophys. Fluid Dyn.*, 62:249–270, 1991.

[235] H. Balthasar and M. Collados. Some properties of an isolated sunspot. *Astron. Astrophys.*, 429:705–711, 2005.

[236] R. G. Giovanelli. An exploratory two-dimensional study of the coarse structure of network magnetic fields. *Sol. Phys.*, 68:49–69, 1980.

[237] R. G. Giovanelli and H. P. Jones. The three-dimensional structure of atmospheric magnetic fields in two active regions. *Sol. Phys.*, 79:267–278, 1982.

[238] S. K. Solanki, W. Finsterle, I. Rüedi, and W. Livingston. Expansion of solar magnetic flux tubes large and small. *Astron. Astrophys.*, 347:L27–L30, 1999.

[239] H. Balthasar and W. Schmidt. Polarimetry and spectroscopy of a simple sunspot. 2: On the height and temperature dependence of the magnetic field. *Astron. Astrophys.*, 279:243–250, 1993.

[240] J. H. M. J. Bruls, S. K. Solanki, R. J. Rutten, and M. Carlsson. Infrared lines as probes of solar magnetic features. VIII. Mg I 12μm diagnostics of sunspots. *Astron. Astrophys.*, 293:225–239, 1995.

[241] M. T. Eibe, G. Aulanier, M. Faurobert, P. Mein, and J. M. Malherbe. Vertical structure of sunspots from THEMIS observations. *Astron. Astrophys.*, 381:290–299, 2000.

[242] W. Henze, E. Tandberg-Hanssen, M. J. Hagyard, E. A. West, B. E. Woodgate, R. A. Shine, J. M. Beckers, M. Bruner, C. L. Hyder, and E. A. West. Observations of the longitudinal magnetic field in the transition region and photosphere of a sunspot. *Sol. Phys.*, 81:231–244, 1982.

[243] J. W. Lee, G. J. Hurford, and D. E. Gary. Microwave emission from a sunspot. I - Implications for the sunspot magnetic structure. *Sol. Phys.*, 144:45–57, 1993.

[244] M. J. Penn and J. R. Kuhn. Imaging spectropolarimetry of the He I 1083 nanometer line in a flaring solar active region. *Atrophys. J. Lett.*, 441:L51–L54, 1995.

[245] H. S. Yun. Magnetic fields in umbral atmospheres under 'similarity' configuration. *Sol. Phys.*, 22:137–139, 1972.

[246] C. Westendorp Plaza, J. C. del Toro Iniesta, B. Ruiz Cobo, and V. Martínez Pillet. Optical tomography of a sunspot. III. Velocity stratification and the Evershed effect. *Astrophys. J.*, 547:1148–1158, 2001.

[247] V. Martínez Pillet. Spectral signature of uncombed penumbral magnetic fields. *Astron. Astrophys.*, 361:734–742, 2000.

[248] J. M. Borrero, S. K. Solanki, L. R. Bellot Rubio, A. Lagg, and S. K. Mathew. On the fine structure of sunspot penumbrae. I. A quantitative comparison of two semiempirical models with implications for the Evershed effect. *Astron. Astrophys.*, 422:1093–1104, 2004.

[249] D. Degenhardt and E. Wiehr. Spatial variation of the magnetic field inclination in a sunspot penumbra. *Astron. Astrophys.*, 252:821–826, 1991.

[250] W. Schmidt, A. Hofmann, H. Balthasar, T. D. Tarbell, and Z. A. Frank. Polarimetry and spectroscopy of a simple sunspot. I - On the magnetic field of a sunspot penumbra. *Astron. Astrophys.*, 264:L27–L30, 1992.

[251] A. M. Title, Z. A. Frank, R. A. Shine, T. D. Tarbell, K. P. Topka, G. Scharmer, and W. Schmidt. On the magnetic and velocity field geometry of simple sunspots. *Astrophys. J.*, 403:780–796, 1993.

[252] K. Langhans, G. B. Scharmer, D. Kiselman, M. G. Löfdahl, and T. E. Berger. Inclination of magnetic fields and flows in sunspot penumbrae. *Astron. Astrophys.*, 436:1087–1101, 2005.

[253] S. K. Solanki and C. A. P. Montavon. Uncombed fields as the source of the broad-band circular polarization of sunspots. *Astron. Astrophys.*, 275:283–292, 1993.

[254] J. Sánchez Almeida. Spectral signature of uncombed penumbral magnetic fields. Comment. *Astron. Astrophys.*, 369:643, 2001.

[255] V. Martínez Pillet. Spectral signature of uncombed penumbral magnetic fields. Reply. *Astron. Astrophys.*, 369:644–645, 2001.

[256] J.-M. Borrero, S. K. Solanki, A. Lagg, H. Socas Navarro, and B. W. Lites. On the fine structure of sunspot penumbrae. III. The vertical structure of penumbral filaments. *Astron. Astrophys.*, 436:33–345, 2005.

[257] H. C. Spruit and G. B. Scharmer. Fine structure, magnetic field and heating of sunspot penumbrae. *Astron. Astrophys.*, in press, 2005.

[258] S. K. Mathew, S. K. Solanki, A. Lagg, M. Collados, J. M. Borrero, and S. Berdyugina. Thermal-magnetic relation in a sunspot and a map of its Wilson depression. *Astron. Astrophys.*, 422:693–701, 2004.

[259] C. E. St. John. Radial motion in Sun-spots. *Astrophys. J.*, 37:322–353, 1913.

[260] P. Maltby. On the velocity field in sunspots. *Astrophysica Norvegica*, 8:205–269, 1964.

[261] K. Ichimoto. Evershed effect observed in various solar photospheric lines. I - Dependence of the velocity distribution across the penumbra on the equivalent width. *Publ. Astron. Soc. Japan*, 39:329–342, 1987.

[262] E. Wiehr. The origin of the Evershed asymmetry. *Astron. Astrophys.*, 298:L17–L20, 1995.

[263] L. H. M. Rouppe van der Voort. Penumbral structure and kinematics from high-spatial-resolution observations of Ca II K. *Astron. Astrophys.*, 389:1020–1038, 2002.

[264] M. J. Penn, W. D. Cao, S. R. Walton, G. A. Chapman, and W. Livingston. Weak infrared molecular lines reveal rapid outflow in cool magnetic sunspot penumbral fibrils. *Atrophys. J. Lett.*, 590:L119–L122, 2003.

[265] E. Wiehr and D. Degenhardt. Spatial structure of the Evershed effect. *Astron. Astrophys.*, 259:313–317, 1992.

[266] K. P. Dere, B. Schmieder, and C. E. Alissandrakis. Flow patterns in a sunspot region observed in the photosphere, chromosphere and transition region. *Astron. Astrophys.*, 233:207–219, 1990.

[267] P. Börner and F. Kneer. High resolution observations of the Evershed flow. *Astron. Astrophys.*, 259:307–312, 1992.

[268] S. K. Solanki, C. A. P. Montavon, and W. Livingston. Infrared lines as probes of solar magnetic features. VII: On the nature of the Evershed effect in sunspots. *Astron. Astrophys.*, 283:221–231, 1994.

[269] C. Westendorp Plaza, J. C. del Toro Iniesta, B. Ruiz Cobo, V. Martinez Pillet, B. W. Lites, and A. Skumanich. Evidence for a downward mass flux in the penumbral region of a sunspot. *Nature*, 389:47, 1997.

[270] L. R. Bellot Rubio, H. Balthasar, M. Collados, and R. Schlichenmaier. Field-aligned Evershed flows in the photosphere of a sunspot penumbra. *Astron. Astrophys.*, 403:L47–L50, 2003.

[271] G. Tsiropoula. Physical parameters and flows along chromospheric penumbral fibrils. *Astron. Astrophys.*, 357:735–742, 2000.

[272] T. L. J. Duvall, S. D'Silva, S. M. Jefferies, J. W. Harvey, and J. Schou. Downflows under sunspots detected by helioseismic tomography. *Nature*, 379:235–237, 1996.

[273] E. N. Parker. Vortex attraction and the formation of sunspots. *Astrophys. J.*, 390:290–296, 1992.

[274] B. W. Lites. Sunspot oscillations - Observations and implications. In N.O. Weiss, J.H. Thomas (Eds.), *Sunspots. Theory and Observations*, pages 261–302, NATO ASI Proc. 375, Kluwer, Dordrecht, 1992.

[275] H. Zirin and A. Stein. Observations of Running Penumbral Waves. *Atrophys. J. Lett.*, 178:L85, 1972.

[276] J. Staude. Sunspot oscillations. In B. Schmieder, A. Hofmann and J. Staude (Eds.), *Third Advances in Solar Physics Euroconference: Magnetic Fields and Oscillations*, pages 113–130, San Francisco: Astronomical Society of the Pacific Conf. Series 184, 1999

[277] Y. Suzuki. On the Wilson effect of the sunspots. *Publ. Astron. Soc. Japan*, 19:220–228, 1967.

[278] M. H. Gokhale and C. Zwaan. The structure of sunspots. I: Observational constraints: Current

sheet models. *Sol. Phys.*, 26:52–75, 1972.

[279] M. Collados, J. C. del Toro Iniesta, and M. Vázquez. A statistical study of the geometrical Wilson effect. *Sol. Phys.*, 112:281–293, 1987.

[280] H. Alfvén. On sunspots and the solar cycle. *Arkiv for Astronomi*, 29:1–17, 1943.

[281] V. Martínez Pillet and M. Vázquez. The continuum intensity-magnetic field relation in sunspot umbrae. *Astron. Astrophys.*, 270:494–508, 1993.

[282] S. K. Solanki, U. Walther, and W. Livingston. Infrared lines as probes of solar magnetic features. VI. The thermal-magnetic relation and Wilson depression of a simple sunspot. *Astron. Astrophys.*, 277:639–647, 1993.

[283] K. Jahn. Current sheet as a diagnostic for the subphotospheric structure of a spot. *Astron. Astrophys.*, 222:264–292, 1989.

[284] K. Jahn and H. U. Schmidt. Thick penumbra in a magnetostatic sunspot model. *Astron. Astrophys.*, 290:295–317, 1994.

[285] E. N. Parker. Sunspots and the physics of magnetic flux tubes. I - The general nature of the sunspot. *Astrophys. J.*, 230:905–913, 1979.

[286] E. N. Parker. Sunspots and the physics of magnetic flux tubes. I - The general nature of the sunspot. II - Aerodynamic drag. *Astrophys. J.*, 230:905–923, 1979.

[287] E. N. Parker. Sunspots and the physics of magnetic flux tubes. IX - Umbral dots and longitudinal overstability. *Astrophys. J.*, 234:333–347, 1979.

[288] E. N. Parker. The Nature of the Sunspot Phenomenon. IV: The Intrinsic Instability of the Magnetic Configuration. *Sol. Phys.*, 40:291–301, 1975.

[289] F. Meyer, H. U. Schmidt, and N. O. Weiss. The stability of sunspots. *Monthly Not. Royal Astron. Soc.*, 179:741–761, 1977.

[290] A. R. Choudhuri. The dynamics of magnetically trapped fluids. I - Implications for umbral dots and penumbral grains. *Astrophys. J.*, 302:809–825, 1986.

[291] J. Zhao, A. G. Kosovichev, and T. L. Duvall. Investigation of mass flows beneath a sunspot by time-distance helioseismology. *Astrophys. J.*, 557:384–388, 2001.

[292] H. C. Spruit. Small scale phenomena in umbras and penumbras - The role of convective processes. In L.E. Cram, J.H. Thomas (Eds.)*The Physics of Sunspots*, pages 359–368, Sunspot, NM, Sacramento Peak Observatory, 1981.

[293] R. Schlichenmaier, K. Jahn, and H. U. Schmidt. Magnetic flux tubes evolving in sunspots. A model for the penumbral fine structure and the Evershed flow. *Astron. Astrophys.*, 337:897–910, 1998.

[294] R. Schlichenmaier, K. Jahn, and H. U. Schmidt. A dynamical model for the penumbral fine structure and the Evershed effect in sunspots. *Astrophys. J.*, 493:L121–L124, 1998.

[295] R. Schlichenmaier and W. Schmidt. Flow geometry in a sunspot penumbra. *Astron. Astrophys.*, 358:1122–1132, 2000.

[296] R. Schlichenmaier and M. Collados. Spectropolarimetry in a sunspot penumbra. Spatial dependence of Stokes asymmetries in Fe I 1564.8 nm. *Astron. Astrophys.*, 381:668–682, 2002.

[297] S. K. Solanki and I. Rüedi. Spatial and temporal fluctuations in sunspots derived from MDI data. *Astron. Astrophys.*, 411:249–256, 2003.

[298] L. Biermann. Gegenwärtiger Stand der Theorie konvektiver Sonnenmodelle. *Mitt. Astron. Ges.*, 76:194–200, 1941.

[299] M. R. E. Proctor and N. O. Weiss. Magnetoconvection. *Rep. Prog. Phys.*, 45:1317–1379, 1982.

[300] H. C. Spruit. Heat flow near obstacles in the solar convection zone. *Sol. Phys.*, 55:3–34, 1977.

[301] H. C. Spruit. Effect of spots on a star's radius and luminosity. *Astron. Astrophys.*, 108:348–355, 1982.

[302] H. C. Spruit. The flow of heat near a starspot. *Astron. Astrophys.*, 108:356–360, 1982.

[303] M. P. Rast, R. W. Meisner, B. W. Lites, P. A. Fox, and O. R. White. Sunspot bright rings: Evidence from case studies. *Astrophys. J.*, 557:864–879, 2001.

[304] M. Waldmeier. Über die Struktur der Sonnenflecken. *Astron. Mitt. Zürich*, 14(138):439–485, 1939.

[305] N. O. Weiss. Magnetoconvection. In B. Schmieder, J.C. del Toro Iniesta, and M. Vázquez, editors, *Advances in Physics of Sunspots*, page 21, San Francisco: Astronomical Society of the Pacific Conf. Series 118, 1997

[306] N. O. Weiss. Umbral and penumbral magnetoconvection. *Astronomische Nachrichten*, 323:371–376, 2002.

[307] M. R. E. Proctor. Magnetoconvection. In J. H. Thomas and N. O. Weiss, editors, *Sunspots: Theory and Observations*, pages 221–224. Kluwer, NATO ASI, C 375, 1992.

[308] N. O. Weiss, D. P. Brownjohn, N. E. Hurlburt, and M. R. E. Proctor. Oscillatory convection

in sunspot umbrae. *Mon. Not. R. Astron. Soc.*, 245:434–452, 1990.

[309] L. Tao, M. R. E. Proctor, and N. O. Weiss. Flux expulsion by inhomogeneous turbulence. *Mon. Not. R. Astron. Soc.*, 300:907–914, 1998.

[310] F. Cattaneo, T. Emonet, and N. Weiss. On the Interaction between Convection and Magnetic Fields. *Astrophys. J.*, 588:1183–1198, 2003.

[311] H. U. Schmidt, H. C. Spruit, and N. O. Weiss. Energy transport in sunspot penumbrae. *Astron. Astrophys.*, 158:351–360, 1986.

[312] R. Schlichenmaier and S. K. Solanki. On the heat transport in a sunspot penumbra. *Astron. Astrophys.*, 411:257–262, 2003.

[313] R. E. Danielson. The Structure of Sunspot Penumbras. II. Theoretical. *Astrophys. J.*, 134:289, 1961.

[314] F. Meyer and H. U. Schmidt. A Model for the Evershed flow in sunspots. *Mitteilungen der Astronomischen Gesellschaft Hamburg*, 25:194–197, 1968.

[315] F. Meyer and H. U. Schmidt. Magnetisch ausgerichtete Strömungen zwischen Sonnenflecken. *Z. Ang. Math. Mech.*, 48:T218–T221, 1968.

[316] D. Degenhardt. On the origin of penumbral line asymmetries. *Astron. Astrophys.*, 277:235–241, 1993.

[317] B. Montesinos and J. H. Thomas. The Evershed effect in sunspots as a siphon flow along a magnetic flux tube. *Nature*, 390:485–487, 1997.

[318] I. Rüedi, S. K. Solanki, and C. U. Keller. Infrared lines as probes of solar magnetic features. XV. Evershed flow in cool, weak penumbral fields. *Astron. Astrophys.*, 348:L37–L40, 1999.

[319] A. M. Title, T. D. Tarbell, and K. P. Topka. On the relation between magnetic field structures and granulation. *Astrophys. J.*, 317:892–899, 1987.

[320] S. K. Solanki. The origin and the diagnostic capabilities of the Stokes V asymmetry observed in solar faculae and the network. *Astron. Astrophys.*, 224:225–241, 1989.

[321] R. Keppens. Sunspot Pores. In B. Schmieder et al., (Eds.), *Encyclopedia of Astronomy and Astrophysics*, pages 3193–3197, Institute of Physics, Bristol, 2001.

[322] C. U. Keller. Resolution of magnetic flux tubes on the sun. *Nature*, 359:307–308, 1992.

[323] H. Lin. On the Distribution of the Solar Magnetic Fields. *Astrophys. J.*, 446:421–430, 1995.

[324] H.C. Spruit, M. Schüssler, and S.K. Solanki. Filigree and flux tube physics. In A.N. Cox, W.C. Livingston, and M.S. Matthews, editors, *Solar Interior and Atmosphere*, pages 890–910, Tucson, 1991. The University of Arizona Press.

[325] S. K. Solanki. Small scale solar magnetic fields - an overview. *Space Sci. Rev.*, 63:1–188, 1993.

[326] G. E. Hale. Invisible sunspots. *Monthly Not. Royal Astron. Soc.*, 82:168, 1922.

[327] H. W. Babcock and H. D. Babcock. The Sun's magnetic field, 1952-1954. *Astrophys. J.*, 121:349–366, 1955.

[328] N. R. Sheeley. Measurements of solar magnetic fields. *Astrophys. J.*, 144:723–732, 1966.

[329] J. M. Beckers and E. H. Schröter. The intensity, velocity and magnetic structure of a sunspot region. I: Observational technique; properties of magnetic knots. *Sol. Phys.*, 4:142–164, 1968.

[330] E. N. Frazier and J. O. Stenflo. On the small-scale structure of solar magnetic fields. *Sol. Phys.*, 27:330–346, 1972.

[331] J. O. Stenflo. Magnetic-field structure of the photospheric network. *Sol. Phys.*, 32:41–63, 1973.

[332] E. Wiehr. A unique magnetic field range for nonspot solar magnetic regions. *Astron. Astrophys.*, 69:279–284, 1978.

[333] J. O. Stenflo and J. W. Harvey. Dependence of the properties of magnetic fluxtubes on area factor or amount of flux. *Sol. Phys.*, 95:99–118, 1985.

[334] S. K. Solanki, C. Keller, and J. O. Stenflo. Properties of solar magnetic fluxtubes from only two spectral lines. *Astron. Astrophys.*, 188:183–197, 1987.

[335] D. Rabin. Spatially extended measurements of magnetic field strength in solar plages. *Astrophys. J.*, 391:832–844, 1992.

[336] D. Rabin. A true-field magnetogram in a solar plage region. *Atrophys. J. Lett.*, 390:L103–L106, 1992.

[337] I. Rüedi, S. K. Solanki, W. Livingston, and J. O. Stenflo. Infrared lines as probes of solar magnetic features. III - Strong and weak magnetic fields in plages. *Astron. Astrophys.*, 263:323–338, 1992.

[338] V. Martínez Pillet, B. W. Lites, and A. Skumanich. Active region magnetic fields. I. Plage fields. *Astrophys. J.*, 474:810–842, 1997.

[339] L. R. Bellot Rubio, B. Ruiz Cobo, and M. Collados. Structure of plage flux tubes from the inversion of stokes spectra. I. Spatially averaged Stokes I and V profiles. *Astrophys. J.*, 535:489–500, 2000.

[340] C. Frutiger and S. K. Solanki. Empirical models of solar magnetic flux-tubes and their non-magnetic surroundings. *Astron. Astrophys.*, 369:646–659, 2001.

[341] H. Zirin and B. Popp. Observations of the 12 micron Mg I lines in various solar features. *Astrophys. J.*, 340:571–578, 1989.

[342] J. H. M. J. Bruls and S. K. Solanki. Infrared lines as probes of solar magnetic features. IX. Mg I 12 μm diagnostics of solar plage. *Astron. Astrophys.*, 293:240–251, 1995.

[343] C. Briand and S. K. Solanki. Velocity fields below the magnetic canopy of solar flux tubes: evidence for high-speed downflows? *Astron. Astrophys.*, 330:1160–1168, 1998.

[344] I. Zayer, J. O. Stenflo, C. U. Keller, and S. K. Solanki. Dependence of the properties of solar magnetic flux tubes on filling factor. II - Results of an inversion approach. *Astron. Astrophys.*, 239:356–366, 1990.

[345] S. K. Solanki, D. Zufferey, H. Lin, I. Rüedi, and J. R. Kuhn. Infrared lines as probes of solar magnetic features. XII. Magnetic flux tubes: evidence of convective collapse? *Astron. Astrophys.*, 310:L33–L36, 1996.

[346] E. V. Khomenko, M. Collados, S. K. Solanki, A. Lagg, and J. Trujillo Bueno. Quiet-Sun inter-network magnetic fields observed in the infrared. *Astron. Astrophys.*, 408:1115–1135, 2003.

[347] I. Domínguez Cerdeña, F. Kneer, and J. Sánchez Almeida. Quiet-Sun magnetic fields at high spatial resolution. *Atrophys. J. Lett.*, 582:L55–L58, 2003.

[348] I. Domínguez Cerdeña, J. Sánchez Almeida, and F. Kneer. Inter-network magnetic fields observed with sub-arcsec resolution. *Astron. Astrophys.*, 407:741–757, 2003.

[349] U. Grossmann-Doerth, M. Knölker, M. Schüssler, and S. K. Solanki. The deep layers of solar magnetic elements. *Astron. Astrophys.*, 285:648–654, 1994.

[350] B. W. Lites, A. Skumanich, and V. Martínez Pillet. Vector magnetic fields of emerging solar flux. I. Properties at the site of emergence. *Astron. Astrophys.*, 333:1053–1068, 1998.

[351] L. H. Strous and C. Zwaan. Phenomena in an Emerging Active Region. II. Properties of the Dynamic Small-Scale Structure. *Astrophys. J.*, 527:435–444, 1999.

[352] N. E. Hurlburt and N. O. Weiss. Interaction between magnetic fields and convection. In E.-H. Schröter, M. Vázquez and A.A. Wyller (Eds.), *The Role of Fine-Scale Magnetic Fields on the Structure of the Solar Atmosphere*, pages 35–46, Cambridge University Press, Cambridge, 1987.

[353] E. N. Parker. Hydraulic concentration of magnetic fields in the solar photosphere. VI - Adiabatic cooling and concentration in downdrafts. *Astrophys. J.*, 221:368–377, 1978.

[354] U. Grossmann-Doerth, M. Schüssler, and O. Steiner. Convective intensification of solar surface magnetic fields: results of numerical experiments. *Astron. Astrophys.*, 337:928–939, 1998.

[355] H. C. Spruit. Convective collapse of flux tubes. *Sol. Phys.*, 61:363–378, 1979.

[356] P. Venkatakrishnan. Inhibition of convective collapse of solar magnetic flux tubes by radiative diffusion. *Nature*, 322:156–157, 1986.

[357] M. Schüssler. Theoretical Aspects of Small-Scale Photospheric Magnetic Fields. In J. O. Stenflo, editor, *Solar Photosphere: Structure, Convection and Magnetic Fields, IAU Symposium 138*, page 161, (Dordrecht, NL: Kluwer), 1990.

[358] M. Schüssler. MHD models of solar photospheric magnetic flux concentrations. In W. Deinzer, M. Knölker. and H.H. Voigt (Eds.), *Small Scale Magnetic Flux Concentrations in the Solar Photosphere*, pages 103–120, Göttingen: Vandenhoeck & Ruprecht), 1986.

[359] A. S. Gadun, S. K. Solanki, V. A. Sheminova, and S. R. O. Ploner. A formation mechanism of magnetic elements in regions of mixed polarity. *Sol. Phys.*, 203:1–7, 2001.

[360] I. Domínguez Cerdeña. Evidence of mesogranulation from magnetograms of the Sun. *Astron. Astrophys.*, 412:L65–L68, 2003.

[361] T. E. Berger, M. G. Loefdahl, R. S. Shine, and A. M. Title. Measurements of Solar Magnetic Element Motion from High-Resolution Filtergrams. *Astrophys. J.*, 495:973–983, 1998.

[362] A. R. Choudhuri, H. Auffret, and E. R. Priest. Implications of rapid footpoint motions of photospheric flux tubes for coronal heating. *Sol. Phys.*, 143:49–68, 1993.

[363] S. F. Martin, S. H. B. Livi, and J. Wang. The cancellation of magnetic flux. II - In a decaying active region. *Australian J. Phys.*, 38:929–959, 1985.

[364] S. H. B. Livi, J. Wang, and S. F. Martin. The cancellation of magnetic flux. I - On the quiet sun. *Australian J. Phys.*, 38:855–873, 1985.

[365] E. R. Priest, C. E. Parnell, and S. F. Martin. A converging flux model of an X-ray bright point and an associated canceling magnetic feature. *Astrophys. J.*, 427:459–474, 1994.

[366] K. P. Topka, T. D. Tarbell, and A. M. Title. Properties of the smallest solar magnetic elements. I - Facular contrast near sun center. *Astrophys. J.*, 396:351–363, 1992.

[367] A. Ortiz, S. K. Solanki, V. Domingo, M. Fligge, and B. Sanahuja. On the intensity contrast of

solar photospheric faculae and network elements. *Astron. Astrophys.*, 388:1036–1047, 2002.

[368] E.N. Frazier. Multi-channel magnetograph observations. III: Faculae. *Sol. Phys.*, 21:42–53, 1971.

[369] T. E. Berger, L. H. M. Rouppe van der Voort, M. G. Löfdahl, M. Carlsson, A. Fossum, V. H. Hansteen, E. Marthinussen, A. Title, and G. Scharmer. Solar magnetic elements at 0.1 arcsec resolution. General appearance and magnetic structure. *Astron. Astrophys.*, 428:613–628, 2004.

[370] L. H. M. Rouppe van der Voort, V. H. Hansteen, M. Carlsson, A. Fossum, E. Marthinussen, M. J. van Noort, and T. E. Berger. Solar magnetic elements at 0.1 arcsec resolution. II. Dynamical evolution. *Astron. Astrophys.*, 435:327–337, May 2005.

[371] K. P. Topka, T. D. Tarbell, and A. M. Title. Properties of the smallest solar magnetic elements. II. Observations versus hot wall models of faculae. *Astrophys. J.*, 484:479–486, 1997.

[372] O. Steiner, P. H. Hauschildt, and J. Bruls. Radiative properties of magnetic elements. I. Why are G-band bright points bright? *Astron. Astrophys.*, 372:L13–L16, 2001.

[373] J. Sánchez Almeida, A. Asensio Ramos, J. Trujillo Bueno, and J. Cernicharo. G-band spectral synthesis in solar magnetic concentrations. *Astrophys. J.*, 555:978–989, 2001.

[374] S. V. Berdyugina, S. K. Solanki, and C. Frutiger. The molecular Zeeman effect and diagnostics of solar and stellarmagnetic fields. II. Synthetic Stokes profiles in the Zeeman regime. *Astron. Astrophys.*, 412:513–527, 2003.

[375] R. J. Rutten, A. G. de Wijn, and P. Sütterlin. DOT tomography of the solar atmosphere. II. Reversed granulation in Ca II H. *Astron. Astrophys.*, 416:333–340, 2004.

[376] J.-P. Delaboudiniere, G. E. Artzner, J. Brunaud, A. H. Gabriel, J. F. Hochedez, F. Millier, X. Y. Song, B. Au, K. P. Dere, R. A. Howard, R. Kreplin, D. J. Michels, J. D. Moses, J. M. Defise, C. Jamar, P. Rochus, J. P. Chauvineau, J. P. Marioge, R. C. Catura, J. R. Lemen, L. Shing, R. A. Stern, J. B. Gurman, W. M. Neupert, A. Maucherat, F. Clette, P. Cugnon, and E. L. van Dessel. EIT: Extreme-Ultraviolet imaging telescope for the SOHO mission. *Sol. Phys.*, 162:291–312, 1995.

[377] B. W. Lites, G. Scharmer, T. E. Berger, and A. M. Title. Three-dimensional structure of the active region photosphere as revealed by high angular resolution. *Sol. Phys.*, 221:65–84, 2004.

[378] J. Hirzberger and E. Wiehr. Solar limb faculae. *Astron. Astrophys.*, 438:1059–1065, 2005.

[379] R. J. Defouw. Wave propagation along a magnetic tube. *Astrophys. J.*, 209:266–269, 1976.

[380] B. Roberts and A. R. Webb. Vertical motions in an intense magnetic flux tube. III - On the slender flux tube approximation. *Sol. Phys.*, 64:77–92, 1979.

[381] G. W. Pneuman, S. K. Solanki, and J. O. Stenflo. Structure and merging of solar magnetic fluxtubes. *Astron. Astrophys.*, 154:231–242, 1986.

[382] A. Ferriz-Mas, M. Schüssler, and V. Anton. Dynamics of magnetic flux concentrations - The second-order thin flux tube approximation. *Astron. Astrophys.*, 210:425–432, 1989.

[383] G. W. Simon, N. O. Weiss, and A. H. Nye. Simple models for magnetic flux tubes. *Sol. Phys.*, 87:65–75, 1983.

[384] O. Steiner, G. W. Pneuman, and J. O. Stenflo. Numerical models for solar magnetic fluxtubes. *Astron. Astrophys.*, 170:126–137, 1986.

[385] H. C. Spruit. Pressure equilibrium and energy balance of small photospheric fluxtubes. *Sol. Phys.*, 50:269–295, 1976.

[386] M. Knölker and M. Schüssler. Model calculations of magnetic flux tubes. IV - Convective energy transport and the nature of intermediate size flux concentrations. *Astron. Astrophys.*, 202:275–283, 1988.

[387] C. U. Keller, M. Schüssler, A. Vögler, and V. Zakharov. On the Origin of Solar Faculae. *Astrophys. J.*, 607:L59–L62, 2004.

[388] M. Carlsson, R. F. Stein, Å. Nordlund, and G. B. Scharmer. Observational manifestations of solar magnetoconvection: Center-to-limb variation. *Atrophys. J. Lett.*, 610:L137–L140, 2004.

[389] O. Steiner. Radiative properties of magnetic elements. II. Center to limb variation of the appearance of photospheric faculae. *Astron. Astrophys.*, 430:691–700, 2005.

[390] C. Briand and S. K. Solanki. Empirical models of solar magnetic elements: constraints imposed by Mg I Stokes profiles. *Astron. Astrophys.*, 299:596–610, 1995.

[391] U. Grossmann-Doerth, M. Schüssler, and S. K. Solanki. Unshifted, asymmetric Stokes V-profiles - Possible solution of a riddle. *Astron. Astrophys.*, 206:L37–L39, 1988.

[392] W. Deinzer, G. Hensler, M. Schüssler, and E. Weisshaar. Model calculations of magnetic flux tubes. I - Equations and method. II - Stationary results for solar magnetic elements. *Astron. Astrophys.*, 139:426–449, 1984.

[393] W. Deinzer, G. Hensler, M. Schussler, and E. Weisshaar. Model Calculations of Magnetic Flux Tubes - Part Two - Stationary Results for Solar Magnetic Elements. *Astron. Astrophys.*, 139:435–449, 1984.

[394] O. Steiner, U. Grossmann-Doerth, M. Knölker, and M. Schüssler. Dynamical interaction of solar magnetic elements and granular convection: results of a numerical simulation. *Astrophys. J.*, 495:468–484, 1998.

[395] R. F. Stein and Å. Nordlund. Realistic Solar Convection Simulations. *Sol. Phys.*, 192:91–108, 2000.

[396] H. C. Spruit, A. Nordlund, and A. M. Title. Solar convection. *Ann. Review of Astronomy and Astrophysics*, 28:263–301, 1990.

[397] A. Nordlund. Modelling of small-scale dynamical processes: Convection and wave generation (Keynote). In S. L. Keil (ed.), *Small-Scale Dynamical Processes in Quiet Stellar Atmospheres*, pages 181–221. National Solar Obs., Sunspot NM, 1984.

[398] M. Asplund, Å. Nordlund, R. Trampedach, C. Allende Prieto, and R. F. Stein. Line formation in solar granulation. I. Fe line shapes, shifts and asymmetries. *Astron. Astrophys.*, 359:729–742, 2000.

[399] Å. Nordlund and R. F. Stein. Solar Magnetoconvection. In J. O. Stenflo, editor, *Solar Photosphere: Structure, Convection and Magnetic Fields, IAU Symp. 138*, page 191, Dordrecht, 1990. Kluwer Academic Publishers.

[400] D. J. Bercik, S. Basu, D. Georgobiani, A. Nordlund, and R. F. Stein. Solar Magneto-Convection. In R. A. Donahue and J. A. Bookbinder, editors, *Cool Stars, Stellar Systems, and the Sun 10*, page 568, San Francisco: Astronomical Society of the Pacific Conf. Series 154, 1998

[401] D. J. Bercik, A. Nordlund, and R. F. Stein. Magnetoconvection and micropores. In *GONG+ 2002. Local and Global Helioseismology: the Present and Future*, page 201, (Nordwijk, NL: European Space Agency), ESA SP-517, 2003

[402] A. Vögler, S. Shelyag, M. Schüssler, F. Cattaneo, Th. Emonet, and T. Linde. Simulation of solar magneto-convection. In N. E. Piskunov, W. W. Weiss, and D. F. Gray, editors, *Modelling of Stellar Atmospheres*, page 157, San Francisco, 2003. Astronomical Society of the Pacific.

[403] A. Vögler and M. Schüssler. Studying magneto-convection by numerical simulation. *Astron. Nachr./AN*, 324:399–404, 2003.

[404] A. Vögler, S. Shelyag, M. Schüssler, F. Cattaneo, T. Emonet, and T. Linde. Simulations of magneto-convection in the solar photosphere. Equations, methods, and results of the MURaM code. *Astron. Astrophys.*, 429:335–351, 2005.

[405] E. V. Khomenko, M. J. Martínez González, M. Collados, A. Vögler, S. K. Solanki, B. Ruiz Cobo, and C. Beck. Magnetic flux in the internetwork quiet Sun. *Astron. Astrophys.*, 436:L27–L30, June 2005.

[406] A. M. Title, T. D. Tarbell, K. P. Topka, S. H. Ferguson, R. A. Shine, and SOUP Team. Statistical properties of solar granulation derived from the SOUP instrument on Spacelab 2. *Astrophys. J.*, 336:475–494, 1989.

[407] M. Schüssler, S. Shelyag, S. Berdyugina, A. Vögler, and S. K. Solanki. Why solar magnetic flux concentrations are bright in molecular bands. *Atrophys. J. Lett.*, 597:L173–L176, 2003.

[408] S. Shelyag, M. Schüssler, S. K. Solanki, S. V. Berdyugina, and A. Vögler. G-band spectral synthesis and diagnostics of simulated solar magneto-convection. *Astron. Astrophys.*, 427:335–343, 2004.

[409] E. N. Parker. Magnetic Neutral Sheets in Evolving Fields - Part Two - Formation of the Solar Corona. *Astrophys. J.*, 264:642–647, 1983.

[410] E. N. Parker. Nanoflares and the solar X-ray corona. *Astrophys. J.*, 330:474–479, 1988.

[411] B. V. Gudiksen and Å. Nordlund. Bulk heating and slender magnetic loops in the solar corona. *Astrophys. J.*, 572:L113–L116, 2002.

[412] R. G. Giovanelli, W. C. Livingston, and J. W. Harvey. Motions in solar magnetic tubes. II - The oscillations. *Sol. Phys.*, 59:49–64, 1978.

[413] B. Fleck, F.-L. Deubner, and W. Schmidt. Observations of waves and oscillations in the solar magnetic fine structure. In H. Zirin, D. Ai and H. Wang (Eds.), *The Magnetic and Velocity Fields of Solar Active Regions*, pages 522–525, San Francisco: Astronomical Society of the Pacific Conf. Ser. 46, 1993.

[414] R. Volkmer, F. Kneer, and C. Bendlin. Short-period waves in small-scale magnetic flux tubes on the Sun. *Astron. Astrophys.*, 304:L1–L4, 1995.

[415] B. Roberts and P. Ulmschneider. Dynamics of flux tubes in the solar atmosphere: Theory. In G.M. Simnett, C.E. Alissandrakis, and L. Vlahos (Eds.), pages 75–101, Lecture Notes in

Physics 489, Berlin, Springer Verlag, 1997.

[416] Z. E. Musielak and P. Ulmschneider. Excitation of transverse magnetic tube waves in stellar convection zones. II. Wave energy spectra and fluxes. *Astron. Astrophys.*, 386:606–614, 2002.

[417] Z. E. Musielak and R. Rosner. On the generation of magnetohydrodynamic waves in a stratified and magnetized fluid. I - Vertical propagation. *Astrophys. J.*, 315:371–384, 1987.

[418] A. R. Webb and B. Roberts. Vertical motions in an intense magnetic flux tube - Part five - Radiative relaxation in a stratified medium. *Sol. Phys.*, 68:87–102, 1980.

[419] G. Herbold, P. Ulmschneider, H. C. Spruit, and R. Rosner. Propagation of nonlinear, radiatively damped longitudinal waves along magnetic flux tubes in the solar atmosphere. *Astron. Astrophys.*, 145:157–169, 1985.

[420] D. Fawzy, P. Ulmschneider, K. Stępień, Z. E. Musielak, and W. Rammacher. Acoustic and magnetic wave heating in stars . II. On the range of chromospheric activity. *Astron. Astrophys.*, 386:983–993, 2002.

[421] S. K. Solanki and B. Roberts. Waves in solar magnetic flux tubes - The observational signature of undamped longitudinal tube waves. *Monthly Not. Royal Astron. Soc.*, 256:13–25, 1992.

[422] S. R. O. Ploner and S. K. Solanki. Influence of kink waves in solar magnetic flux tubes on spectral lines. *Astron. Astrophys.*, 325:1199–1212, 1997.

[423] S. R. O. Ploner and S. K. Solanki. Influence of torsional waves in solar magnetic flux tubes on spectral lines. *Astron. Astrophys.*, 345:986–998, 1999.

[424] W. C. Livingston and J. Harvey. A new component of solar magnetism - The inner network fields. *Bulletin of the American Astronomical Society*, 7:346, 1975.

[425] H. Zirin. Evolution of weak solar magnetic fields. *Australian J. Phys.*, 38:961–969, 1985.

[426] J. Zhang, G. Lin, J. Wang, H. Wang, and H. Zirin. The evolution of intranetwork magnetic elements. *Astron. Astrophys.*, 338:322–328, 1998.

[427] H. Socas-Navarro and B. W. Lites. Observational Evidence for Small-Scale Mixture of Weak and Strong Fields in the Quiet Sun. *Astrophys. J.*, 616:587–593, 2004.

[428] L. R. Bellot Rubio and M. Collados. Understanding internetwork magnetic fields as determined from visible and infrared spectral lines. *Astron. Astrophys.*, 406:357–362, 2003.

[429] J. O. Stenflo and L. Lindegren. Statistical analysis of solar Fe I lines - Magnetic line broadening. *Astron. Astrophys.*, 59:367–378, 1977.

[430] J. O. Stenflo. The Hanle effect and the diagnostics of turbulent magnetic fields in the solar atmosphere. *Sol. Phys.*, 80:209–226, 1982.

[431] M. Faurobert-Scholl, N. Feautrier, F. Machefert, K. Petrovay, and A. Spielfiedel. Turbulent magnetic fields in the solar photosphere: diagnostics and interpretation. *Astron. Astrophys.*, 298:289–302, 1995.

[432] M. Faurobert, J. Arnaud, J. Vigneau, and H. Frisch. Investigation of weak solar magnetic fields. New observational results for the Sr I 460.7 nm linear polarization and radiative transfer modeling. *Astron. Astrophys.*, 378:627–634, 2001.

[433] J. O. Stenflo, C. U. Keller, and A. Gandorfer. Differential Hanle effect and the spatial variation of turbulent magnetic fields on the Sun. *Astron. Astrophys.*, 329:319–328, 1998.

[434] S. V. Berdyugina and D. M. Fluri. Evidence for the Hanle effect in molecular lines. *Astron. Astrophys.*, 417:775–784, 2004.

[435] J. Trujillo Bueno, N. Shchukina, and A. Asensio Ramos. A substantial amount of hidden magnetic energy in the quiet Sun. *Nature*, 430:326–329, 2004.

[436] C. Fröhlich. Solar irradiance variations. In A. Wilson (ed.), *Solar Variability as an Input to the Earth's Environment*, pages 183–193, (Nordwijk, NL: European Space Agency), ESA SP-535, 2003

[437] C. L. Wolff and J. R. Hickey. Solar irradiance change and special longitudes due to r-modes. *Science*, 235:1631–1633, 1987.

[438] J. R. Kuhn and R. F. Stein. Accounting for the solar acoustic and luminosity variations from the deep convection zone. *Atrophys. J. Lett.*, 463:L117–L119, 1996.

[439] S. Sofia and L. H. Li. Irradiance or luminosity changes? In A. Wilson (ed.), *The Solar Cycle and Terrestrial Climate, Solar and Space weather*, pages 107–111, (Nordwijk, NL: European Space Agency), ESA SP-463, 2000.

[440] G. A. Chapman. Variations of solar irradiance due to magnetic activity. *A&AR*, 25:633–667, 1987.

[441] P. Foukal. Solar luminosity variation. In K.L. Harvey (ed.), *The Solar Cycle*, pages 439–449, San Francisco: Astronomical Society of the Pacific Conf. Ser. 27, 1992

[442] N. A. Krivova, S. K. Solanki, M. Fligge, and Y. C. Unruh. Reconstruction of solar irradiance variations in cycle 23: Is solar surface magnetism the cause? *Astron. Astrophys.*, 399:L1–L4, 2003.

[443] I. Ermolli, B. Caccin, M. Centrone, and V. Penza. Modeling solar irradiance variations through full-disk images and semi-empirical atmospheric models. *Memorie della Societa Astronomica Italiana*, 74:603, 2003.

[444] G. B. Gelfreikh. Radio measurements of coronal magnetic fields. In V. Rusin, P. Heinzel, and J.-C. Vial, editors, *Solar coronal structures*, volume 144 of *IAU Colloquium*, pages 21–28, Bratislava, Slovakia, 1994. VEDA Publishing Company.

[445] S. M. White and M. R. Kundu. Radio observations of gyroresonance emission from coronal magnetic fields. *Solar Phys.*, 174:31–52, 1997.

[446] T. R. Metcalf, Litao Jiao, A. N. McClymont, R. C. Canfield, and H. Uitenbroek. Is the solar chromosperic magnetic field force-free?. *Astrophys. J.*, 439:474–481, 1995.

[447] V. Bommier and J. L. Leroy. Global pattern of the magnetic field vectors above neutral lines from 1974 to 1982: Pic-du-Midi observations of prominences. In D. Webb, B. Schmieder, and D. Rust, editors, *IAU Colloq. 167: New Perspectives on Solar Prominences*, pages 434–348, San Francisco: Astronomical Society of the Pacific Conf. Series 150, 1998

[448] H. Socas-Navarro, J. Trujillo Bueno, and B. Ruiz Cobo. Anomalous circular polarization profiles in sunspot chromospheres. *Astrophys. J.*, 544:1141–1154, 2000.

[449] S. K. Solanki, A. Lagg, J. Woch, N. Krupp, and M. Collados. Three-dimensional magnetic field topology in a region of solar coronal heating. *Nature*, 425:692–695, 2003.

[450] A. Lagg, J. Woch, N. Krupp, and S. K. Solanki. Retrieval of the full magnetic vector with the He I multiplet at 1083 nm. Maps of an emerging flux region. *Astron. Astrophys.*, 414:1109–1120, 2004.

[451] J. Arnaud. Observed polarization of the Fe XIV 5303 coronal emission line. *Astron. Astrophys.*, 112:350–354, 1982.

[452] N.-E. Raouafi, S. Sahal-Bréchot, and P. Lemaire. Linear polarization of the O VI λ 1031.92 coronal line. II. Constraints on the magnetic field and the solar wind velocity field vectors in the coronal polar holes. *Astron. Astrophys.*, 396:1019–1028, 2002.

[453] H. Lin, M. J. Penn, and S. Tomczyk. A new precise measurement of the coronal magnetic field strength. *Astrophys. J. Lett.*, 541:L83–L86, 2000.

[454] P. G. Judge. Spectral lines for polarization measurements of the coronal magnetic field. I. Theoretical intensities. *Astrophys. J.*, 500:1009–1022, 1998.

[455] J. R. Kuhn, R. M. MacQueen, J. Streete, G. Tansey, I. Mann, P. Hillebrand, R. Coulter, H. Lin, D. Edmunds, and P. Judge. Probable Detection of a Bright Infrared Coronal Emission Line of Si IX near 3.93 Microns. *Astrophys. J.*, 521:478–482, 1999.

[456] P. G. Judge, S. Tomczyk, W. C. Livingston, C. U. Keller, and M. J. Penn. Spectroscopic Detection of the 3.934 Micron Line of Si IX in the Solar Corona. *Astrophys. J. Lett.*, 576:L157–L160, 2002.

[457] M. D. Altschuler and G. Newkirk. Magnetic fields and the structure of the solar corona. *Solar Phys.*, 9:131–149, 1969.

[458] M. J. Hagyard and A. A. Pevtsov. Studies of solar helicity using vector magnetograms. *Solar Phys.*, 189:25–43, 1999.

[459] S. Bao and H. Zhang. Patterns of current helicity for solar cycle 22. *Astrophys. J.*, 496:L43–L46, 1998.

[460] P. Démoulin, S. Cuperman, and M. Semel. Determination of force-free magnetic fields above the photosphere using three-component boundary conditions: II. Analysis and minimization of scale-related growing modes and of computational induced singularities. *Astron. Astrophys.*, 263:351–360, 1992.

[461] A. N. McClymont, L. Jiao, and Z. Mikić. Problems and progress in computing three-dimensional coronal active region magnetic fields from boundary data. *Solar Phys.*, 174:191–218, 1997.

[462] N. Seehafer. Determination of constant α force-free solar magnetic fields from magnetograph data. *Solar Phys.*, 58:215–223, 1978.

[463] J. B Taylor. Relaxation of toroidal plasma and generation of reversed magnetic fields. *Phys. Rev. Lett.*, 33:1139–1141, 1974.

[464] J. J. Aly. On the reconstruction of the nonlinear force-free coronal magnetic field from boundary data. *Solar Phys.*, 120:19–48, 1989.

[465] T. Sakurai. Computational modeling of magnetic fields in solar active regions. *Space Sc. Rev.*, 51:11–48, 1989.

[466] J. J. Aly and N. Seehafer. Coronal force-free magnetic field: Source-surface model. *Solar Phys.*, 144:243–254, 1993.

[467] G. Roumeliotis. The stress-and-relax method for reconstructing the coronal magnetic field from vector magnetograph data. *Astrophys. J.*, 473:1095–1103, 1996.

[468] T. Amari, J. J. Aly, J. F. Luciani, T. Z. Boulmezaoud, and Z. Mikić. Reconstructing the solar coronal magnetic field as a force-free magnetic field. *Solar Phys.*, 174:129–149, 1997.

[469] T. Amari, T. Z. Boulmezaoud, and Z. Mikić. An iterative method for the reconstruction of the solar coronal field. I. Method for regular solutions. *Astron. Astrophys.*, 350:1051–1959, 1999.

[470] M. S. Wheatland, P. A. Sturrock, and G. Roumeliotis. An Optimization Approach to Reconstructing Force-free Fields. *Astrophys. J.*, 540:1150–1155, 2000.

[471] Y. Yan and T. Sakurai. New boundary integral equation representation for finite energy force-free magnetic fields in open space above the Sun. *Solar Phys.*, 195:89–109, 2000.

[472] J.-Q. Li, J.-X. Wang, and W. Feng-Si. A fluid dynamics approach for the computation of non-linear force-free magnetic field. *Chinese J. Astron. Astrophys.*, 3:247–256, 2003.

[473] J. A. Linker, Z. Mikić, D. A. Biesecker, R. J. Forsyth, S. E. Gibson, A. J. Lazarus, A. Lecinski, P. Riley, A. Szabo, and B. J. Thompson. Magnetohydrodynamic modeling of the solar corona during Whole Sun Month. *J. Geophys. Res.*, 104:9809–9830, 1999.

[474] Z. Mikić, J. A. Linker, D. D. Schnack, R. Lionello, and A. Tarditi. Magnetohydrodynamic Modelling of the Global Solar Corona. *Phys. Plasma*, 6:2217–2224, 1999.

[475] T. Wiegelmann and B. Inhester. Magnetic modeling and tomography: First steps towards a consistent reconstruction of the solar corona. *Solar Phys.*, 214:287–312, 2003.

[476] M. J. Aschwanden, A. I. Poland, and D. M. Rabin. The new solar corona. *Ann. Rev. Astron. Astrophys.*, 39:175–210, 2001.

[477] H. P. Jones and R. G. Giovanelli. Magnetic canopies in unipolar regions. *Solar Phys.*, 87:37–42, 1983.

[478] M. Faurobert-Scholl. Hanle effect of magnetic canopies in the solar chromosphere. *Astron. Astrophys.*, 285:655–662, 1994.

[479] M. Bianda, J. O. Stenflo, and S. K. Solanki. Hanle diagnostics of solar magnetic fields: the Sr II 4078 Å line. *Astron. Astrophys.*, 337:565–578, 1998.

[480] M. Bianda, J. O. Stenflo, and S. K. Solanki. Hanle effect observations with the Ca I 4227 Å line. *Astron. Astrophys.*, 350:1060–1070, 1999.

[481] S. K. Solanki and O. Steiner. How magnetic is the solar chromosphere? *Astron. Astrophys.*, 234:519–529, 1990.

[482] T. R. Ayres and L. Testerman. Fourier Transform Spectrometer observations of solar carbon monoxide. I - The fundamental and first overtone bands in the quiet sun. *Astrophys. J.*, 245:1124–1140, 1981.

[483] T. R. Ayres, L. Testerman, and J. W. Brault. Fourier transform spectrometer observations of solar carbon monoxide. II - Simultaneous cospatial measurements of the fundamental and first-overtone bands, and Ca II K, in quiet and active regions. *Astrophys. J.*, 304:542–559, 1986.

[484] S. K. Solanki, W. Livingston, and T. Ayres. New Light on the Heart of Darkness of the Solar Chromosphere. *Science*, 263:64–66, 1994.

[485] T. R. Ayres. Does the Sun Have a Full-Time COmosphere? *Astrophys. J.*, 575:1104–1115, 2002.

[486] A. M. Title and C. J. Schrijver. The Sun's Magnetic Carpet. In *Cool Stars, Stellar Systems, and the Sun*, pages 345–358, San Francisco: Astronomical Society of the Pacific Conf. Series 154, 1998

[487] T. E. Berger, B. de Pontieu, C. J. Schrijver, and A. M. Title. High-resolution imaging of the solar chromosphere/corona transition region. *Astrophys. J. Lett.*, 519:L97–L100, 1999.

[488] C. J. Schrijver and A. M. Title. The Magnetic Connection between the Solar Photosphere and the Corona. *Astrophys. J. Lett.*, 597:L165–L168, 2003.

[489] M. D. Altschuler, D. E. Trotter, and F. Q. Orrall. Coronal holes. *Solar Phys.*, 26:354–365, 1972.

[490] R. H. Munro and G. L. Withbroe. Properties of a coronal hole derived from extreme-ultraviolet observations. *Astrophys. J.*, 176:511–520, 1972.

[491] S. R. Cranmer, J. L. Kohl, G. Noci, E. Antonucci, G. Tondello, M. C. E. Huber, L. Strachan, A. V. Panasyuk, L. D. Gardner, M. Romoli, S. Fineschi, D. Dobrzycka, J. C. Raymond, P. Nicolosi, O. H. W. Siegmund, D. Spadaro, C. Benna, A. Ciaravella, S. Giordano, S. R. Habbal, M. Karovska, X. Li, R. Martin, J. G. Michels, A. Modigliani, G. Naletto, R. H. O'Neal, C. Pernechele, G. Poletto, P. L. Smith, and R. M. Suleiman. An Empirical Model of a Polar Coronal Hole at Solar Minimum. *Astrophys. J.*, 511:481–501, 1999.

[492] I. A. Belenko. Coronal Hole Evolution During 1996-1999. *Solar Phys.*, 199:23–35, 2001.

[493] Y.-M. Wang and N. R. Sheeley. Sunspot activity and the long-term variation of the Sun's open magnetic flux. *J. Geophys. Res.*, 107:1302–1317, 2002.

[494] Y.-M. Wang, S. H. Hawley, and N. R. Sheeley. The magnetic nature of coronal holes. *Science*, 271:464–469, 1996.

[495] K. Wilhelm, I. E. Dammasch, E. Marsch, and D. M. Hassler. On the source regions of the fast solar wind in polar coronal holes. *Astron. Astrophys.*, 353:749–756, 2000.

[496] E. C. Sittler and M. Guhathakurta. Semiempirical two-dimensional magnetohydrodynamic model of the solar corona and interplanetary medium. *Astrophys. J.*, 523:812–826, 1999.

[497] T. Wiegelmann and S. K. Solanki. Similarities and Differences between Coronal Holes and the Quiet Sun: Are Loop Statistics the Key? *Sol. Phys.*, 225:227–247, 2004.

[498] K. Stucki, S. K. Solanki, U. Schühle, I. Rüedi, K. Wilhelm, J. O. Stenflo, A. Brković, and M. C. E. Huber. Comparison of far-ultraviolet emission lines formed in coronal holes and the quiet Sun. *Astron. Astrophys.*, 363:1145–1154, 2000.

[499] K. Stucki, S. K. Solanki, C. D. Pike, U. Schühle, I. Rüedi, A. Pauluhn, and A. Brković. Properties of ultraviolet lines observed with the Coronal Diagnostic Spectrometer (CDS/SOHO) in coronal holes and the quiet Sun. *Astron. Astrophys.*, 381:653–667, 2002.

[500] Y.-M. Wang and N. R. Sheeley. Solar Implications of ULYSSES Interplanetary Field Measurements. *Astrophys. J. Lett.*, 447:L143–L146, 1995.

[501] T. R. Sanderson, T. Appourchaux, J. T. Hoeksema, and K. L. Harvey. Observations of the Sun's magnetic field during the recent solar maximum. *J. Geophys. Res.*, 108:1035–1042, 2003.

[502] C. E. DeForest, J. T. Hoeksema, J. B. Gurman, B. J. Thompson, S. P. Plunkett, R. Howard, R. C. Harrison, and D. M. Hassler. Polar Plume Anatomy: Results of a Coordinated Observation. *Solar Phys.*, 175:393–410, 1997.

[503] Y.-M. Wang and N. R. Sheeley. Coronal plumes and their relationship to network activity. *Astrophys. J.*, 452:457–461, 1995.

[504] K. Wilhelm, E. Marsch, B. N. Dwivedi, D. M. Hassler, P. Lemaire, A. H. Gabriel, and M. C. E. Huber. The Solar Corona above Polar Coronal Holes as Seen by SUMER on SOHO. *Astrophys. J.*, 500:1023–1038, 1998.

[505] L. Del Zanna, A. W. Hood, and A. W. Longbottom. An MHD model for solar coronal plumes. *Astron. Astrophys.*, 318:963–969, 1997.

[506] C. J. Schrijver. Relations between activity and magnetic field. In P. Ulmschneider, E. R. Priest, and R. Rosner, editors, *Mechanisms of chromospheric and coronal heating.*, pages 257–272. Springer, Berlin, 1991.

[507] E. E. Benevolenskaya, A. G. Kosovichev, J. R. Lemen, P. H. Scherrer, and G. L. Slater. Large-scale solar coronal structures in soft X-rays and their relationship to the magnetic Flux. *Astrophys. J. Lett.*, 571:L181–L185, 2002.

[508] Y.-M. Wang, N. R. Sheeley, S. H. Hawley, G. E. Kraemer, G. E. Brückner, R. A. Howard, C. M. Korendyke, D. J. Michels, N. E. Moulton, D. G. Socker, and R. Schwenn. Green-line corona and its relation to the photospheric magnetic field. *Astrophys. J.*, 485:419–429, 1997.

[509] L. M. Green, M. C. López Fuentes, C. H. Mandrini, P. Démoulin, L. Van Driel-Gesztelyi, and J. L. Culhane. The Magnetic Helicity Budget of a CME-Prolific Active Region. *Solar Phys.*, 208:43–68, 2002.

[510] P. Démoulin, C. H. Mandrini, L. van Driel-Gesztelyi, B. J. Thompson, S. Plunkett, Z. Kovári, G. Aulanier, and A. Young. What is the source of the magnetic helicity shed by CMEs? The long-term helicity budget of AR 7978. *Astron. Astrophys.*, 382:650–665, 2002.

[511] A. Bleybel, T. Amari, L. van Driel-Gesztelyi, and K. D. Leka. Global budget for an eruptive active region. I. Equilibrium reconstruction approach. *Astron. Astrophys.*, 395:685–695, 2002.

[512] S. Régnier, T. Amari, and E. Kersalé. 3D Coronal magnetic field from vector magnetograms: non-constant-alpha force-free configuration of the active region NOAA 8151. *Astron. Astrophys.*, 392:1119–1127, 2002.

[513] E. Marsch, T. Wiegelmann, and L. D. Xia. Coronal plasma flows and magnetic fields in solar active regions: Combined observations from SOHO and NSO/Kitt Peak. *Astron. Astrophys.*, 428:629–645, 2004.

[514] T. Wiegelmann, A. Lagg, S. K. Solanki, B. Inhester, and J. Woch. Comparing magnetic field extrapolations with measurements of magnetic loops. *Astron. Astrophys.*, 433:701–705, April 2005.

[515] J. A. Klimchuk, S. K. Antiochos, and D. Norton. Twisted Coronal Magnetic Loops. *Astrophys. J.*, 542:504–512, 2000.

[516] F. Reale and G. Peres. TRACE-derived Temperature and Emission Measure Profiles along Long-lived Coronal Loops: The Role of Filamentation. *Astrophys. J. Lett.*, 528:L45–L48, 2000.

[517] M. J. Aschwanden, R. W. Nightingale, and D. Alexander. Evidence for nonuniform heating of coronal loops inferred from multithread modeling of TRACE data. *Astrophys. J.*, 541:1059–1077, 2000.

[518] M. J. Aschwanden and C. J. Schrijver. Analytical approximations to hydrostatic solutions and scaling laws of coronal loops. *Astrophys. J. Supp*, 142:269–283, 2002.

[519] Z. Mikić, D. D. Schnack, and G. van Hoven. Dynamical evolution of twisted magnetic flux tubes. I - Equilibrium and linear stability. *Astrophys. J.*, 361:690–700, 1990.

[520] G. van Hoven, Y. Mok, and Z. Mikić. Coronal loop formation resulting from photospheric convection. *Astrophys. J. Lett.*, 440:L105–L108, 1995.

[521] A. A. Pevtsov. Active-Region Filaments and X-ray Sigmoids. *Solar Phys.*, 207:111–123, 2002.

[522] S. E. Gibson, Y. Fan, C. Mandrini, G. Fisher, and P. Demoulin. Observational consequences of a magnetic flux rope emerging into the corona. *Astrophys. J.*, 617:600–613, 2004.

[523] N. Seehafer. Electric current helicity in the solar atmosphere. *Solar Phys.*, 125:219–232, 1990.

[524] D. M. Rust and A. Kumar. Helical magnetic fields in filaments. *Solar Phys.*, 155:69–97, 1994.

[525] D. M. Rust and A. Kumar. Evidence for helically kinked magnetic flux ropes in solar eruptions. *Astrophys. J.*, 464:L199–L202, 1996.

[526] E. Tandberg-Hanssen. *The nature of solar prominences.*, volume 199 of *Astrohysics and space library*. Kluwer Academic Publishers, 1995.

[527] S.F. Martin. Conditions for the formation and maintainance of filaments. *Solar Phys.*, 182:107–137, 1998.

[528] T. Amari, J. F. Luciani, Z. Mikić, and J. Linker. A twisted flux rope model for coronal mass ejections and two-ribbon flares. *Astrophys. J. Lett.*, 529:L49–L52, 2000.

[529] M. Kuperus and M. A. Raadu. The Support of Prominences Formed in Neutral Sheets. *Astron. Astrophys.*, 31:189–193, 1974.

[530] A. A. Van Ballegooijen. Photospheric motions as a source of twist in coronal magnetic fields. In M. R. Brown, R. C. Canfield, and A. A. Pevtsov, editors, *Magnetic helicity in space and Laboratory plasmas*, pages 213–219, Geophysical Monograph 111, (Washingthon, DC: American Geophysical Union), 1999

[531] C. R. DeVore and S. K. Antiochos. Dynamical formation and stability of helical prominence magnetic fields. *Astrophys. J.*, 539:954–963, 2000.

[532] R. Lionello, Z. Mikić, J. A. Linker, and T. Amari. Magnetic Field Topology in Prominences. *Astrophys. J.*, 581:718–725, 2002.

[533] A. A. Pevtsov, R. C. Canfield, and T. R. Metcalf. Longitudinal variation of helicity of photospheric magnetic fields. *Astrophys. J. Lett.*, 440:L109–L112, 1995.

[534] J. B. Zirker, S. F. Martin, K. Harvey, and V. Gaizauskas. Global magnetic patterns of chirality. *Solar Phys.*, 175:27–44, 1997.

[535] S. F. Martin and A. H. McAllister. The Skew of X-ray Coronal Loops Overlying Hα Filaments. In Y. Uchida and al., editors, *IAU Colloq. 153: Magnetohydrodynamic Phenomena in the Solar Atmosphere - Prototypes of Stellar Magnetic Activity*, pages 497–498. Kluwer Academic Publishers, 1996.

[536] N. R. Sheeley, Y.-M. Wang, S. H. Hawley, G. E. Brueckner, K. P. Dere, R. A. Howard, M. J. Koomen, C. M. Korendyke, D. J. Michels, S. E. Paswaters, D. G. Socker, O. C. St. Cyr, D. Wang, P. L. Lamy, A. Llebaria, R. Schwenn, G. M. Simnett, S. Plunkett, and D. A. Biesecker. Measurements of Flow Speeds in the Corona between 2 and 30 R$_\odot$. *Astrophys. J.*, 484:472–478, 1997.

[537] A. A. van Ballegooijen and P. C. H. Martens. Formation and eruption of solar prominences. *Astrophys. J.*, 343:971–984, 1989.

[538] A. A. van Ballegooijen and P. C. H. Martens. Magnetic fields in quiescent prominences. *Astrophys. J.*, 361:283–289, 1990.

[539] B. Inhester, J. Birn, and M. Hesse. The evolution of line-tied coronal arcades including a converging footpoint motion. *Solar Phys.*, 138:257–281, 1992.

[540] T. Amari, J. F. Luciani, Z. Mikić, and J. Linker. Three-dimensional solutions of magnetohydrodynamic equations for prominence magnetic support: twisted magnetic flux rope. *Astrophys. J. Lett.*, 518:L57–L60, 1999.

[541] B. C. Low. Solar activity and the corona. *Solar Phys.*, 167:217–265, 1996.

[542] D. H. Mackay, E. R. Priest, V. Gaizauskas, and A. A. van Ballegooijen. Role of Helicity in the Formation of Intermediate Filaments. *Solar Phys.*, 180:299–312, 1998.

[543] E. R. Priest. A dynamic dextral-sinistral model for the structure and evolution of prominence magnetic fields. In D. Webb, B. Schmieder, and D. Rust, editors, *IAU Colloq. 167: New Perspectives on Solar Prominences*, pages 453–462, San Francisco: Astronomical Society of the Pacific Conf. Series 150, 1998

[544] H. S. Hudson and E. W. Cliver. Observing coronal mass ejections without coronagraphs. *J. Geophys. Res.*, 106(A11):25199–25214, 2001.

[545] D. M. Rust. Magnetic helicity in solar filaments and coronal mass ejections. In M. R. Brown, R. C. Canfield, and A. A. Pevtsov, editors, *Magnetic helicity in space and Laboratory plasmas*, Geophysical Monograph 111, pages 221–227, (Washingthon, DC: American Geophysical Union), 1999

[546] V. Bothmer and R. Schwenn. The structure and origin of magnetic clouds in the solar wind. *Ann. Geophys.*, 16:1–24, 1998.

[547] A. Kumar and D. M. Rust. Interplanetary magnetic clouds, helicity conservation, and current-core flux-ropes. *J. Geophys. Res.*, 101:15667–15684, 1996.

[548] S. P. Plunkett, A. Vourlidas, S. Šimberová, M. Karlický, P. Kotrč, P. Heinzel, Y. A. Kupryakov, W. P. Guo, and S. T. Wu. Simultaneous SOHO and ground-based observations of a large eruptive prominence and coronal mass ejection. *Solar Phys.*, 194:371–391, 2000.

[549] E. R. Priest and C. J. Schrijver. Aspects of Three-Dimensional Magnetic Reconnection. *Solar Phys.*, 190:1–24, 1999.

[550] Y. Lau and J. M. Finn. Three-dimensional kinematic reconnection in the presence of field nulls and closed field lines. *Astrophys. J.*, 350:672–691, 1990.

[551] T. N. Bungey, V. S. Titov, and E. R. Priest. Basic topological elements of coronal magnetic fields. *Astron. Astrophys.*, 308:233–247, 1996.

[552] D. S. Brown and E. R. Priest. The topological behaviour of 3D null points in the Sun's corona. *Astron. Astrophys.*, 367:339–346, 2001.

[553] D. W. Longcope and A. A. Van Ballegooijen. A Three-dimensional Dynamical Model of Current Sheet Formation in a Coronal Loop. *Astrophys. J.*, 578:573–589, 2002.

[554] I. J. D. Craig and P. G. Watson. Optimized magnetic reconnection solutions in three dimensions. *Solar Phys.*, 194:251–268, 2000.

[555] C. Beveridge, E. R. Priest, and D. S. Brown. Magnetic topologies due to two bipolar regions. *Solar Phys.*, 209:333–347, 2002.

[556] G. L. Withbroe and R. W. Noyes. Mass and energy flow in the solar chromosphere and corona. *Ann. Rev. Astron. Astrophys.*, 15:363–387, 1977.

[557] M. J. Aschwanden, T. D. Tarbell, R. W. Nightingale, C. J. Schrijver, A. Title, C. C. Kankelborg, P. Martens, and H. P. Warren. Time variability of the "quiet" Sun observed with TRACE. II. Physical parameters, temperature evolution, and energetics of extreme-ultraviolet nanoflares. *Astrophys. J.*, 535:1047–1065, 2000.

[558] P. K. Browning. Mechanisms of solar coronal heating. *Plasma Phys. Contr. Fusion*, 33(6):539–572, 1991.

[559] M. J. Aschwanden, C. J. Schrijver, and D. Alexander. Modelling of EUV loops observed with TRACE. I. Hydrostatic solutions with nonuniform heating. *Astrophys. J.*, 550:1036–1050, 2001.

[560] A. J. Hundhausen, A. L. Stanger, and S. A. Serbicki. Mass and energy contents of coronal mass ejections: SMM results from 1980 and 1984-1987. In *Solar dynamic phenomena and solar wind consequences*, Proc. of the Third SOHO Workshop, Estes Park Colorado, page 409, 1994.

[561] E. N. Parker. Topological dissipation and small-scale fields in turbulent gases. *Astrophys. J.*, 174:499, 1972.

[562] J. Feynman and S. F. Martin. The initiation of coronal mass ejections by newly emerging magnetic flux. *J. Geophys. Res.*, 100(A3):3355–3367, 1995.

[563] Y.-M. Wang and N. R. Sheeley. Filament Eruptions near Emerging Bipoles. *Astrophys. J. Lett.*, 510:L157–L160, 1999.

[564] A. O. Benz and S. Krucker. Energy Distribution of Microevents in the Quiet Solar Corona. *Astrophys. J.*, 568:413–421, 2002.

[565] A. Brković, S. K. Solanki, and I. Rüedi. Analysis of blinkers and EUV brightenings in the quiet Sun observed with CDS. *Astron. Astrophys.*, 373:1056–1072, 2001.

[566] A. R. Winebarger. Energetic Implications of Transient Dynamic Events. In J. J. Hunt and V. Domingo (eds.), *SOHO 13 Waves, Oscillations and Small-Scale Transients Events in the Solar Atmosphere: Joint View from SOHO and TRACE*, pages 223–228, (Nordwijk, NL: European Space Agency), ESA SP-547, 2004

[567] J. Heyvaerts and E. R. Priest. Coronal heating by reconnection in DC current system. A theory based on Taylor's hypothesis. *Astron. Astrophys.*, 137:63–78, 1984.

[568] K. Galsgaard and Å. Nordlund. Heating and activity of the solar corona 1. Boundary shearing of an initially homogeneous magnetic field. *J. Geophys. Res.*, 101(A6):13445–13460, 1996.

[569] W. Grossmann and R. A. Smith. Heating of solar coronal loops by resonant absorption of

Alfvén waves. *Astrophys. J.*, 332:476–498, 1988.

[570] P. Ulmschneider, E. R. Priest, and R. Rosner, editors. *Mechanisms of Chromospheric and Coronal Heating.* Springer, Berlin, 1991.

[571] M. Goossens, J. Andries, and M. J. Aschwanden. Coronal loop oscillations. An interpretation in terms of resonant absorption of quasi-mode kink oscillations. *Astron. Astrophys.*, 394:L39–L42, 2002.

[572] T. Van Doorsselaere, J. Andries, S. Poedts, and M. Goossens. Damping of coronal loop oscillations: calculation of resonantly damped kink oscillations of one-dimensional nonuniform loops. *Astrophys. J.*, 606:1223–1232, 2004.

[573] V. M. Nakariakov, L. Ofman, E. E. Deluca, B. Roberts, and J. M. Davila. TRACE observation of damped coronal loop oscillations: Implications for coronal heating. *Science*, 285:862–864, 1999.

[574] C. J. Schrijver, M. J. Aschwanden, and A. M. Title. Transverse oscillations in coronal loops observed with TRACE - I. An overview of events, movies, and a discussion of common properties and required conditions. *Solar Phys.*, 206:69–98, 2002.

[575] T. J. Wang, S. K. Solanki, W. Curdt, D. E. Innes, I. E. Dammasch, and B. Kliem. Hot coronal loop oscillations observed with SUMER: Examples and statistics. *Astron. Astrophys.*, 406:1105–1121, 2003.

[576] I. De Moortel and A. W. Hood. The damping of slow MHD waves in solar coronal magnetic fields. *Astron. Astrophys.*, 408:755–765, 2003.

[577] C. J. Schrijver, A. M. Title, T. E. Berger, L. Fletcher, N. E. Hurlburt, R. W. Nightingale, R. A. Shine, T. D. Tarbell, J. Wolfson, L. Golub, J. A. Bookbinder, E. E. Deluca, R. A. McMullen, H. P. Warren, C. C. Kankelborg, B. N. Handy, and B. de Pontieu. A new view of the solar outer atmosphere by the Transition Region and Coronal Explorer. *Solar Phys.*, 187:261–302, 1999.

[578] H. Grad. Some new variational properties of hydromagnetic equilibria. *Phys. Fluids*, 7:1283–1292, 1964.

[579] J. B Taylor. Relaxation and magnetic reconnection in plasmas. *Rev. Mod. Phys.*, 58:741–763, 1986.

[580] D. Biskamp. *Nonlinear Magnetohydrodynamics.*, volume 1 of *Cambridge Monographs on Plasma Physics.* Cambridge University Press, Cambridge, UK, 1993.

[581] M. A. Berger. Rigorous new limits on magnetic helicity dissipation in the solar corona. *Geophys. Astrophys. Fluid Dyn.*, 30:79, 1984.

[582] G. Hornig and L. Rastätter. The role of helicity in the reconnection process. *Adv. Space Res.*, 19:1789, 1997.

[583] J. A. Klimchuk, R. C. Canfield, and J. E. Rhoads. The practical application of the magnetic virial theorem. *Astrophys. J.*, 385:327–343, 1992.

[584] J. J. Aly. On some properties of force-free magnetic fields in infinite regions of space. *Astrophys. J.*, 283:349–362, 1984.

[585] J. J. Aly. How much energy can be stored in a three-dimensional force-free magnetic field. *Astrophys. J. Lett.*, 375:L61–L64, 1991.

[586] P. A. Sturrock. Maximum energy of semi-infinite magnetic field configurations. *Astrophys. J.*, 380:655–659, 1991.

[587] M. A. Berger and G. B. Field. The topological properties of magnetic helicity. *J. Fluid Mech.*, 147:133–148, 1984.

[588] J. M. Finn and T. M. Antonsen. Magnetic helicity: What is it and what is it good for? *Comm. Plasma Phys. Contr. Fusion*, 9(3):111–126, 1985.

[589] P. Démoulin and M. A. Berger. Magnetic Energy and Helicity Fluxes at the Photospheric Level. *Solar Phys.*, 215:203–215, 2003.

[590] C. R. DeVore. Magnetic helicity generation by solar differential rotation. *Astrophys. J.*, 539:944–953, 2000.

[591] M. A. Berger and A. Ruzmaikin. Rate of helicity production by solar rotation. *J. Geophys. Res.*, 105:10481–10490, 2000.

[592] P. Démoulin, C. H. Mandrini, L. Van Driel-Gesztelyi, M. C. Lopez Fuentes, and G. Aulanier. The Magnetic Helicity Injected by Shearing Motions. *Solar Phys.*, 207:87–110, 2002.

[593] L. van Driel-Gesztelyi, P. Démoulin, and C. H. Mandrini. Observations of magnetic helicity. *Adv. Space Res.*, 32:1855–1866, 2003.

[594] J. W. Bieber, P. A. Evenson, and W. H. Matthaeus. Magnetic helicity of the Parker field. *Astrophys. J.*, 315:700–705, 1987.

[595] M. C. López Fuentes, P. Démoulin, C. H. Mandrini, A. A. Pevtsov, and L. van Driel-Gesztelyi. Magnetic twist and writhe of active regions: On the origin of deformed flux tubes. *Astron.*

Astrophys., 397:305–318, 2003.

[596] F. Mariani and F. M. Neubauer. The interplanetary magnetic field. In R. Schwenn and E. Marsch, editors, *Physics of the inner heliosphere 1*, volume 20 of *Physics and Chemistry in Space*, pages 183–206. Springer, Berlin, 1990.

[597] L. F. Burlaga, C. Wang, J. D. Richardson, and N. F. Ness. Evolution of magnetic fields in corotating interaction regions from 1 to 95 AU: Order to chaos. *Astrophys. J.*, 590:554–566, 2003.

[598] M. Neugebauer. The solar-wind and heliospheric magnetic field in three dimensions. In A. Balogh, R. G. Mardsen, and E. J. Smith, editors, *The heliosphere at solar minimum - The Ulysses perspective*, Springer books in astrophysics and astronomy, pages 43–106. Springer, Berlin, 2001.

[599] Y.-M. Wang, N. R. Sheeley, J. L. Phillips, and B. E. Goldstein. Solar Wind Stream Interactions and the Wind Speed-Expansion Factor Relationship. *Astrophys. J. Lett.*, 488:L51–L54, October 1997.

[600] C. N. Arge and V. J. Pizzo. Improvement in the prediction of solar wind conditions using near-real time solar magnetic field updates. *J. Geophys. Res.*, 105:10465–10480, 2000.

[601] J. T. Hoeksema. The Large-Scale Structure of the Heliospheric Current Sheet During the ULYSSES Epoch. *Space Sc. Rev.*, 72:137–148, 1995.

[602] A. Balogh and E. J. Smith. The heliospheric field at solar maximum: Ulysses observations. *Space Sc. Rev.*, 97:147–160, 2001.

[603] G. H. Jones and A. Balogh. The global heliospheric magnetic field polarity distribution as seen at Ulysses. *Ann. Geophys.*, 21:1377–1382, 2003.

[604] E. J. Smith, R. G. Marsden, A. Balogh, G. Gloeckler, J. Geiss, D. J. McComas, R. B. McKibben, R. J. MacDowall, L. J. Lanzerotti, N. Krupp, H. Krueger, and M. Landgraf. The Sun and Heliosphere at Solar Maximum. *Science*, 302:1165–1169, 2003.

[605] Y.-M. Wang, N. R. Sheeley, and M. D. Andrews. Polarity reversal of the solar magnetic field during cycle 23. *J. Geophys. Res.*, 107(A12):1465–1471, 2002.

[606] H. Alfvén. Electric currents in cosmic plasmas. *Rev. of Geophys. Space Phys.*, 15:271–284, 1977.

[607] L. F. Burlaga. *Interplanetary Magnetohydrodynamics.*, volume 3 of *International series on Astron. Astrophys.* Oxford University Press, Oxford, UK, 1995.

[608] J. De Keyser, M. Roth, H. De Sterk, and S. Poedts. A survey of field-aligned Mach number and plasma beta in the solar wind. *Space Sc. Rev.*, 97:201–204, 2001.

[609] J. L. Phillips, S. J. Bame, A. Barnes, B. L. Barraclough, W. C. Feldman, B. E. Goldstein, J. T. Gosling, G. W. Hoogeveen, D. J. McComas, M. Neugebauer, and S. T. Suess. Ulysses solar wind plasma observations from pole to pole. *Geophys. Res. Lett.*, 22:3301–3304, 1995.

[610] J. Woch, W. I. Axford, U. Mall, B. Wilken, S. Livi, J. Geiss, G. Gloeckler, and R. J. Forsyth. SWICS/Ulysses observations: The three-dimensional structure of the heliosphere in the declining/minimum phase of the solar cycle. *Geophys. Res. Lett.*, 24:2885–2888, 1997.

[611] Y.-M. Wang, N. R. Sheeley, D. G. Socker, R. A. Howard, and N. B. Rich. The dynamical nature of coronal streamers. *J. Geophys. Res.*, 105(A11):25133–25142, 2000.

[612] E. N. Parker. Dynamics of the Interplanetary Gas and Magnetic Fields. *Astrophys. J.*, 128:664–676, 1958.

[613] E. J. Weber and L. J. Davis. The Angular Momentum of the Solar Wind. *Astrophys. J.*, 148:217–227, 1967.

[614] V. Pizzo, R. Schwenn, E. Marsch, H. Rosenbauer, K.-H. Mühlhäuser, and F. Neubauer. Determination of the solar wind angular momentum flux from Helios data – An observational test of the Weber and Davis theory. *Astrophys. J.*, 335:1983, 271.

[615] E. Marsch and A. K. Richter. Distribution of solar wind angular momentum between particles and fields : Inferences about the Alfvén critical point from Helios observations. *J. Geophys. Res.*, 89:5386–5394, 1984.

[616] E. J. Smith, M. E. Burton, A. Balogh, R. Forsyth, and R. P. Lepping. Radial and azimuthal components of the heliospheric magnetic field - ULYSSES observations. *Adv. Space Res.*, 20:47–53, 1997.

[617] E. J. Smith and A. Balogh. Open Magnetic Flux: Variation with Latitude and Solar Cycle. In *Solar Wind Ten*, pages 67–70, Melville, NY: American Institute of Physics Conf. Proc. 679, 2003.

[618] Y.-M. Wang and N. R. Sheeley. Sunspot activity and the long-term variation of the Sun's open magnetic flux. *J. Geophys. Res.*, 107(A10):1302–1316, 2002.

[619] L. A. Fisk and N. A. Schwadron. Origin of the Solar Wind: Theory. *Space Sc. Rev.*, 97:21–33, 2001.

[620] J. Bertaux, E. Quémerais, and R. Lallement. Observations of a sky Lyman α groove related to enhanced solar wind mass flux in the neutral sheet. *Geophys. Res. Lett.*, 23:3675–3678, 1996.

[621] R. J. Forsyth, A. Balogh, E. J. Smith, G. Erdös, and D .J. McComas. The underlying Parker spiral structure in the Ulysses magnetic field observations, 1990-1994. *J. Geophys. Res.*, 101:395–403, 1996.

[622] J. R. Jokipii and B. Thomas. Effects of drift on the transport of cosmic rays. IV - Modulation by a wavy interplanetary current sheet. *Astrophys. J.*, 243:1115–1122, 1981.

[623] A. Balogh, V. Bothmer, N. U. Crooker, R. J. Forsyth, G. Gloeckler, A. Hewish, M. Hilchenbach, R. Kallenbach, B. Klecker, J. A. Linker, E. Lucek, G. Mann, E. Marsch, A. Posner, I. G. Richardson, J. M. Schmidt, M. Scholer, Y.-M. Wang, R. F. Wimmer-Schweingruber, M. R. Aellig, P. Bochsler, S. Hefti, and Z. Mikić. The Solar Origin of Corotating Interaction Regions and Their Formation in the Inner Heliosphere. *Space Sc. Rev.*, 89:141–178, 1999.

[624] R. J. Forsyth and J. T. Gosling. Corotating and transient structures in the heliosphere. In A. Balogh, R. G. Mardsen, and E. J. Smith, editors, *The heliosphere at solar minimum - The Ulysses perspective*, Springer books in astrophysics and astronomy, pages 107–166. Springer, Berlin, 2001.

[625] V. J. Pizzo. Global, quasi-steady dynamics of the distant solar wind 2: Deformation of the heliospheric current sheet. *J. Geophys. Res.*, 99(A3):4185–4191, 1994.

[626] V. J. Pizzo and J. T. Gosling. 3-D simulation of high-latitude interaction regions: Comparison with ULYSSES results. *Geophys. Res. Lett.*, 21:2063–2066, 1994.

[627] J. T. Gosling and V. J. Pizzo. Formation and evolution of corotating interaction regions and their three dimensional structure. *Space Sc. Rev.*, 89:21–52, 1999.

[628] L. F. Burlaga, N. F. Ness, and J. W. Belcher. Radial evolution of corotating merged interaction regions and flows between $\sim$ 14 AU and $\sim$ 43 AU. *J. Geophys. Res.*, 102:4661–4672, 1997.

[629] J. T. Gosling, S. J. Bame, D. J. McComas, J. L. Phillips, B. E. Goldstein, and M. Neugebauer. The speeds of coronal mass ejections in the solar wind at mid heliographic latitudes: ULYSSES. *Geophys. Res. Lett.*, 21:1109–1112, 1994.

[630] J. T. Gosling, D. J. McComas, J. L. Phillips, L. A. Weiss, V. J. Pizzo, B. E. Goldstein, and R. J. Forsyth. A new class of forward-reverse shock pairs in the solar wind. *Geophys. Res. Lett.*, 21:2271–2274, 1994.

[631] R. J. Forsyth, A. Balogh, and E. J. Smith. Latitudinal variation of the underlying heliospheric magnetic field direction: comparisons of the Ulysses first and second orbits. *Space Sc. Rev.*, 97:161–164, 2001.

[632] P. Riley, J. A. Linker, Z. Mikić, D. Odstrcil, T. H. Zurbuchen, D. Lario, and R. P. Lepping. Using an MHD simulation to interpret the global context of a coronal mass ejection observed by two spacecraft. *J. Geophys. Res.*, 108(A7):1272–1267, 2003.

[633] V. Bothmer and R. Schwenn. Eruptive prominences as sources of magnetic clouds in the solar wind. *Space Sc. Rev.*, 70:215–221, 1994.

[634] V. Bothmer, M. I. Desai, R. G. Marsden, T. R. Sanderson, K. J. Trattner, K.-P. Wenzel, J. T. Gosling, A. Balogh, R. J. Forsyth, and B. E. Goldstein. ULYSSES observations of open and closed magnetic field lines within a coronal mass ejection. *Astron. Astrophys.*, 316:493–498, 1996.

[635] D. Odstrčil and V. J. Pizzo. Three-dimensional propagation of CMEs in a structured solar wind flow: 1. CME launched within the streamer belt. *J. Geophys. Res.*, 104:483–492, 1999.

[636] D. Odstrčil and V. J. Pizzo. Three-dimensional propagation of coronal mass ejections in a structured solar wind flow 2. CME launched adjacent to the streamer belt. *J. Geophys. Res.*, 104:493–504, 1999.

[637] I. I. Roussev, T. I. Gombosi, I. V. Sokolov, M. Velli, W. Manchester, D. L. DeZeeuw, P. Liewer, G. Tóth, and J. Luhmann. A Three-dimensional Model of the Solar Wind Incorporating Solar Magnetogram Observations. *Astrophys. J.*, 595:L57–L61, 2003.

[638] C. P. T. Groth, D. L. De Zeeuw, T. I. Gombosi, and K. G. Powell. Global three-dimensional MHD simulation of a space weather event: CME formation, interplanetary propagation, and interaction with the magnetosphere. *J. Geophys. Res.*, 105(A11):25053–25078, 2000.

[639] W. B. Manchester, T. I. Gombosi, I. Roussev, D. L. De Zeeuw, I. V. Sokolov, K. G. Powell, G. Tóth, and M. Opher. Three-dimensional MHD simulation of a flux rope driven CME. *J. Geophys. Res.*, 109:1102–1118, 2004.

[640] J. W. Belcher and L. Davis. Large-amplitude Alfvén waves in the interplanetary medium, 2. *J. Geophys. Res.*, 76:3534–3563, 1971.

[641] E. J. Smith, M. Neugebauer, A. Balogh, S. J. Bame, R. P. Lepping, and B. T. Tsurutani. ULYSSES observations of latitude gradients in the heliospheric magnetic field: Radial

component and variances. *Space Sc. Rev.*, 72:165–170, 1995.

[642] C.-Y. Tu and E. Marsch. MHD structures, waves and turbulence in the solar wind: Observations and theories. *Space Sc. Rev.*, 73:1–210, 1995.

[643] E. Marsch and C.-Y. Tu. Spatial evolution of the magnetic field spectral exponent in the solar wind: Helios and Ulysses comparison. *J. Geophys. Res.*, 101(A5):11149–11152, 1996.

[644] C.-Y. Tu and E. Marsch. Two-fluid model for heating of the solar corona and accelaration of the solar wind by high-frequency Alfvén waves. *Solar Phys.*, 171:363–391, 1997.

[645] W. I. Axford and J. F. McKenzie. The origin of high speed solar wind streams. In E. Marsch and R. Schwenn (Eds.), *Solar Wind Seven*, pages 1–5, Oxford: Pergamon Press, 1992.

[646] W. H. Matthaeus, G. P. Zank, C. W. Smith, and S. Oughton. Turbulence, Spatial Transport, and Heating of the Solar Wind. *Phys. Rev. Lett.*, 82:3444–3447, 1999.

[647] C. W. Smith, W. H. Matthaeus, G. P. Zank, N. F. Ness, S. Oughton, and J. D. Richardson. Heating of the low-latitude solar wind by dissipation of turbulent magnetic fluctuations. *J. Geophys. Res.*, 106(A5):8253–8272, 2001.

[648] W. I. Axford. The interaction of the solar wind with the interstellar medium. In C. P. Sonett, P. J. Coleman, and J. M. Wilcox (Eds.), *Solar Wind*, pages 609ff, Washington, D.C.: NASA volume SP-308, 1972.

[649] T. E. Holzer. Interaction between the solar wind and the interstellar medium. *Ann. Rev. Astron. Astrophys.*, 27:199–234, 1989.

[650] G. P. Zank. Interaction of the solar wind with the local interstellar medium: a theoretical perspective. *Space Sc. Rev.*, 89:413–688, 1999.

[651] L. F. Burlaga, N. F. Ness, M. H. Acuña, R. P. Lepping, J. E. P. Connerney, E. C. Stone, and F. B. McDonald. Crossing the termination shock into the heliosheath: magnetic fields. *Science*, 309:2027–2029, 2005.

[652] R. Lallement. Relations Between ISM Inside and Outside the Heliosphere. *Space Sc. Rev.*, 78:361–374, 1996.

[653] M. Witte, M. Banaszkiewicz, and H. Rosenbauer. Recent Results on the Parameters of the Interstellar Helium from the Ulysses/Gas Experiment. *Space Sc. Rev.*, 78:289–296, 1996.

[654] A. Barnes. Interaction of the local interstellar medium with the heliosphere: interior and exterior magnetic fields. In K. Scherer, H. Fichtner, H. J. Fahr, and E. Marsch, editors, *The outer heliosphere: the next frontiers*, volume 11 of *COSPAR colloquia series*, pages 43–52, Amsterdam, 2001. Pergamon, Elsevier Science.

[655] R. Ratkiewicz, A. Barnes, G. A. Molvik, J. R. Spreiter, S. S. Stahara, M. Vinokur, and S. Venkateswaran. Effect of varying strength and orientation of the local interstellar magnetic field configuration of exterior heliosphere: 3D simulations. *Astron. Astrophys.*, 335:363–369, 1998.

[656] R. Ratkiewicz and J. F. McKenzie. Interstellar magnetic field effects on the termination shock, heliopause, and bow shock: Aligned MHD flow. *J. Geophys. Res.*, 108(A2):1071–1079, 2003.

[657] L. F. Burlaga, N. F. Ness, Y.-M. Wang, and N. R. Sheeley. Voyager 1 studies of the HMF to 81 AU during the ascending phase of solar cycle 23. In *Solar Wind Ten*, pages 39–42, Melville, NY: American Institute of Physics Conf. Proc. 679, 2003.

[658] P. A. Isenberg, C. W. Smith, and W. H. Matthaeus. Turbulent Heating of the Distant Solar Wind by Interstellar Pickup Protons. *Astrophysical Journal*, 592:564–573, 2003.

[659] H. J. Fahr and K. Scherer. Diamagnetic effects of heliospheric Pick-up ions and magnetic fluxes in the outer heliosphere. *Astron. Astrophys. Letters*, 421:L9–L12, 2004.

[660] H. Washimi and T. Tanaka. 3D magnetic field and current system in the heliosphere. *Space Sc. Rev.*, 78:85–94, 1996.

[661] T. Linde, T. I. Gombosi, P. L. Roe, K. G. Powell, and D. L. DeZeeuw. The heliosphere in the magnetized local interstellar medium: Results of a 3D MHD simulation. *J. Geophys. Res.*, 103:1889–1904, 1998.

[662] Y. C. Whang, L. F. Burlaga, and N. F. Ness. Locations of the termination shock and the heliopause. *J. Geophys. Res.*, 100(A9):17015–17024, 1995.

[663] G. P. Zank and H.-R. Müller. The dynamical heliosphere. *J. Geophys. Res.*, 108(A6):1240–1235, 2003.